

The Barkhausen effect

Gianfranco Durin¹ and Stefano Zapperi²

¹ *Istituto Elettrotecnico Nazionale Galileo Ferraris, strada delle Cacce 91, I-10135 Torino, Italy*

² *INFM SMC and UdR Roma 1, Dipartimento di Fisica,
Università "La Sapienza", P.le A. Moro 2, 00185 Roma, Italy*

We review key experimental and theoretical results on the Barkhausen effect, focusing on the statistical analysis of the noise. We discuss the experimental methods and the material used and review recent measurements. The picture emerging from the experimental data is that Barkhausen avalanche distributions and power spectra can be described by scaling laws as in critical phenomena. In addition, there is growing evidence that soft ferromagnetic bulk materials can be grouped in different classes according to the exponent values. Soft thin films still remain to be fully explored both experimentally and theoretically. Reviewing theories and models proposed in the recent past to account for the scaling properties of the Barkhausen noise, we conclude that the domain wall depinning scenario successfully explains most experimental data. Finally, we report a translation from German of the original paper by H. Barkhausen.

Contents

I. Introduction	2
II. Experiments and materials	3
A. Experimental setup	3
1. Inductive measurements	3
2. Magneto-optical Kerr effect measurements	5
B. Magnetic materials	5
III. Experimental results	6
A. Barkhausen signal and avalanches distributions	6
B. Power spectra and avalanche shapes	10
1. Avalanche shapes	12
2. High order power spectra	14
C. Thin films	17
IV. Models and theories of magnetization dynamics	20
A. General properties of ferromagnetic systems	20
1. Exchange energy	20
2. Magnetostatic energy	21
3. Magnetocrystalline anisotropy and magnetoelastic energies	22
4. Disorder	22
5. Micromagnetic equations	23
B. Random energy models	24
C. Spin models	25
1. The random field Ising model	25
2. Random bonds, random anisotropies and other effects	27
D. Domain wall models	29
1. Energetics of a domain wall	29
2. Domain wall dynamics and depinning transition	32
V. Discussion of theoretical results	37
A. Avalanches distributions	37
B. The power spectrum	39
C. The avalanche shape	41
D. Two dimensions	43
VI. Conclusions and perspectives	44

VII. Acknowledgments

45

A. Translation of the original paper by Barkhausen

45

References

47

I. INTRODUCTION

”Eisen gibt beim Unmagnetisieren ein Geräusch; bei ganz gleichmäßigen Änderung der magnetomotorischen Kraft klappen die Molekularmagnete sprungweise in ihre neue Lage und erzeugen dadurch in einer darüber geschobenen Spule unregelmäßige Induktionsstöße, die sich im Telephon als Geräusch erkenntlich machen” [1] [As the magnetomotive force is smoothly varied, the molecular magnets flip in jumps to their new position. Because of this, they generate irregular induction pulses in a coil wound around the sample, that can then be heard as a noise in a telephone.](See the Appendix for a complete translation of the original paper).

All the essential elements of the magnetization noise as discovered by H. Barkhausen are contained in his words introducing the famous paper of 1919. A piece of iron, the simplest magnetic material, produces a jerky noise when magnetized by a field smoothly changing in time as, for instance, given by the slow movement of a magnetic yoke driven by a hand. This noise is irregular, in contrast with the regularity of the applied field, and can be easily heard with a microphone. This was the first indirect evidence of the existence of magnetic domains, postulated a few years before by Weiss [2]: actually, Barkhausen believed that the noise was produced by the sudden reversal of the entire magnetic domains (the ”molecular magnets”). Only several years later, in 1938, Elmore [3] made the first observation of the motion of domain boundaries in a cobalt crystal (described theoretically in 1932 by Bloch and thus referred as Bloch walls) under the application of an external field. Curiously, Elmore did not recognize this motion as the source of the noise heard by Barkhausen. This instead was successively evidenced by Williams and Shockley measuring a SiFe single crystal [4]. It is worth noting that in this very year, Kittel in his famous *Physical theory of ferromagnetic domains*, warned ”it may be well to correct the widespread notion” that the Barkhausen effect is connected to the complete domain reversal, as Williams and Shockley showed ”quite clearly [...] that the Barkhausen discontinuities correspond to irregular fluctuations in the motion of a domain boundary (Bloch wall)” [from [5], pg. 9].

Once the origin of Barkhausen (BK) noise was understood, it was soon realized that it could be used as an effective probe to investigate and understand the magnetization dynamics in soft magnetic materials, and explain some of their hysteresis properties. At the same time, it was also clear that the task was far from being easy. As significantly noted ”the Barkhausen effect research is both simple and hard” [Ref. [6], pg. 46], in the sense that it is relatively easy to perform a measurement, but it is much more difficult to interpret it. This is due to the stochastic character of domain wall (DW) motion, which proceeds in jumps, or avalanches, when slowly magnetized. This dynamics is strongly affected by material microstructure, and other effects such as the demagnetizing field, external stress, etc. For this reason, earlier studies were focused on materials having the simplest domain structure, like the SiFe single crystals (see for instance [7]), where it is possible to obtain a single DW in frame-type samples.

The intense activity of Barkhausen studies up to the 70s, both from the theoretical and experimental side, are extensively described in the reviews of Rudyak [8], and of McClure and Schöeder [6]. Both papers report a large series of experimental data on the statistical properties of the noise: distribution of duration and size of the avalanches, power spectra, pulse propagation along the sample, etc. The approach followed to interpret the data is fully phenomenological, without a precise connection with the DW dynamics. For instance, power spectra [9, 10] and cross spectra using two separated coils [11] are described by a proper superposition of *elementary* independent jumps, whose spectral characteristic are defined *at priori*. These elementary jumps are not strictly related to well specified DW displacements. Another approach tried to mimic the active interactions on a DW considering the effect of a series of springs on a rigid wall, and calculating the resulting power spectrum [12, 13].

Both reviews also present an exhaustive discussion on the possible effects of the measuring setup on the detected signal, considering the effect of the dimensions of both the solenoid and the pick-up coils, the different time constants related to the electrical circuits, and, more importantly, the effect of the eddy currents. This detailed analysis testifies the accuracy and capability in doing BK experiments in that period. Most of the methodology is still valid and should be strictly followed, even if this has not always happened in the recent literature.

The difficulties to correctly interpret the experimental data were partially explained by the observation of Wiegman and ter Stege [14] first, and later of Bertotti *et. al* [15], who noticed as the statistical properties of the noise typically vary along the hysteresis loop. Only considering a region where the DW motion is the dominant or better the unique magnetization process, as around the coercive field, it is possible to obtain a stationary signal and to correctly perform a statistical analysis. This observation triggered a new series of detailed experiments, which were quite well described by a new DW model, known as ABBM [16, 17]. Even if still phenomenological, this model has the merit to describe

the statistical properties of the noise on the basis of some simple assumptions verified experimentally, and to be analytically tractable.

This new experimental determination of the noise properties put in evidence a series of interesting characteristics. The BK noise is self-similar, and shows scaling invariance and power laws. In other words, it has the typical features of a critical phenomenon, whose detailed nature has been the subject of an intense debate. Following this line of interpretation, in 1991, Cote and Meisel [18, 19] claimed that the Barkhausen effect is a particular example of a "self-organized critical" system [20], in which there is no need to fine tune a control parameter, as in usual second-order transitions. Following this suggestion, new experiments and models were published quite regularly in the literature. After nearly 15 years, it is necessary to review this large production of data and ideas and, taking into account the important result previously appeared in the literature, to propose a single framework to interpret the phenomenon. This is particularly important in order to deal with recent observations of the Barkhausen noise lacking a coherent interpretation, such as for measurements in thin films, hard materials, and low dimensional systems.

II. EXPERIMENTS AND MATERIALS

In the vast literature about the Barkhausen noise, there is such a large production and analysis of experimental data that there is a serious risk of confusion and misunderstanding. Data have been collected on nearly all possible soft magnetic materials, and considering many different properties, so that one can, in principle, assume them as sufficiently exhaustive and reliable. The absence of a coherent interpretation could then be ascribed to the lack of a proper theoretical model.

Paradoxically, the situation is very different. Despite the large production of data, the number of reliable results is quite small, and is restricted, with only a few exceptions, to last decades of studies. There are many reasons for this, as we will discuss in detail in the following. One of the main points is that there is no general agreement about a 'standard' experimental setup which would allow for a meaningful comparison of the results. In fact, different experimental procedures can all produce "nice" Barkhausen data, but their interpretation could widely differ. The way the measurement is performed influences significantly the details of the magnetization process. Thus, there has been a strong effort in the last years to set experiments in the simplest and most controlled way, avoiding unnecessary complications. This opened the way to a convincing theoretical interpretation based on relatively simple models. It is only through well defined experiments that parameters can be estimated and used in the theory.

As discussed in the introduction, a crucial observation is that the noise properties, such as the power spectrum, change along the hysteresis loop [14, 15]. As a consequence, it is important to measure the noise only around the coercive field in the steepest part of the loop, where domain wall motion is the dominant (and often the unique) magnetization mechanism, and the Barkhausen signal is stationary. This point questions the reliability of many experimental results previously reported in the literature.

It is convenient to critically discuss the experimental procedures proposed in the recent literature, in order to identify a series of practical rules to establish a 'standard' setup. This will enable the direct comparison of different experimental data, and the development of a common theoretical framework in which to analyze and understand the magnetization process.

A. Experimental setup

As shown in the introduction, earlier experiments, starting from the original one by Barkhausen, are all based on the induction of a flux change into some concatenated coils in response to a slowly varying external field. The regularity of the applied field contrasts with the irregular character of the induced pulses, as a result of the random motion of the DW. More recent experiments make use of magneto-optical methods based on the Kerr effect (MOKE) and are more suitable to investigate the noise properties of thin films, as we will describe in detail (see Sec. III C).

1. Inductive measurements

The essential elements of an inductive Barkhausen noise measurement are simply identified: an external solenoid or a Helmholtz coil, able to produce a sufficiently homogeneous field along the sample, and a certain number of pick-up (secondary) coils wound around the sample to detect the induced flux. In general, it is a good practise to use a solenoid much longer than the sample to ensure a uniform applied field. Also in the case of application of an external tensile stress, it is preferable to use a non-magnetic ribbon glued to the sample and attached to a weight (as done in Ref. [21] using amorphous materials), so that the sample remains in the center of the solenoid. To make measurements

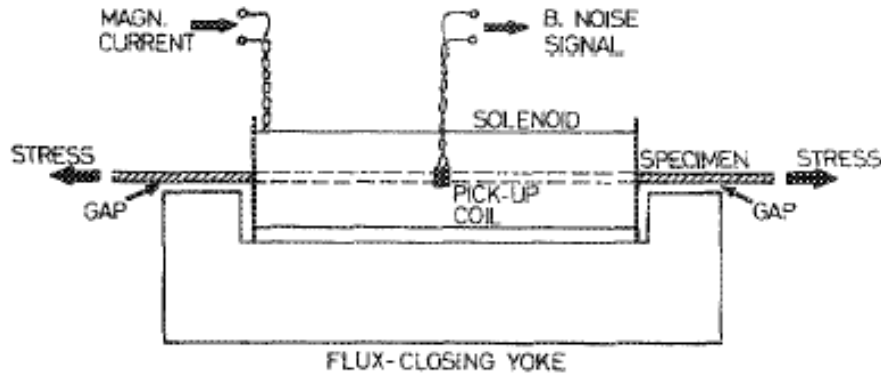


FIG. 1: Schematic representation of a setup for inductive measurements. In this case, the sample is longer than the solenoid, so that the applied field is not uniform. The flux-closing yoke is used to change the apparent permeability [From [17], Fig. 1, p. 2909]

at different permeability there are two alternatives with both advantages and disadvantages: as in [22], a magnetic yoke with a variable gap can be used, but, obviously, with a sample longer than the solenoid (see Fig. 1); otherwise, the sample can be progressively cut, as in Ref. [21].

The induced signal $\dot{\Phi}$ both detects the contribution of the applied field H across the pick-up coil (having a cross section A_{pickup}) and of the material itself, so that $\dot{\Phi} = A_{pickup}\mu_o\dot{H} + A\dot{I}$, where A is the material cross section, and I the magnetization. This expression is valid as long as the eddy current shielding is negligible, as happens for the usual measurements performed at very low frequency (usually up to no more than a few Hz). In high permeability magnetic materials and for A not too small in respect to A_{pickup} , the contribution of the external field can be neglected for frequency up to several kHz, thus the induced flux contains all the information about the material properties. On the contrary, with low permeability materials, or when $A \ll A_{pickup}$, as for instance, in thin films, it is necessary to compensate for the induced flux in air in order to have $\dot{\Phi} \approx A\dot{I}$. This is usually performed using another pickup coil with the same number of turns and the same cross section, but wound in the opposite direction. A more refined solution requires a further coil put in air to get a finer compensation [14, 23]. This solution is particularly important when it is necessary to measure the hysteresis properties of thin films using inductive methods [24].

In the simplest experimental conditions, as for a material having only two opposite domains and thus a single DW, the induced flux is simply proportional to the DW velocity v , as $\dot{\Phi} = N(2I_s dv)$, where I_s is the saturation magnetization, d the sample thickness, and N is the number of turns. In the more common case of a multiplicity of DWs, one can assume that v measures the velocity of the active DWs, even if this must be considered just as a rough approximation. In fact, the induced signal indirectly collects, in a very complicated and unpredictable way, the changes coming from all the rest of the sample because of long range spatial interactions, and/or propagation of local deformations of DWs. This latter effect has been quantitatively studied, showing that the flux variation decays roughly exponentially with a typical scale of the order of a few cm [11]. This suggests to keep the width of the pickup coil as small as possible (a few mm, in practice). A measurement obtained with N turns is thus a good approximation of a measurement in a single cross-section of the material, with the advantage of the amplification of the signal by the factor N . There is also an additional effect suggesting to keep the width of the coils small. The magnetostatic field in an open sample produces a counterfield known as demagnetizing field, which essentially depends on the sample shape and on the domain structure. This field is spatially constant only in a sample having the form of ellipse and *at saturation*, otherwise it varies, as for instance, when a domain structure is present. The demagnetizing effect has a strong effect on the DW dynamics, limiting for instance the maximum size of a jump (see Sec. III A): it is thus convenient to consider a constant demagnetizing field, and this is again obtained limiting the width of the secondary coils. A notable example not following this rule is the setup used by Spasojević *et al.* [25] where the pickup coil has a length of 5.5 cm, while the sample is only 4 cm long. This seriously questions the interpretation of the data and the obtained scaling exponents given the strong spatial variation of the demagnetizing field.

Even following all these experimental prescriptions, we must clarify that the inductive measurement is always a collective detection of many moving DWs, where propagation and long range interactions still play a significant role. We emphasize it as the most successful models proposed in the literature (see Sec. IV) are based on the dynamics of a single domain wall. It is thus necessary to clarify what is the reason of their success and, at the same time, understand their limitations. In particular, we will describe in detail how the open problems, still under severe theoretical and

experimental investigation, could be possibly understood introducing more complicated magnetization models which have not been considered so far.

A strict consequence of this collective detection of DWs motion is that the measured signal cannot distinguish between single BK jumps and a superposition in space and/or time of them. This limitation has strong consequences on the interpretation of the statistical distributions of BK jumps, and in particular on the effect of the external field rate (Sec. III A). Quite reasonably, it has been noted [26] that at zero driving rate (the so called adiabatic limit) the signal should be considered a sequence of Barkhausen *avalanches*, i.e. of elementary jumps without any superposition. On the contrary, at finite driving rates, the signal appears a sequence of *pulses* containing a certain number of avalanches. We adopt this distinction, as it is necessary to understand theoretically the effect of the driving rate on the scaling exponents. Clearly, there is a practical difficulty to establish the low frequency regime which approximates the adiabatic limit.

In order to further simplify the measurements, we finally note that the applied field has usually a triangular shape instead of the common sinusoidal waveform used in hysteresis loop measurements. As the noise is taken around the coercive field, as said, this ensures to have constant magnetization rate, which is the fundamental parameter to describe the variation of the BK statistical distributions (Sec. III A), and of the power spectra (Sec. III B).

2. Magneto-optical Kerr effect measurements

As described above, earlier measurements on thin films were done using inductive setups, with fine compensation of air flux [14, 23, 27]. These measurements focused both on the noise power spectra [27], and on the avalanche statistical distributions, detected along the hysteresis loop [14]. The authors were able to observe the noise in films down to a thickness of 40 nm. This is a very surprising result, as we must consider that the size of avalanches roughly diminish with the sample thickness, and thus can be considerably small at such thickness. In ref. [14] the largest avalanche size detected is of the same order of magnitude ($\sim 10^{-8}$ Wb) found in ribbons (cfr. Fig. 4), while the largest duration is two orders of magnitude smaller. This means that the 83-17 NiFe film used has DWs with an extremely high mobility. In other materials, the situation cannot be so favorable. For instance, we have recently used a similar setup to detect the noise in Co-base thin films. For thickness below 1 μm , the BK signal becomes undistinguishable from the instrumental background noise, so that the measurement is practically impossible. Thus the only valid alternative is to use optical methods, based on the magneto-optical Kerr effect (MOKE), which is the change of polarization of the light reflected by a magnetic material. This technique is extensively used to investigate the domain structure of most magnetic materials [28]. There are fundamentally two variations of the basic MOKE setup applied to the investigation of the Barkhausen noise and in particular to the statistical distributions. The first was introduced by Puppini *et al.* [29], who added an optical stage to tune the laser spot size onto the film, with values ranging from 20 μm up to 700 μm . The reduction of the background noise is obtained using a photoelastic birefringence modulator working at 50 kHz, while the signal is detected with a lock-in amplifier at 100 kHz to enhance the signal-to-noise ratio. This system allowed to estimate the distribution of avalanche sizes in a Fe thin films [30, 31] (see Sec. III C).

The second solution makes use of an advanced video processing technique to directly observe the domains and their motion [32, 33]. The main instruments used are an objective of numerical aperture of 0.9 having a $\times 1000$ magnification. The domain images are obtained at the rate of 30 frames/s in real time and a spatial resolution of 400 nm [33]. In this particular setup, the external field is applied with an electromagnet up to nearly 99% of the coercive field starting from the saturation. Barkhausen jumps are thus triggered only by thermal fluctuations, so that any sweep rate effect is completely eliminated. The experiment is performed repeatedly imaging the same film area, using up to 1000 repetitions. The BK jump size is defined as the area having two end points *outside* the image; this choice raises some problems in the interpretation of the experimental data, as we will discuss later (Sec. III C).

B. Magnetic materials

Nearly all soft magnetic materials have been studied using the Barkhausen noise technique. But despite the large amount of published papers, a systematic identification of material properties appears intrinsically hard to perform, because of the large differences between the same type of material, the possible annealing procedures, etc. Up to now, the only identification of different classes of behavior (the "universality classes" deeply discussed in Sec. IV D 2) has been reported for SiFe polycrystalline ribbons with high Si content and amorphous FeCoBSi alloys [21], which show two distinctive scaling exponents ruling the Barkhausen distributions. This difference is understood in terms of a different DW dynamics, as it will be discussed extensively.

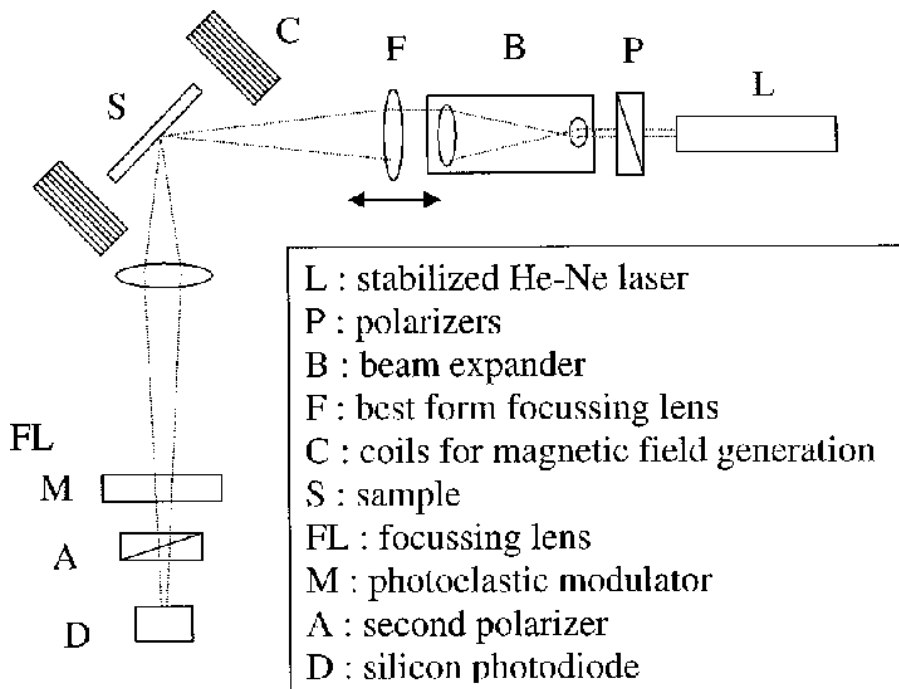


FIG. 2: The focused magneto-optical Kerr magnetometer with variable laser spot sizes used to investigate the avalanche size distributions in thin films [From [29], Fig. 1, p. 1753]

Earlier fundamental studies have been performed in frame-type single crystals to eliminate the effect of the demagnetizing field, where a single DW is present (see Ref. 34, 35, 36, 37 for 3% wt. SiFe, ref. 4 for 3.8% SiFe, Ref. 7, 38 for 4% SiFe, and Ref. 10 for 4.5% and 6.5 % SiFe). The most studied polycrystalline materials are the traditional non-oriented 3% wt. SiFe strips [15, 17, 39, 40, 41, 42], or the 1.8% ones [43], as well as the GO SiFe alloys [11, 15, 44, 45, 46, 47, 48]. Other interesting SiFe alloys are the ribbons (thickness about 50-60 μm) with high Si content (% 6.5-7) produced by planar flow casting, which reveal interesting noise characteristics [21, 49, 50]. A large attention has received also the NiFe alloys, such as the Permalloy ($\text{Ni}_{80}\text{Fe}_{20}$) and similar [12, 14, 41, 51, 52] or the Perminvar (30 % Fe, 45 % Ni, 25 % Co) [53, 54], particularly when a strong disorder is induced by precipitation of some crystalline phases.

In more recent years, many studies have been focused on amorphous materials, especially the iron-based family: some commercial ribbons, like the Metglass 2605 [18, 19, 55, 56], the Metglass 2826 [57], or the Vitrovac 6025 [25], and the vast production of various laboratories with different composition and additives [21, 48, 49, 50, 58, 59, 60, 61]. On the contrary, Co-based amorphous alloys have received a very limited attention [41], due to their high permeability values connected to the usual presence of a single large BK jump.

Despite the large variety of compositions used, we should stress here that not all the soft magnetic materials are appropriate for BK measurements. Especially, materials having very nice 'soft' properties (high permeability, small losses, etc.) show reduced or no BK noise, like the Co-base amorphous alloys or a well prepared Permalloy, with limited structural defects. In fact, the essential ingredients for a 'nice' noise are the presence of a consistent structural disorder, hindering the motion of DW, and a non-negligible demagnetizing effect, limiting the size of avalanches. Also the thickness appears to be an important factor to take into account, as it sets the limits of eddy current shielding effect. For instance, SiFe ribbons having thickness of the order of hundreds of μm , have to be magnetized at very low frequencies to detect well defined BK jumps [17, 40].

III. EXPERIMENTAL RESULTS

A. Barkhausen signal and avalanches distributions

In Fig. 3, we show some typical experimental BK data obtained in a polycrystalline Fe-Si 7.8 wt.% ribbon and in an amorphous $\text{Fe}_{64}\text{Co}_{21}\text{B}_{15}$ ribbon, the latter measured under moderate tensile stress. The different sequences, acquired during the same time interval, correspond to increasing applied field rates. At low rates, the BK signal clearly comes

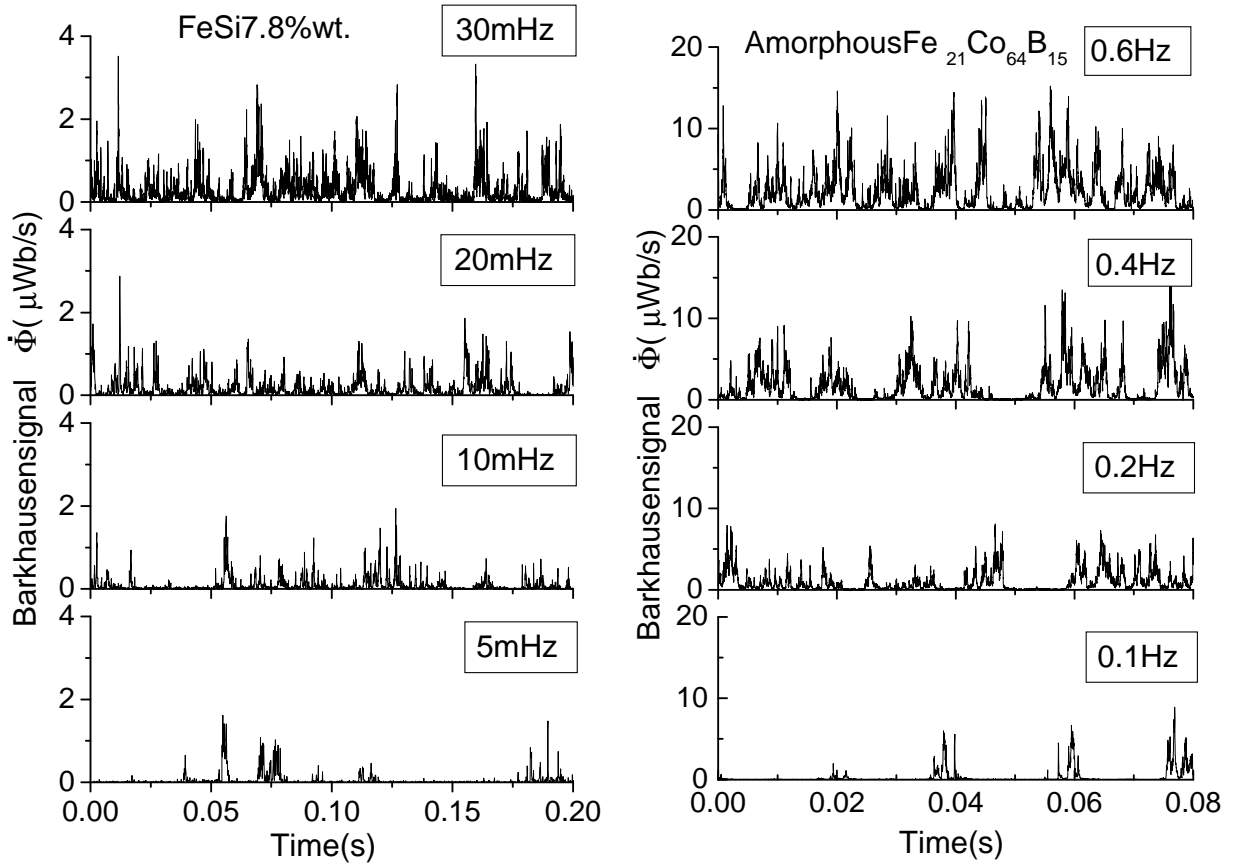


FIG. 3: Time sequences of Barkhausen noise measured in a polycrystalline FeSi 7.8 % wt. ribbon (left) and an amorphous $\text{Fe}_{21}\text{Co}_{64}\text{B}_{15}$ under moderate tensile stress (right). The labels indicate the frequency of the applied field.

out as a sequence of distinguishable and well separated avalanches: at larger rates, this separation is progressively lost and the noise resembles a continuous sequence of peaks. This feature is common to both materials, even if this similarity is only seeming, as their statistical properties are very different and appear to be representative of two types of behavior, the 'universality classes', with different DW dynamics, as we will describe in detail.

To investigate the statistical distribution of BK jumps is necessary to univocally define the size and the duration of an individual jump. This poses a delicate problem, given the self-similar fractal nature of the BK signal, and the fact that, in addition, the background noise limits the detection of smaller avalanches. The common way to solve this problem is to define a threshold, a 'resolution coefficient' [19, 23, 51, 62, 63], in order to set the temporal limits of a single avalanche. This procedure has been justified in the context of the fractal properties of the signal, as it is possible to associate to it a random Cantor dust, with a fractal dimension ≤ 1 , which can be used to calculate the critical exponents [63]. The determination of the threshold can vary, but in general we found the results are nearly insensitive to changes in its value [63], as long as it is not too small or too large. Because the BK signal amplitude v follows a power law of the type

$$P(v) = v^{-(1-c)} f(v/v_0), \quad (1)$$

where c is proportional to the driving rate, we usually assume the threshold between 5 and 15 % of v_0 .

With this definition, the duration T and the size S (the integral within the time limits) are unambiguously defined. Like the signal amplitude, also the distributions of T and S follow power laws

$$P(T) = T^{-\alpha} g(T/T_0), \quad (2)$$

and

$$P(S) = S^{-\tau} f(S/S_0), \quad (3)$$

Ref.	Material	Type	Dimensions	τ	α	$1/\sigma\nu z$	Rate dep.
[51]	81%NiFe	Wire	50cm x Φ 1 mm	1.73	2.28	1.63	Yes
[25]	Vitrovax 6025X	Ribbon	4 cm x 1 cm x 30 μ m	1.77	2.22	1.51	?
[54]	Perminvar	Strip	5 cm x 2 cm x 100 μ m	1.33	-	-	No
[64]	Annealed steel	Strip	2.5 cm x 13 cm x 840 μ m	1.24;1.27	-	-	No
[21] [65]	Fe ₆₄ Co ₂₁ B ₁₅ , Fe ₂₁ Co ₆₄ B ₁₅ amorph. (tensile stress)	Ribbon	28 cm x 1 cm x 20 μ m	1.3	1.5	\sim 1.77	No
[66]	Fe ₂₁ Co ₆₄ B ₁₅ amorph. (no stress)	Ribbon	21 cm x 1 cm x 20 μ m	1.46	1.74	1.70	No
[43]	SiFe 1.8%	Strip	20 cm x 1 cm x 180 μ m	1.5	2	-	Yes
[21]	SiFe 6.5%, SiFe 7.8%, Fe ₆₄ Co ₂₁ B ₁₅ partially cryst.	Ribbon	28 cm x 0.5 cm x 48 μ m 30 cm x 0.5 cm x 60 μ m 30 cm x 1 cm x 20 μ m	1.5	2	\sim 2	Yes

TABLE I: Experimental critical exponents reported in the literature which can be considered sufficiently accurate and reliable. Exponents τ , and α are the critical exponent of the size and duration distributions, respectively. The exponent $1/\sigma\nu z$ relates the average size of an avalanche to its duration (see text). "Rate dep." indicates if the exponents τ and α depend on the applied field rate.

where T_0 and S_0 are two cutoffs, and α and τ the critical exponents.

It is interesting to note that, despite the large number of papers regarding the BK noise, the reliable estimates of these critical exponents are very limited. We report in Tab. I the results presented in the literature we believe are sufficiently accurate to be considered and analyzed. We leave out, for instance, the results of the quite famous papers of Cote and Meisel [18, 19], who first suggested the BK exhibits self-organized criticality [20], because they are based on a very poor statistics. At first sight, the measured exponents span a quite large range of values, and no general behavior can be easily guessed. But it is worth to consider in detail each experiment analyzing the particular conditions of the material and of the measurement to find a possible explanation for this large variability. In particular, two key factors appear to affect the results, and should thus be carefully checked: the applied field rate dependence of the critical exponents, and if the data are taken in a small bin around the coercive field or along all the hysteresis loop. After this warning, we proceed to analyze the literature results in more detail:

1. The 81%NiFe used in Ref. 51 is the only wire which has been measured accurately. The authors use 3 different samples with different annealing conditions, but do not report any indication about the structural characteristic of the materials. They also did notice a dependence of the statistics on the applied field rate, but to simplify matter, they made the measurements at the same *magnetization rate*, which later has been established to be the correct parameter to take into account [16, 17]. As it is not explicitly mentioned, the noise has been probably recorded along all the hysteresis loop and it is thus likely that it is not statistically stationary.
2. Similar critical exponents have been reported by Spasojević *et al.* [25], with a completely different material. As mentioned in Sec. II A, this experiment has some serious drawbacks due to the large extension of the pickup coil in respect the sample length, which have been shown to affect the size distributions [6]. The data are taken in a small field interval, presumably around the coercive field, but it is not clear from the paper if the applied field is large enough to saturate the material. The rate dependence of the critical exponents has not been discussed.
3. The Perminvar used in [54] has been subjected to an annealing at 450 °C for 24 h. This prolonged treatment has the effect to induce the precipitation of micro-crystalline phases, which create a large number of strong pinning centers for the DW, resulting in a low permeability of about 250. The estimation of the critical exponent is limited to the size exponent τ , but it is made with high accuracy.
4. A comparable size critical exponent has been measured for a sheet of interstitial-free, low-carbon, annealed steel [64]. The external field is applied both parallel and perpendicular to the rolling direction. The corresponding hysteresis loops show a different permeability, which affects the value of the cutoff S_0 , and slightly the critical exponent τ . As matter of fact, the estimation at the lowest permeability (smaller S_0) appear much less accurate, due to the limited region of the power law dependence.
5. Ref. [43] reports the first estimation of the critical exponents in a polycrystalline SiFe strips (1.8 % wt.). Within the experimental errors, the critical exponents show a linear dependence on the applied field rate, expressed by $\alpha = 2 - c$, and $\tau = 1.5 - c/2$, where c is the parameter comparing in Eq. 1.

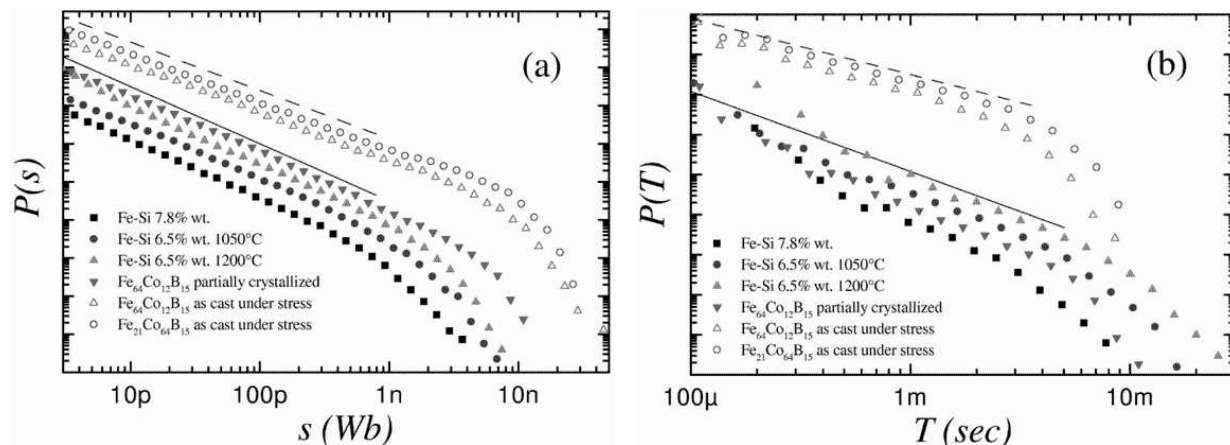


FIG. 4: (Left) Distributions of Barkhausen jump sizes measured in different materials. The solid line has a slope $\tau \sim 1.5$ while for the dashed one $\tau \sim 1.27$. (Right) Similar plot for duration distributions. The solid line has a slope $\alpha \sim 2$, while for the dashed one $\alpha \sim 1.5$. [From [21], Fig. 1, p. 4706]

- In Ref. 21, we have reported measurements of the critical exponents in polycrystalline SiFe ribbons (with high Si contents) and amorphous alloys with composition $\text{Fe}_x\text{Co}_{85-x}\text{B}_{15}$. We also measured a partially crystallized $\text{Fe}_{64}\text{Co}_{21}\text{B}_{15}$, obtained after annealing for 30 min at 350 °C and then for 4h at 300 °C under an applied tensile stress of 500 MPa. This induces the formation of α -Fe crystals of about 50 nm, with a crystal fraction of $\sim 5\%$ [67]. The SiFe alloys and the partially crystallized alloy show $\tau \sim 1.5$ and $\alpha \sim 2$, measured at the lowest possible frequency $f = 3\text{-}5$ mHz (see Fig. 4-left). They also show a linear dependence on the applied field rate, as shown in Fig. 5-left [43, 63]. The highly magnetostrictive $\text{Fe}_x\text{Co}_{85-x}\text{B}_{15}$ alloys ($\lambda_s \sim 30 - 50 \times 10^{-6}$) have been measured under a tensile stress of $\sigma \sim 100$ MPa. The applied stress is found to enhance the signal-noise ratio, reducing biases in the distributions, but does not change the exponents [68], as long a small stress is applied (see below). These alloys yield $\tau \sim 1.27$ and $\alpha \sim 1.5$ (Fig. 4- right), independent of the applied field rate, as shown in Fig. 5-right. In contrast, the shape of the cutoff changes drastically as the rate increases.
- The authors of Ref. 66 used the same type of amorphous alloy of Ref. 21, but without the application of a tensile stress. The resulting critical exponents are larger, and the authors have no a simple explanation of the difference. As they claimed, the residual stress may be the origin of the anomaly. We can confirm that unstressed amorphous materials have in general hysteresis loops with restricted regions of linear permeability, thus the determination of the exponents can be difficult and less accurate.

In Tab. I we also report the values of another critical exponent $1/\sigma\nu z$ relating the average size $\langle S \rangle$ to the duration T as $\langle S \rangle \sim T^{1/\sigma\nu z}$. This exponent has been shown to be in strict relation with the power spectrum exponent. (see Secs. III B and V A).

To understand the origin of the variability of the critical exponents is important to first focus on the values which has been found to be close in different samples and experiments. In addition, it is better to consider the data recorded in a small bin around the coercive field, that can thus be considered as stationary. Two sets of exponents emerges: one is measured in polycrystalline alloys or with embedded grains, characterized by $\tau \approx 1.5$, and $\alpha \approx 2$, with a linear dependence on the applied field rate. The other is measured in materials where the crystalline matrix is absent (amorphous samples under tensile stress) or progressively lost by induction of a strong disorder (like in the Perminvar of Ref. [54]). They show $\tau \approx 1.3$, and $\alpha \approx 1.5$, and no rate dependence is found. These results support the idea that there are (at least) two kinds of behavior, the *universality classes*, to which correspond different sets of critical exponents. We will come back to this matter in more detail in Sec. V A, where we will also try to explain the occurrence of the other experimental exponents.

Given the variability of the number shown above, it is quite clear that the sole comparison of the values of the exponents τ and α can be misleading. In other words, it necessary to determine other experimental critical exponents which can confirm the existence of the two universality class. In this respect, an important suggestion has been given by Perković *et al.*, who pointed out that "an explanation for the experiment must involve collective motion of many domains; it must provide an explanation for the power-law scaling regions, *an it must provide an explanation for the cutoff* [From [69], pg. 4528]. We have already stressed the importance of the demagnetizing effect in the DW dynamics, so that we investigated in detail the effect of the change of the demagnetizing factor k on the power-

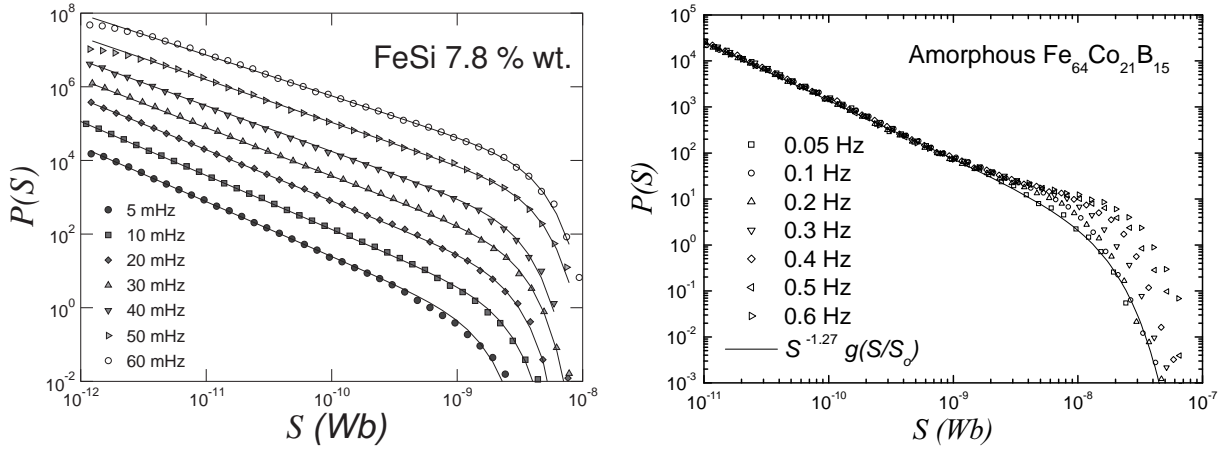


FIG. 5: Distributions of the avalanche sizes S for the polycrystalline SiFe (left) and the amorphous (right) material at different applied field frequencies. In the polycrystalline sample, the critical exponent τ varies linearly with the frequency [43, 63] between 1.5 and 1.15, while it is independent in the amorphous one $\tau \sim 1.27$.

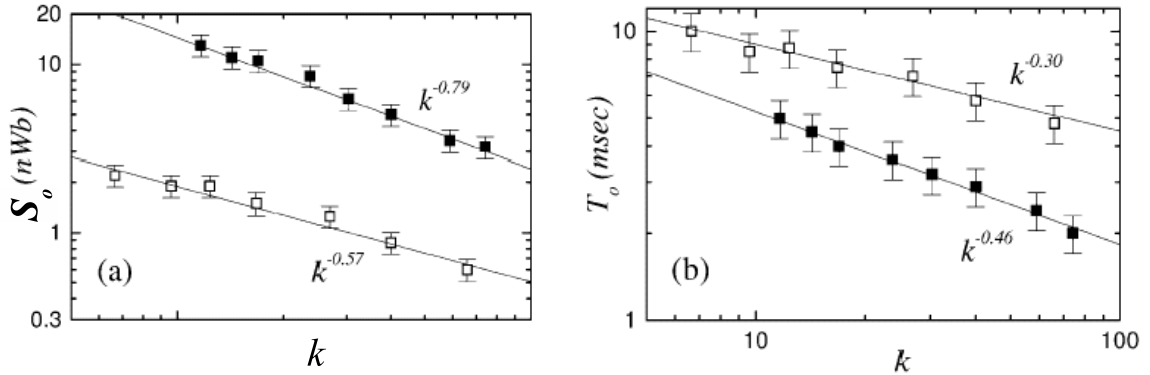


FIG. 6: The cutoff of the Barkhausen size (a) and duration (b) distributions as a function of the demagnetizing factor k in Fe-Si 6.5 wt% alloy (empty symbols) and an amorphous $\text{Fe}_{21}\text{Co}_{64}\text{B}_{15}$ sample under constant tensile stress (filled symbols).

law distributions. We used two samples belonging to the different universality classes, and measured the avalanche distributions, progressively cut the samples to change the apparent permeability μ_{app} , and thus calculate the factor k using the well known expression $\mu_{app} = \mu/(1 + k\mu)$, with μ the intrinsic permeability. We verified that the cutoffs S_0 and T_0 strongly depend on k , as in Fig. 6, and follow the scaling relations $S_0 \sim k^{-1/\sigma_k}$, and $T_0 \sim k^{-\Delta_k}$. Best fit estimation of the exponents gives $1/\sigma_k \sim 0.57$, $\Delta_k \sim 0.30$ for the polycrystalline class, and $1/\sigma_k \sim 0.79$, $\Delta_k \sim 0.46$ for the amorphous one.

B. Power spectra and avalanche shapes

If we merely count the huge number of papers in the literature concerning the spectral properties of the BK noise, the contrast with those considering scaling exponents results clearly. Since the earlier papers, but especially during the 70s-80s, almost all the authors publishing about the BK effect considered the problem of the detection and explanation of the power spectrum. The main reason for this abundant production is related to the practical need to reduce the spectral noise in applications where soft materials are used. In addition, it seemed easy to explain all the details the power spectral shape in terms of a superposition of 'elementary' Barkhausen jumps (see for instance [9]). These elementary units were generally defined *a priori*, for instance, as exponential or square events: a proper superposition of these independent jumps can give practically any measured power spectrum shape. Even if successful to give a general description of the power spectrum shape, this approach was not able to account for the microscopic magnetization

events and the details of the DW dynamics, so it really did not represent a significant step towards the fundamental understanding of the BK noise. Remarkably, after the publication of the two seminal papers by Alessandro *et al.* [16, 17], introducing the ABBM model (Sec. IV B), the investigation of the power spectrum apparently lost interest, even though the problem remained basically a puzzle. Only recently the subject, seen under a completely new point of view, received a new impulse.

As it should be clear from the discussion in the preceding sections, the detection of stationary or non-stationary Barkhausen signals has a strong effect also on the estimation of spectral properties. More precisely, traditional power spectral calculations using FFT must be applied only to stationary data, otherwise they can give unpredictable results. A non-constant value of the permeability, for instance, introduces low frequency components unrelated to the BK noise. Thus we must consider only two types of spectral estimation: i) those taken *with a single DW at constant velocity*, as in [10, 36, 57, 70], where a feedback setup keeps the flux rate constant, and ii) those taken in a small bin around the coercive field, as first performed in [14, 15].

Measurements of power spectrum of type (i) are particularly important. In fact, not only they are a measure of the time correlation of the BK signal (in the frequency domain), but more they are a measurement of the spatial fluctuation of local fields which are needed to unpin the DW. In other words, these measurements describe the spatial spectrum of the random pinning field (see Sec. IV B). Measurements on single crystal of SiFe give a f^{-2} power spectrum, and thus a k^{-2} spectrum of the pinning field [10, 36], because of the linear relation between f and k at constant v . It is curious to note that measurements on a toroidal Metglass sample gave a $k^{-1.7}$ spectrum [57]. Even if a single measurement cannot be taken as conclusive, this result can be regarded as a manifestation of a different universality class, similar to what reported for the avalanche critical exponents.

As anticipated, the most accurate report of power spectra in a polycrystalline material has been presented in Ref. [17]. A strip of non-oriented 3% SiFe, having a grain size of about 100 μm is measured under a small tensile stress (~ 5 MPa), and at variable apparent permeability obtained varying the air gap with a mumetal yoke (see Fig. 1). The effect of the grain size on similar materials is reported in Ref. [71]. Successively, a few other papers have reported the power spectra of single crystal and polycrystalline SiFe materials [72], as well as of amorphous materials [59, 73].

There some general common characteristics that can be summarized as follows:

1. The spectrum $F(\omega)$ has a typical $1/f^\vartheta$ shape at high frequency, with $\vartheta = 1.7 \div 2$, and scales linearly with the average magnetization rate \dot{I} , so that the spectra normalized with the average flux $F(\omega)/S\dot{I}$ coincide at high frequency (Fig. 7);
2. At lower frequency, the spectrum shows a marked peek at a frequency roughly proportional to $\dot{I}^{1/2}$, with an amplitude which takes a constant value at low rates, as shown in Fig. 7. This amplitude roughly scales with the permeability, as $\mu^{1.5}$ [17];
3. At frequencies lower than the peek, the spectrum scales as f^ψ , with $\psi \sim 0.6$, or ~ 1 .

These general features describe only qualitatively the observed results. More precisely, there are at least four different typical shapes, as shown in Figs. 8-9.

Single crystal and polycrystalline SiFe strips show the simplest power spectrum, with $\vartheta \sim 2$, and $\psi \sim 0.6$. The polycrystalline SiFe ribbons at high Si content keep the same exponents, but present a large region at intermediate frequencies where the spectrum strongly deviates from the simple $1/f^2$ law. Amorphous materials under tensile stress show instead $\vartheta = 1.7 \div 1.8$, and $\psi \sim 1$, as shown in Fig. 9. Similar data are found in the unstressed case, $\vartheta = 1.73 \pm 0.08$ and $\psi \sim 1$, for the same amorphous alloy [66] (private communication). Amorphous materials, where a proper annealing induces a partial crystallization, show a sort of intermediate case: the high frequency part is more similar to the polycrystalline SiFe samples with $\vartheta \sim 2$, while $\psi \sim 1$ keeps the values of a pure amorphous material. The former property is not a merely coincidence, as we observed a corresponding change in the critical exponents of size and duration distributions towards the values measured in SiFe, as shown in Tab. I. Curiously, all the spectra, despite these differences, show the same dependence of the peek frequency on $\dot{I}^{1/2}$.

The interpretation of all these complicated details still represents a challenging puzzle, although some progress has been recently made [65, 74]. Earlier estimates of the exponent ϑ ([51], and similarly in [25, 69, 75]) led to the conclusion that "the asymptotic decay of the spectrum is not given by the shape of the pulses, but is exclusively determined by the distribution of the pulse duration and the correlation between the size and the duration" [Adapted from [51], pg. 15]. In our notation, $\vartheta = 1 + 2\sigma\nu z - \alpha$, or analogously $(3 - \tau)/\sigma\nu z$ (see also Sec. V B). Using the data of Tab. I, this implies $\vartheta \sim 3$, much larger than the experiments. This result was successively found to be valid only for $\tau > 2$, while for $\tau < 2$, Kuntz and Sethna [74] calculated $\vartheta = 1/\sigma\nu z$, which is the same critical exponent relating the average avalanche size to the duration (Tab. I). This prediction agrees pretty well with the experiments, as we can see in Fig. 10. In particular, it works for the amorphous material in an extended frequency range; the same is

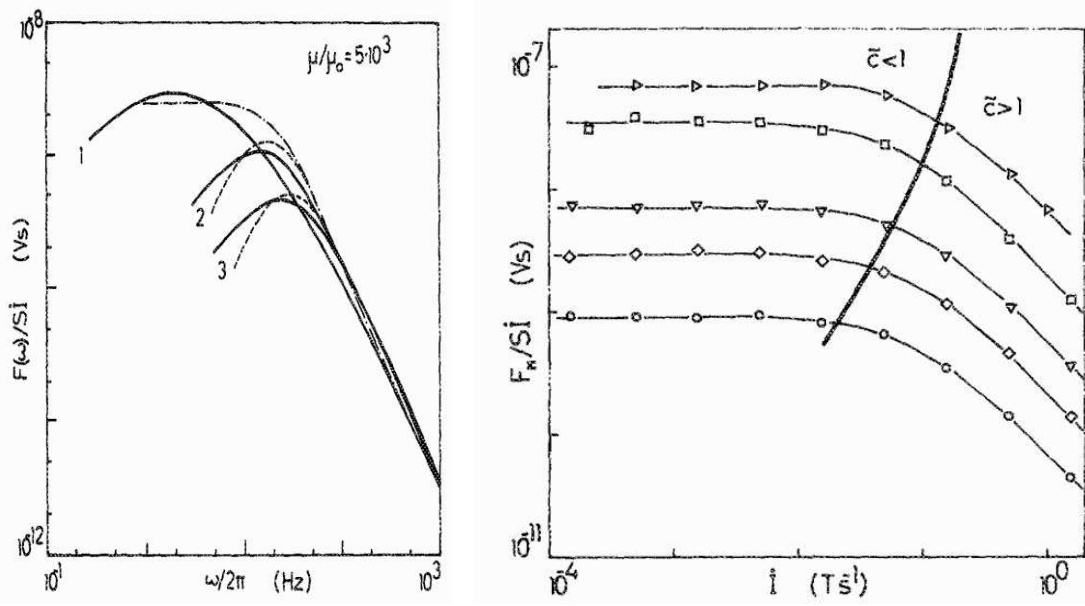


FIG. 7: (Left) Normalized power spectra $F(\omega)/SI$ at fixed permeability of a polycrystalline 3% SiFe strip. The solid lines are the experimental results while the dotted lines are the prediction of the ABBM model (Sec. IV B); (right) Normalized maximum of the power spectra F_M/SI for permeability ranging from 2500 (o) up to 60,000 (\triangleright). Continuous lines are guide to eyes only. The bold line is the boundary between the intermittent ($\bar{c} < 1$) and the continuous ($\bar{c} > 1$) DW motion. Here \bar{c} is equivalent of the exponent c of eq. 1. [From Ref. [17], figs. 7 and 10, pg. 2912-2913]

not valid for the polycrystalline SiFe ribbon, and the reason will be discussed after introducing the hypothesis at the base of the calculations by Kuntz and Sethna.

1. Avalanche shapes

The simple result $\vartheta = 1/\sigma\nu z$ obtained by Kuntz and Sethna [74] is based on the existence of a certain number of scaling relations and on a few hypothesis, like the complete separation of the avalanches in time. We leave the discussion of these important aspects to a further section (see Sec. V B), focusing here on the new proposed scaling relations which can be tested experimentally. These relations involve universal scaling functions whose *shape* could provide a critical test for model, as "a sharper tool for discriminating between different universality classes than critical exponents" [66, 76].

The first relation states that the average avalanche shape scales in a universal way so that

$$v(t, T) = T^{1/\sigma\nu z - 1} f_{shape}(t/T), \quad (4)$$

where v is the BK signal, t is the time and $f_{shape}(t/T)$ is the universal scaling function. Similar to this relation, we can consider the voltage as a function of magnetization $s = \int_0^T v dt$ to get

$$v(s, S) = S^{1-\sigma\nu z} g_{shape}(s/S) \quad (5)$$

A third relation deals with the fluctuations of avalanche sizes, and considers the probability $P(v|S)$ that a voltage v occurs in an avalanche of size S . This probability scales as:

$$P(v|S) = v^{-1} f_{voltage}(vS^{\sigma\nu z - 1}) \quad (6)$$

and, again, $f_{voltage}$ is another universal scaling function.

A partial experimental verification of these relations has been reported in a couple of papers [65, 66]. In Fig. 11, we show the complete universal scaling laws of Eqs. 4 and 5 for the same 7.8 % SiFe ribbon and the amorphous sample of Fig. 3, scaled using the theoretical estimation of the critical exponent $\sigma\nu z$. The experimental data are compared

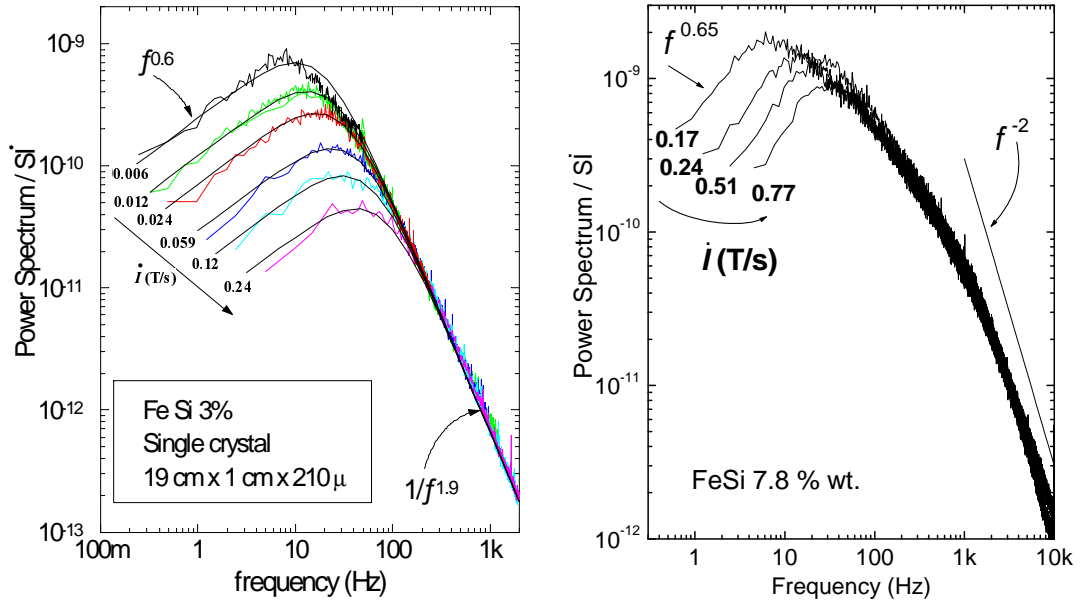


FIG. 8: Normalized power spectra of a single crystal 3% SiFe strip (left, reproduced from [72], Fig. 3, pg. 580), and a polycrystalline 7.8 % SiFe ribbon (right) as a function of the magnetization rate \dot{I} .

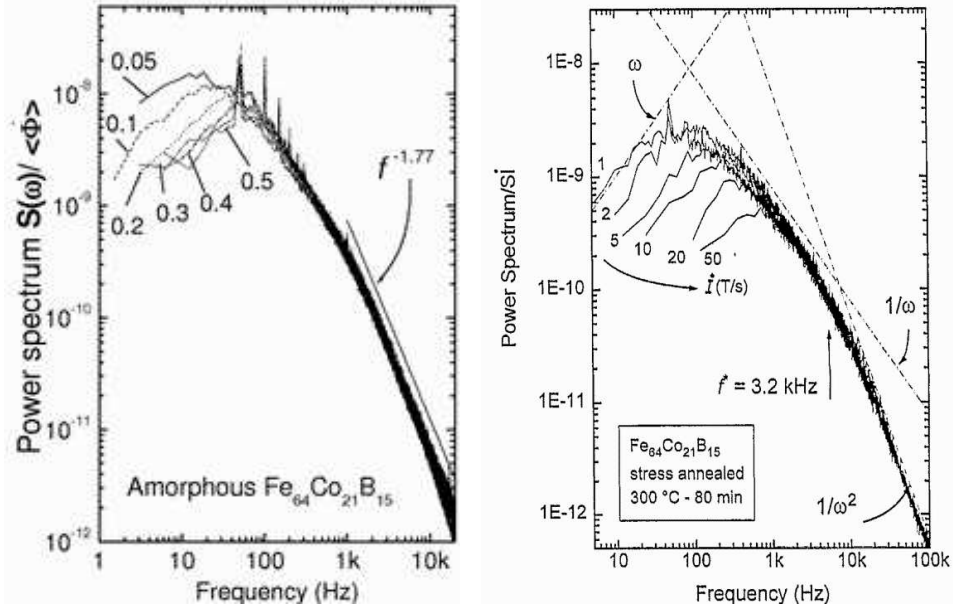


FIG. 9: Normalized power spectra of the same amorphous material of Fig. 5 (left), and of a partially crystallized (16%) sample induced by annealing (right, reproduced from [59], Fig. 2, pg. 300) as a function of the magnetization rate \dot{I} . In the left Fig., f^* is roughly the frequency where the shape changes from f^{-1} to f^{-2} .

with the theoretical average shape predicted using the ABBM model (see Eqs. 101-102). In the case of the amorphous material, the scaling is pretty good, except for the magnetization signal at small sizes. In particular, both time signals show a marked time asymmetry, similar to what found in [25] where the average of avalanches is made without any scaling. The asymmetry is also visible in the magnetization signal, even if less marked. Here, the shape calculated using the ABBM (see Eq. 102 and Sec. V C) reproduces pretty well the experiments, except for the small sizes in the amorphous material. It is interesting to note that all the models presented in the literature predict symmetric time

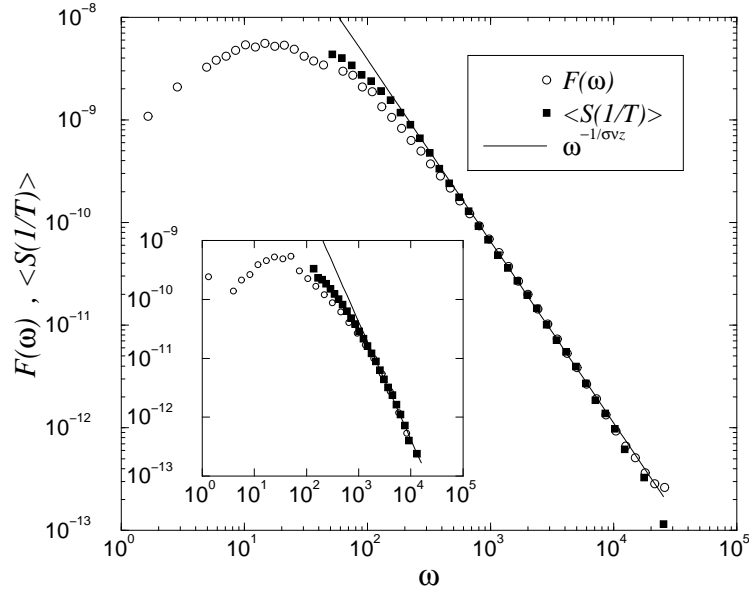


FIG. 10: Comparison of the power spectrum $F(\omega)$ with the average size $\langle S \rangle$ as a function of the inverse of duration T , for the amorphous material and the polycrystalline SiFe ribbon (7.8 %, inset) of Fig. 4. The theoretical prediction of Ref. [74] is also shown, with $1/\sigma\nu z$ equal to 1.77 and 2 [From [65], fig. 1, pg. 1086]

and magnetization signals. In Sec. V C, we will discuss the relevance of the shape of the scaling function as indicator of universality class.

The scaling of time signal data of 7.8 % SiFe ribbon using the theoretical exponent $1/\sigma\nu z = 2$ is clearly incorrect. The reason is illustrated in Fig. 12, where we plot the average avalanche size $\langle S \rangle$ as a function of duration T . The exponent $1/\sigma\nu z$ (the slope of the curve in the log-log plot) slightly varies from ~ 2 down to about 1.75. If we use this 'variable' exponent $1/\sigma\nu z^*$, the rescaling of the time signal is highly satisfying.

The third universal scaling function (Eq. 6) has been reported in [65] for an amorphous material, as shown in Fig. 13. This confirms the validity of scaling relations proposed in [74], at least for the amorphous material. In fact, the relation in Eq. 6 does not hold so well for the 7.8 % SiFe ribbon.

2. High order power spectra

In Ref. [55], O'Brien and Weissman introduced a further statistical characterization of BK signal calculating power spectra of order higher than those shown in the previous section. This analysis is motivated by the possibility to prove the BK as a real example of SOC [20], lacking of any inertial effect unlike, for instance, grain falling in sandpiles. In fact, the mere "existence of pulses with a range of sizes and durations should not be taken as conclusive evidence for SOC" [From [55], pg. 3446]. Thus it is important to understand if the observed scaling properties reflect a real self-organization involving "cooperative avalanche processes invoked by SOC", or simply reflect the scaling properties of the pinning field, or, alternatively, the vague proximity of a disorder-driven critical transition [69].

The high order spectra involve correlations between different temporal scales, so for instance, could clarify if events on a certain scale systematically precede event on another scale, as in the case of systems showing precursors such as earthquakes. Another important aspect, more specific of BK noise, is the possibility to distinguish whether the high frequency spectrum $1/f^\theta$ primarily comes from short independent pulses, as often assumed, or conversely from the fine structure of longer pulses [73]. This is addressed considering the 1.5 power spectrum $S_{1.5}(f_2, f_1)$, involving a third moment of time signal $v(t)$, defined as:

$$S_{1.5}(f_2, f_1) = \frac{F\{v(t)\}F\{H(t, f_1)\}^*}{\langle H(t, f_1) \rangle} \quad (7)$$

where $H(t, f_1)$ is the time-dependent Haar power at the frequency f_1 , $F\{\cdot\}$ is the usual Fourier transform those

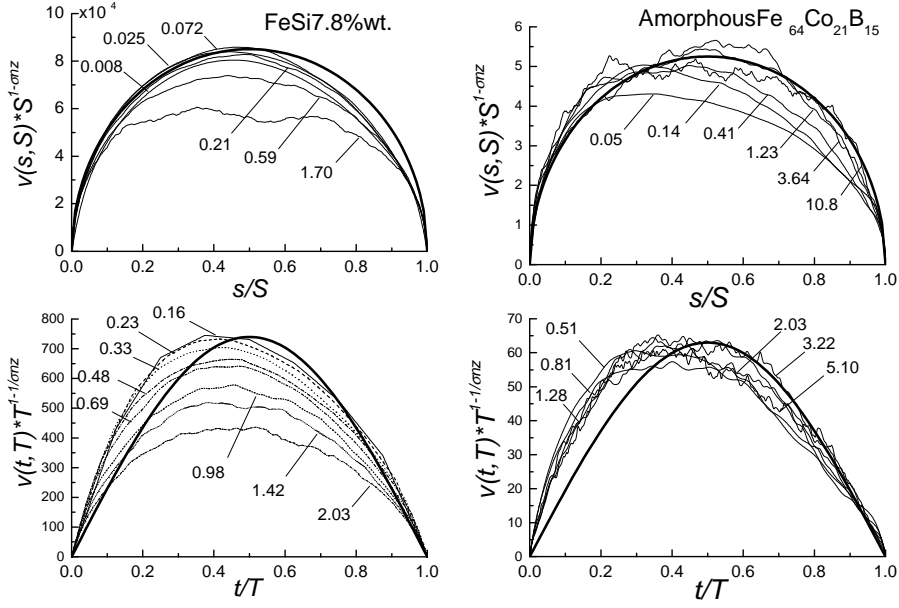


FIG. 11: Average avalanche shapes for the 7.8 % SiFe ribbon (left) and the amorphous sample (right) of Fig. 3. Time signal $v(t, T)$ and magnetization signal $v(s, S)$ are scaled according to Eqs. 4-5. Bold lines are the theoretical predictions of Eqs. 101-102, a semicircle and an arc of sinusoid, respectively (see Sec. V C). Numbers in the graphs denote avalanche size (in nWb, upper figures) and duration (in milliseconds, lower figures).

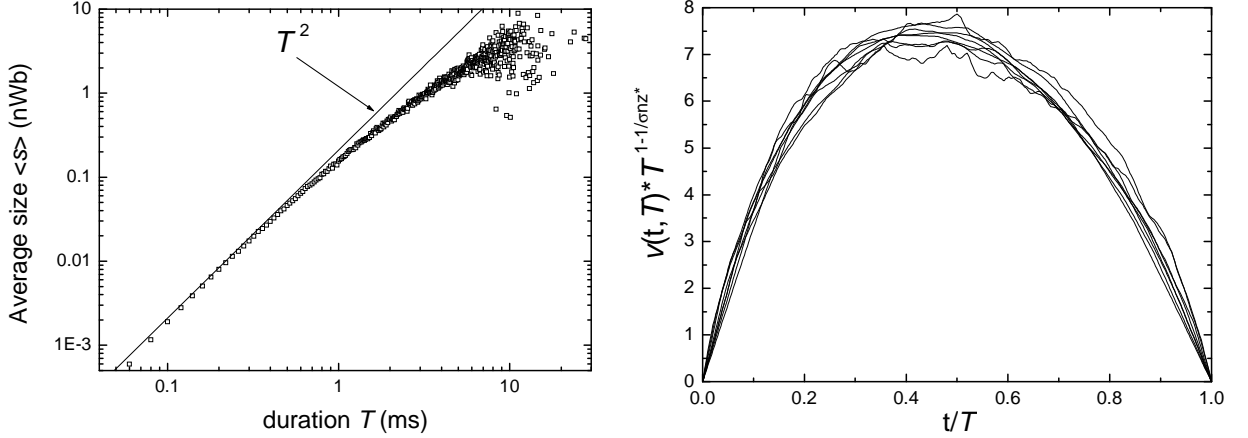


FIG. 12: Average avalanche size as a function of the duration for the 7.8 % SiFe ribbon (left). Time signals are rescaled as in Eq. 4 using a variable exponent $1/\sigma v z^*$, deduced by the plot on the left.

components are calculated at frequency f_2 [73]. Similarly, the second spectrum $S_2(f_2, f_1)$ is defined as:

$$S_2(f_2, f_1) = \frac{F\{H(t, f_1)\}F\{H(t, f_1)\}^*}{\langle H(t, f_1) \rangle^2} \quad (8)$$

A complete presentation of these spectra have been reported in Ref. [73] for a $\text{Fe}_{21}\text{Co}_{64}\text{B}_{15}$ amorphous ribbon (in the unstressed state). In Fig. 14 we show the 1.5 power spectrum. The weak independence of $\text{Re}\{S_{1.5}(f_2, f_1)\}$ on f_1 indicates that the high frequency spectrum $1/f^\nu$ contains a large contribution from pulses with duration much longer than $1/f_1$. This definitely demonstrates that, in this case, the power spectrum does not come from independent short pulses. The imaginary part, instead, is sensitive to the asymmetry of the time signal. The positive sign of $\text{Im}\{S_{1.5}(f_2, f_1)\}/\text{Re}\{S_{1.5}(f_2, f_1)\}$ suggests that, on average, high frequency components precede the low frequency ones. This is in accord with the time asymmetry of the average avalanche shape of Fig. 11.

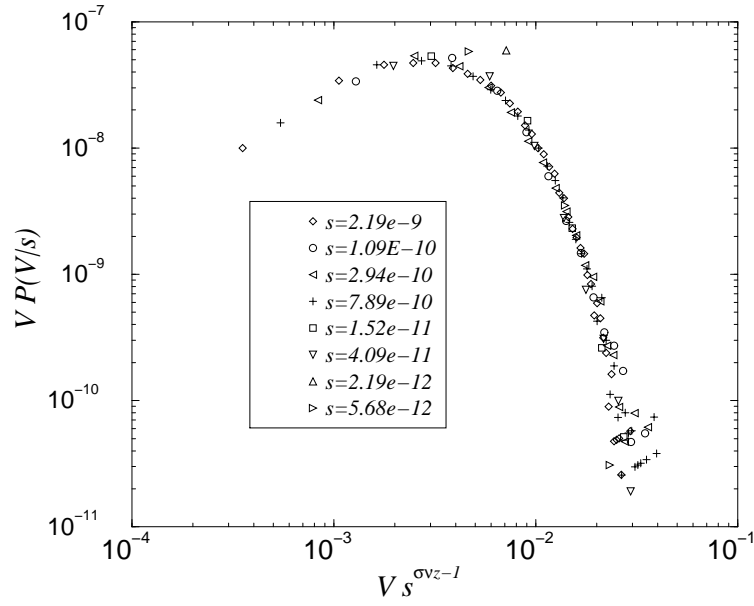


FIG. 13: Distribution of time signal at fixed size as predicted by Eq. 6 for the amorphous material using the theoretical scaling exponent $1/\sigma\nu z = 1.77$. [From [65], Fig. 3, pg. 1087]

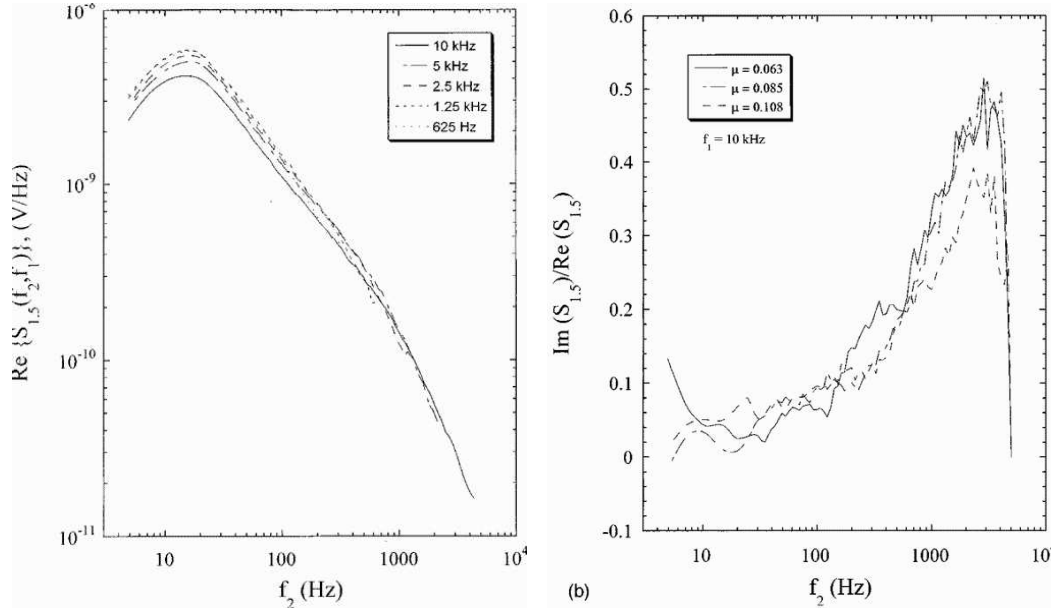


FIG. 14: The 1.5 power spectrum defined in Eq. 7 for a $\text{Fe}_{21}\text{Co}_{64}\text{B}_{15}$ amorphous ribbon in the unstressed state, at 5 different frequencies f_1 . [From [73], figs. 6 and 9, pg. 6366-6367]

Interestingly, high order power spectra of 1.8 % SiFe single crystals have a completely different behavior [77], as shown in Fig. 15. Here $S_2(f_2, f_1)$ is nearly flat as a function of f_2 and falls off as $f_1^{-1.2}$, which indicates that most of the power at f_1 comes from separated pulses of duration $1/f_1$. The 1.5 power spectrum confirms this hypothesis, as it strongly depends on f_1 , in contrast with the weak dependence in the amorphous ribbon. In this case, it is appropriate to assume the power spectrum as a superposition of individual independent pulses.

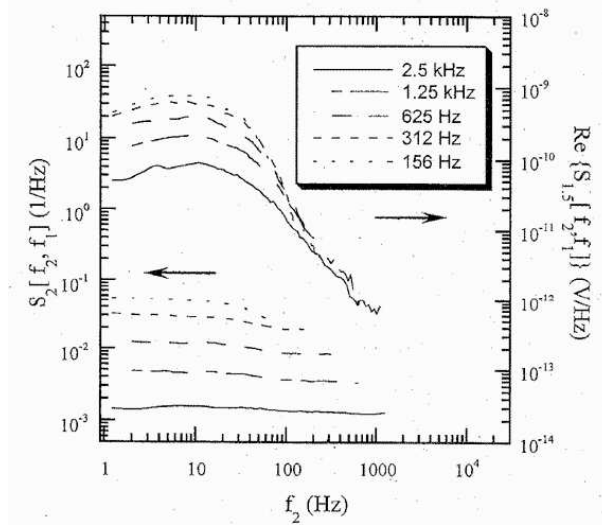


FIG. 15: Second spectra S_2 and 1.5 power spectra $S_{1.5}$ for a 1.8 % SiFe single crystal [From [77], Fig. 3, pg. 1172].

C. Thin films

All the results presented so far are related to materials which are essentially three-dimensional, with the sole exception of the wire reported in Ref. 51 (see Tab. I). The behavior of the BK noise in 2D thin films is much less known, and the number of papers reporting a complete set of experimental results is very limited [14, 23, 27, 30, 32]. Many questions remain to be solved, both on the experimental and the theoretical side, so that the topic represents an interesting and promising field of study for the near future.

Contrary to bulk three dimensional systems with a relatively simple magnetic structure of nearly parallel DWs, thin films show richer and often more complicated DW patterns. The film thickness plays a fundamental role because of the increasing importance of stray fields in the direction perpendicular to the sample, as first pointed out by Néel [78]. In addition to usual Bloch DWs, other different types exist, such as symmetric and non-symmetric Néel walls, and the cross-tie walls, a complicated pattern of 90° Néel walls. A complete description of the existing configurations together with many experimental images can be found in the excellent book of Hubert and Schäfer [28]. To have an idea of the complexity, it is worth reporting their very words about the role of film thickness: "The typical DW in very thin films, i.e. the symmetric Néel wall, needs basically a one-dimensional description of its magnetization structure. The stray field of this wall reaches out into the space above and below the film, however, and cannot be treated one-dimensionally. Cross-tie walls in thin films need at least a two-dimensional description for the magnetization and a three-dimensional treatment of the stray field. Bloch walls in thick films and their relatives are two-dimensional both in the magnetization and in the stray field. Most complex are cross-tie walls in thicker films (100 nm for Permalloy), which need a three-dimensional description of both magnetization and field and which have never been analysed theoretically up to now" [From Ref. [28], pg. 241].

It is clear that the experimental BK data can be understood only through a precise knowledge of the active DWs, and their role in the magnetization process. Considering that the present research is still at a preliminary stage, the task will surely require some time to be fulfilled. Nevertheless, it is worth to discuss in detail the main results presented in the literature. A quite impressive work has been done in the Ph.D thesis of N.J. Wiegman in 1979 [23], who explored the properties of Permalloy thin films using an inductive setup. A selected number of results had been previously reported in a couple of papers [14, 27].

The simple visual comparison of a typical noise data of Permalloy films with those of SiFe or amorphous samples (see Fig. 3) reveals striking differences. As shown in Fig. 16, the BK avalanches appear as sharp peaks, well separated in time, with nearly no inner structure. This behavior is confirmed by the data of the size and duration distributions, where the maximum duration is nearly two orders of magnitude less than the corresponding value in ribbons, as noted before, while the same does not occur for the maximum size. In other words, the avalanches in these films are rather sharp peaks of short duration, reversing a magnetization volume comparable to the value observed in ribbons. The behavior of the critical exponents τ (α_1 in Wiegman's notation) and α (δ_1), shown in Fig. 17, as a function of the film thickness is quite intriguing. The exponents do not show any strong thickness dependence, except for the increasing fluctuations below 100 nm, which, by the way, is the region where complex cross-tie walls are observed. In the same

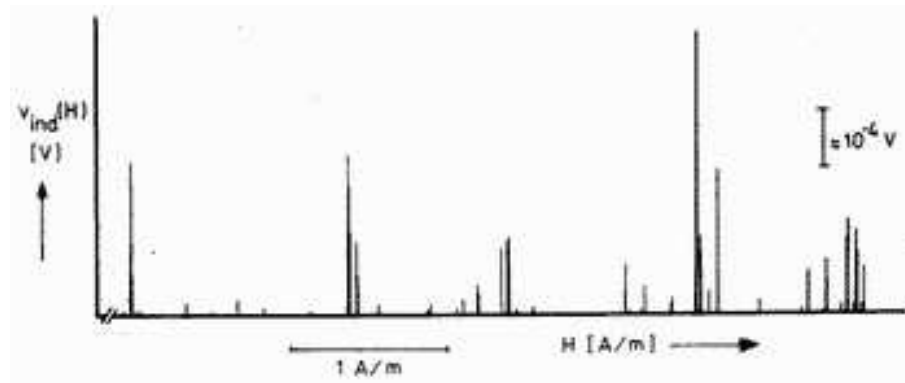


FIG. 16: A typical time signal for a permalloy thin film [From [23], Fig. 3.2, pg. 44].

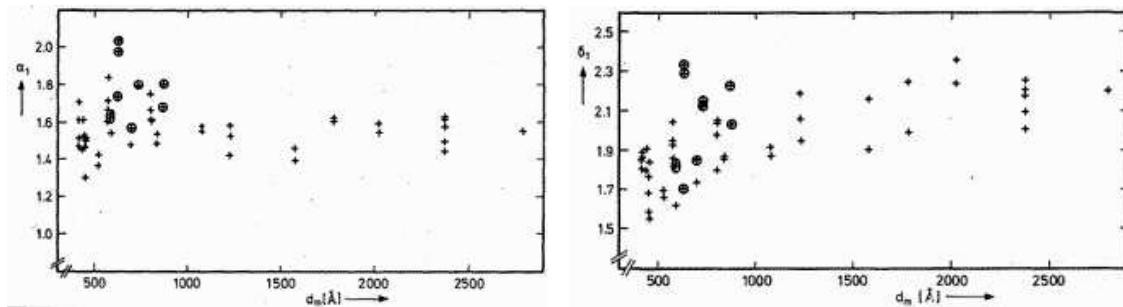


FIG. 17: Values of the critical exponents τ (α_1 in Wiegman's notation, left) and α (δ_1 , right) for permalloy films as a function of the thickness. [From [23], Figs. 3.10 and 3.14, pg. 57;62]

region, the critical exponent $1/\sigma\nu z$ (χ) displays a sharp transition of from 2 to 1.5, as clearly shown in Fig. 18.

These interesting results should be considered as the basis for further investigations. In fact, the critical exponents have the same values observed in polycrystalline ribbons ($\tau \sim 1.5$, $\alpha \sim 2$, $1/\sigma\nu z \sim 2$) for thicknesses down to 100 nm, suggesting a typical three-dimensional behavior with predominant long-range interactions. The situation at smaller thicknesses is more complicated and the role of DW pattern, such as cross-tie walls, is not clear. While an accurate estimate of the critical exponents is desirable, it is also necessary to perform an extended scaling analysis,

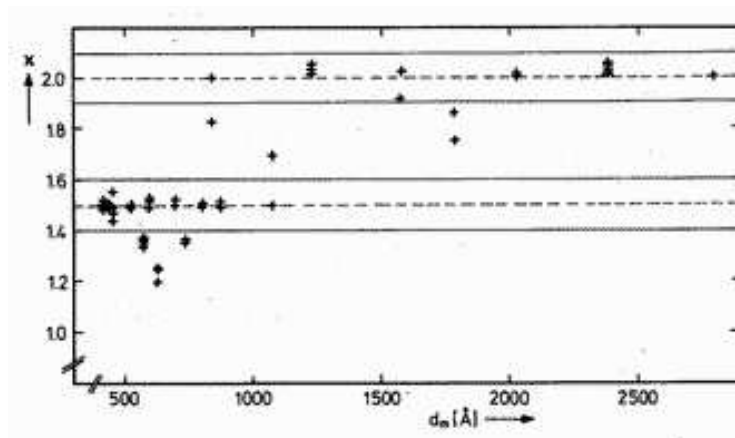


FIG. 18: The critical exponent $1/\sigma\nu z$ (χ in Wiegman's notation) for permalloy films as a function of the thickness. [From [23], Fig. 3.7, pg. 53].

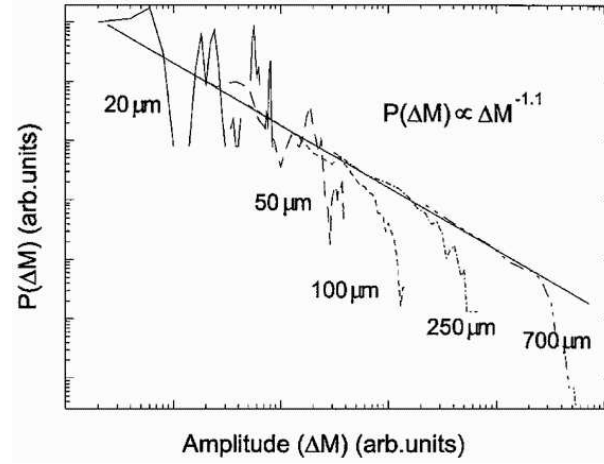


FIG. 19: Distribution of magnetization steps ΔM in a 90 nm Fe film. Data taken at different laser spots are properly rescaled to show a single distribution [From [30], Fig. 5, pg. 5418].

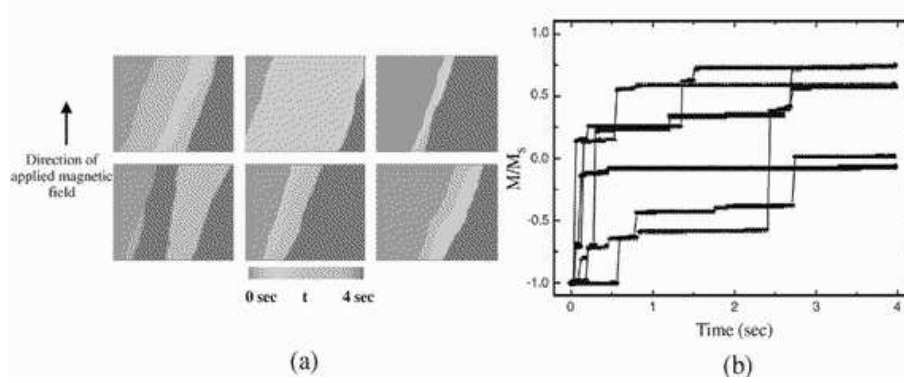


FIG. 20: (a) Domain images of same $400 \times 320 \mu\text{m}^2$ area for a 25-nm Co film between 0 and 4 sec. The sample was saturated downward first, and then a constant field was applied upward, denoted by the solid arrow, during observation. (b) Magnetization reversal curves obtained from the corresponding domain patterns of (a) [From [32], Fig. 2, pg. 087203-2].

not restricted to a single exponent (i.e. τ as in most recent studies).

In Ref. [30], the critical exponent τ is estimated in a Fe film of 90 nm using the MOKE setup (Sec. II A), and considering different laser spot sizes from 20 to $700 \mu\text{m}$. A single distribution $P(\Delta M)$ is obtained properly rescaling the size of the avalanche ΔM and the distribution P , as shown in Fig. 19. Unfortunately, data at small spot sizes are not averaged over different positions, so that the overall distribution appears quite unreliable under $100 \mu\text{m}$. Given that, the estimated exponent is $\tau = 1.1 \pm 0.05$. A successive estimation using a spot of $20 \mu\text{m}$ averaged over 10 different locations yields $\tau = 1.14$ [31]. It worth noting that these values are much smaller than the ones observed in permalloy, a fact we will comment very soon. The other critical exponents are not considered, even if their estimation appears possible.

The paper of Kim *et al.* [32] reports an estimate of the critical exponent τ in Co films, using a different MOKE setup able to visualize directly the DWs. As shown in Fig. 20, both ends of the DWs are usually outside the frame, so that the authors deliberately neglect those jumps having one of the ends inside the frame. The resulting power-law distribution has an exponent close to 1.33, averaged over 4 different thicknesses, from 5 to $50 \mu\text{m}$. As we explain more extensively in Sec. V D, this exponent is different from τ , which should be evaluated, in principle, considering only the jumps fully inside the frame. As a matter of fact, this appears quite difficult to perform, given the limited number of such jumps.

It worth noting that a similar comment could be appropriate also for the previous experiment of Puppini. In that case, it is not possible to distinguish between jumps fully inside the laser spot and the others. Moreover, the relative probability of the two types of events is not known, so that in principle we cannot be sure if the exponent τ is correctly

estimated. With many others, this could be one of the reasons to get the lower value in respect to the permalloy. But, as discussed above, all these matters have been confirmed by further experiments.

IV. MODELS AND THEORIES OF MAGNETIZATION DYNAMICS

A theory of the Barkhausen effect should explain the statistical features of the noise such as the power spectrum, the avalanche distributions and the pulse shape. In particular, the theory should be able to predict the values of the scaling exponents characterizing the distributions and possibly link the noise properties to microstructural details of the material under study. It is thus important to establish a controlled pathway from the microscopic reversal processes and the resulting macroscopic noise response.

We can list here a set of crucial questions that need to be addressed by the theory:

1. an explanation for the occurrence of scaling and quantitative estimates for the exponents.
2. the origin of cutoff in the scaling regime.
3. the effect of microstructural parameters (lattice structure, anisotropies, spin interactions) on the noise statistics.

Clearly these questions are particularly broad and it is dubious that a single answer will be valid for all materials and experimental situations. The observation of scaling laws, however, can signify that relatively simple models could capture and reproduce a wide class of experiments. This is what is expected in critical phenomena, where universality implies that only the main symmetries and conservation laws influence the behavior of the system, while many other quantitative details are irrelevant. Thus, if the Barkhausen effect reflects the presence of an underlying critical phenomenon, one expects relatively broad universality classes spanning different materials, as it is indeed observed.

Discussing the main theoretical approaches proposed to understand the Barkhausen effect, we will pay particular attention to the way each theory addresses the main questions reported above. In order to put the models into context, we first discuss the general properties of ferromagnetic materials in terms of the micromagnetic free energy. This represents a natural microscopic starting point to build up mesoscopic models and theories amenable to an analytic treatment and large scale numerical simulations.

A. General properties of ferromagnetic systems

A ferromagnetic material can be represented as an ensemble of localized magnetic moments or spins, interacting between each other and with the external magnetic field \vec{H} . The macroscopic properties of the material, such as the Barkhausen noise and the hysteresis loop, are due to microscopic rotations of the spins and could in principle be described by a microscopic theory. As a first step in this direction, we will discuss the interactions governing the dynamics of the local magnetization and the associated energetic contributions. In particular, we can write the energy of a ferromagnetic material as a sum of different terms

$$E = E_{ex} + E_m + E_{an} + E_{dis}, \quad (9)$$

where E_{ex} represents exchange interactions, E_m the magnetostatic energy, E_{an} the anisotropy and E_{dis} the disorder. The detailed form of these terms, as a function of the local magnetization $\vec{M}(\vec{r})$ will be discussed in the following sections.

1. Exchange energy

The most important energetic contribution comes from exchange interactions, which are typically short-ranged and tend to align spins. For a set of spins $\vec{s}(\vec{r}_i)$ on the lattice, the exchange energy can be written as

$$E_{ex} = \sum_{ij} J(|\vec{r}_i - \vec{r}_j|) \vec{s}(\vec{r}_i) \cdot \vec{s}(\vec{r}_j), \quad (10)$$

where $J(x)$ decays rapidly for large x and the sum is over all atom pairs. Eq. 10 can be approximated in the continuum limit, through an elastic approximation which involves the removal of all small scale details. The set of spins $\vec{s}(\vec{r}_i)$

are replaced by a continuous field $\vec{M}(\vec{r})$ and the exchange energy can be written as

$$E_{ex} = A \int d^3r \sum_{\alpha=1}^3 (\vec{\nabla} M_{\alpha}(\vec{r}))^2, \quad (11)$$

where A is the exchange coupling, which can be derived from $J(x)$.

2. Magnetostatic energy

The magnetostatic energy is due to the interactions between the spins and the external field and to dipole-dipole interactions between different spins. For a uniformly magnetized sample the contribution of the external field to the magnetostatic energy is simply given by

$$E_m = -\frac{\mu_0}{8\pi} V \vec{M} \cdot \vec{H}, \quad (12)$$

where \vec{M} is the magnetization and V is the volume.

In addition, we should consider the energy due to the demagnetizing field \vec{H}_{dm} , the magnetostatic field generated by the local magnetization. In order to compute H_{dm} , it is useful to define “magnetic charges” associated to the discontinuities of the normal component of the magnetization. For a surface separating two regions of magnetizations \vec{M}_1 and \vec{M}_2 , the surface charge density is given by

$$\sigma = \hat{n} \cdot (\vec{M}_1 - \vec{M}_2) \quad (13)$$

where \hat{n} is the vector normal to the surface. For instance, at the boundary of the sample, where the magnetization varies abruptly from M_s to zero, the charge density is given by $M_s \cos \theta$, where θ is the angle between the magnetization direction and \hat{n} . It is important to remark that magnetic charges are not physical charges, but are a convenient tool to compute the demagnetizing field and magnetostatic energy of magnetized bodies. Everything proceeds as in electrostatics provided we replace electric charge with magnetic charges and the electric field with the demagnetizing field which is thus given by

$$\vec{H}_{dm}(\vec{r}) = -\vec{\nabla} \cdot \int \frac{dS' \sigma}{|\vec{r} - \vec{r}'|}, \quad (14)$$

where the integral is over the surface separating two regions of constant magnetization. For a uniformly magnetized ellipsoid \vec{H}_{dm} is constant and proportional to magnetization vector

$$\vec{H}_{dm} = -k\vec{M}, \quad (15)$$

where k is a geometry dependent demagnetizing factor. In this case the total magnetostatic energy is simply obtained by replacing \vec{H} in Eq. 12 by $\vec{H} + \vec{H}_{dm}$.

In general the demagnetizing field is not constant and Eq. 12 has to be replaced by an integral

$$E_m = -\frac{\mu_0}{8\pi} \int d^3r \vec{M} \cdot (\vec{H} + \vec{H}_{dm}(\vec{r})), \quad (16)$$

where H_{dm} is given by the contribution of surface charges (i.e. Eq. 14) summed to the contribution due to the bulk variation of the magnetization. The bulk dipolar energy can be written explicitly as

$$E_m = -\frac{\mu_0}{8\pi} \int d^3r d^3r' \sum_{\alpha,\beta=1}^3 \left(\frac{\delta_{\alpha\beta}}{|\vec{r} - \vec{r}'|^3} - \frac{3(r_{\alpha} - r'_{\alpha})(r_{\beta} - r'_{\beta})}{|\vec{r} - \vec{r}'|^5} \right) M_{\alpha}(\vec{r}) M_{\beta}(\vec{r}'). \quad (17)$$

As in the case of the surface term Eq. 17, can also be rewritten in terms of the density of magnetic volume charges $\rho(\vec{r}) = \vec{\nabla} \cdot \vec{M}(\vec{r})$ as

$$E_m = -\frac{\mu_0}{8\pi} \int \frac{d^3r d^3r' \rho(\vec{r}) \rho(\vec{r}')}{|\vec{r} - \vec{r}'|}. \quad (18)$$

3. Magnetocrystalline anisotropy and magnetoelastic energies

The magnetization in a ferromagnetic material typically has preferential directions corresponding to the crystallographic axis of the material. Therefore, it is easier to magnetize the sample along the easy directions. This observation can also be expressed in terms of the energy of magnetocrystalline anisotropy

$$E_{an} = \int d^3r \sum_{\alpha,\beta} K_{\alpha\beta} M_\alpha M_\beta, \quad (19)$$

where M_α is the α component of the vector \vec{M} and K_{ij} is a symmetric tensor, describing the anisotropy of the material. In the simplest case of a uniaxial crystal, Eq. 19 reduces to

$$E_{an} = \int d^3r K_0 (\vec{M} \cdot \hat{e})^2 = \int d^3r K_0 M^2 \sin^2 \phi \quad (20)$$

where ϕ is the angle between the easy axis \hat{e} and the magnetization vector and K_0 is the uniaxial anisotropy constant.

The variations of the magnetization inside a ferromagnetic sample can cause deformation in the lattice structure, a phenomenon known as magnetostriction. Conversely, when an external mechanical stress is applied to the sample the magnetic structure can in principle be modified. To describe this effect it is useful to introduce the magnetoelastic energy, which in the most general form can be written as

$$E_{an} = \int d^3r \sum_{\alpha,\beta,\gamma,\delta} \lambda_{\alpha\beta\gamma\delta} \sigma_{\alpha\beta} M_\gamma M_\delta, \quad (21)$$

where $\sigma_{\alpha\beta}$ is the stress tensor and $\lambda_{\alpha\beta\gamma\delta}$ is the magnetoelastic tensor. For a crystal with isotropic magnetostriction, under a uniaxial stress σ the anisotropy energy takes the simple form of Eq. 20 with K_0 replaced by $K_0 + 3/2\lambda\sigma$, where λ is the uniaxial magnetostriction constant.

4. Disorder

In the previous discussion we have considered only an homogenous system, in which the interactions are globally defined and do not depend on position. In general, however, different sources of inhomogeneities are found in virtually all ferromagnetic materials. The presence of structural disorder is essential to understand the fluctuations in the Barkhausen noise, which would be strongly suppressed in a perfectly ordered system. The nature of the disorder can be inferred from the microscopic structure of the material under study.

We can thus distinguish several contributions to the magnetic free energy due to the disorder: in a crystalline materials disorder is due to the presence of vacancies, dislocations or non-magnetic impurities. In polycrystalline materials we should add to these defects the presence of grain boundaries and variations of the anisotropy axis in different grains. Finally in amorphous alloys disorder is primarily due to internal stresses and the random arrangement of the atoms. It is important to notice that in the following we will consider the disorder as quenched (or “frozen”): it does not evolve on the timescales of the magnetization processes under study. It is not always simple to quantify the energetic contributions of the different sources of disorder but we can highlight here the main effects.

The presence of randomly distributed non-magnetic inclusions give rise to a magnetostatic contribution, due to the magnetic charges that form at the boundaries of the inclusions [79]. The energetic contribution due to a collection of those inclusions can be expressed as a local fluctuation of the dipolar coupling. A similar discussion can be repeated in the case of exchange interactions, leading to a fluctuating exchange coupling. The typical fluctuations of the coupling depend on the volume fraction v of the non magnetic inclusions: the typical strength of the (exchange or dipolar) coupling $g(\vec{r})$ will be of the order of $\bar{g} \simeq (1 - v)g_0$ and the fluctuations $\langle (g - \bar{g})^2 \rangle \simeq v g_0^2$, where g_0 is the coupling without impurities. This type of disorder is conventionally called of random-bond type and should also be present in amorphous alloys, due to the random arrangements of the atoms.

In polycrystalline samples, each grain has a different crystalline anisotropy. In particular, the direction of the anisotropy axes will fluctuate in space and in the simple case of uniaxial anisotropies the anisotropy energy will be given by $E_{an} = \int d^3r K(\vec{r}) (\vec{M} \cdot \hat{e}(\vec{r}))^2$, where \hat{e} is a random function of position reflecting the grain structure of the material under study.

In magnetostrictive samples internal stresses play a similar role than anisotropies, as we discussed in the previous section. In particular, a random distribution of internal stresses produces an random energy of the type of Eq. 20 with a random anisotropy constant $K(\vec{r}) \propto K_0 + 3/2\lambda\sigma(\vec{r})$. While internal stresses can have multiple origins, it is possible

to compute explicitly their distribution in some particular cases, such as in a crystal with a random distribution of parallel dislocations. The stress in \vec{r} due to a dislocation in the origin is given in cylindrical coordinates by $\sigma_{\alpha\beta} = b\mu C_{\alpha\beta}(\theta)/r$, where b is the Burgers vector, μ is the shear modulus and $C_{\alpha\beta}$ is an angular function depending on the dislocation type [80]. The distribution of the internal stresses is formally given by

$$P(\vec{\sigma}_{\alpha\beta}) = \int d^{2N}r D(\vec{r}_1, \dots, \vec{r}_N) \delta(\vec{\sigma}_{\alpha\beta} - \sum_k \sigma_{\alpha\beta}(\vec{r} - \vec{r}_k)), \quad (22)$$

where D is the distribution of the position of the dislocations. The internal stress distribution has been evaluated in the case of a random short-range correlated dislocation arrangement: $P(\sigma)$ is Gaussian for small stresses, with variance $\langle \Delta\sigma^2 \rangle \propto \rho$, where ρ is the dislocation density and at larger stresses displays a power law tail, scaling as σ^{-3} [81]. It is interesting to remark that $P(\sigma)$ is an experimentally accessible quantity, since it is directly related to the X-ray spectrum [82].

We have discussed two common contributions to the disorder energy in ferromagnetic materials: random bonds and random anisotropies. To conclude the discussion, we remark that some diluted antiferromagnets in a field can be effectively described by a random-field type disorder, with energy given by

$$E_{dis} = \int d^3r \vec{h}(\vec{r}) \cdot \vec{M} \quad (23)$$

where \vec{h} is randomly distributed in space. Despite the fact that random field disorder is not present in ferromagnetic materials, it provides a useful theoretical ingredient to understand the role of disorder in hysteresis, as we will discuss in the following.

5. Micromagnetic equations

In the previous sections we have discussed the different energetic contributions to ferromagnetic materials. Collecting all the terms, considering for simplicity a uniaxial material, we can write the energy

$$E = \sum_{\alpha=1}^3 \int d^3r [A(\vec{\nabla} M_\alpha)^2 + K(M_\alpha e_\alpha)^2 - (H_\alpha + H_{dem}^{(\alpha)})M_\alpha], \quad (24)$$

A , K and e_α in principle depend on position and $H_{dem}^{(\alpha)}$ is the component α of the demagnetizing field, discussed in section IV A 2.

The energy function reported in Eq. 24 can in principle be used to compute the equilibrium properties of a ferromagnetic materials. This problem is in general very complex and we do not attempt to treat it here. In fact, to describe the Barkhausen effect we are interested in the evolution of the magnetization in response of an increasing external field. The equation of motion for the magnetization can readily be obtained from Eq. 24

$$\frac{\partial \vec{M}}{\partial t} = \gamma \vec{M} \times \vec{H}_{eff} \quad (25)$$

where γ is the charge to mass ratio and $\vec{H}_{eff} \equiv -\delta E / \delta \vec{M}$. Eq. 25 does not include dissipation mechanism and would predict an indefinite precession of the magnetization vector. This problem can be overcome introducing phenomenological laws for the dissipation. This results for instance in the Landau-Lifshitz-Gilbert equation whose numerical integration for different microstructures and boundary conditions is the subject of micromagnetism.

It is tempting to use a micromagnetic approach describe collective effects arising in the Barkhausen effect from first principles. An attempt on this direction was made in Refs. [83, 84, 85], where a Montecarlo version of the micromagnetic equation was used to simulate the Barkhausen effect in polycrystals.

The model consists in a chain of N magnetic moments with orientations defined by two angles ϕ_i and θ_i . The total energy of the system is given by

$$E = \frac{1}{2} \sum_i (\sin^2 \alpha_i + 2H \cos \theta_i + m \sin^2 \theta_i \sin^2 \phi_i - 2a \cos \beta_{i,i+1}), \quad (26)$$

where α_i is the angle between the magnetic moment and the local (random) easy axis, H is the magnetic field, a is the exchange-anisotropy energy ratio and m controls the magnetostatic energy. The last term takes into account the interaction between magnetic moments and $\beta_{i,j}$ is the angle between the moments in i and j .

The evolution of the magnetization is dictated by a Montecarlo algorithm. As the external field is slowly increased the magnetic moments rotate in bursts which are associated with the Barkhausen jumps. The results obtained for the jump distributions are in some range of parameters reminiscent of the experiments (i.e. a power law with a cutoff) but a quantitative comparison with experiments would be questionable. The model treats very accurately some aspects of ferromagnetic system, namely spin rotations, nucleation and random anisotropies, but completely neglects the fundamental aspects of the problem: dimensionality (the model is one dimensional), the range of interactions (only nearest-neighbor interactions are present, while in reality dipolar interactions give rise to long-range terms decaying as $1/r^3$) and demagnetizing effects. For these reasons, this model is not able to reproduce quantitatively the scaling properties of the Barkhausen effect. To this end, it would be necessary to study three dimensional models with long-range interactions, a task that promises to be computationally very demanding.

B. Random energy models

The difficulties arising in the direct analysis of the micromagnetic equations naturally lead to search for simplified models that could capture the essential mechanism underlying the Barkhausen noise without excessive complications. The main ingredient of any model for the Barkhausen effect is the presence of disorder, thus the simplest approach is to neglect most of the details of the micromagnetic energy, keeping only a uniform magnetostatic term E_m and replacing the rest with a random function of the magnetization m

$$E = F(m) - mH_{eff}, \quad (27)$$

where $H_{eff} = H + H_{dem}$. The rationale behind this approximation can be understood considering a single rigid domain wall dividing the sample in two domains. In this case the magnetization is proportional to the wall position x : $m = M_s(2x/L - 1)$, where M_s is the saturation magnetization and L is the sample width. The sample is magnetized as the applied magnetic field pushes the domain wall across a disordered landscape represented by the random potential $F(m)$. In order to define completely the problem, one needs to specify the statistical features of $F(m)$, such as its distribution and correlations.

Néel was the probably the first to use a random energy model to study the hysteresis loop properties at low fields in his theory of the Rayleigh loops [86, 87]. In the Néel model the random function was schematized as a series of parabolas with randomly distributed curvatures. The Barkhausen noise can be constructed from the random energy model by a visual inspection of the pinning field $W(m) \equiv -\frac{dF}{dm}$ as shown in Fig. 21. As the effective field is increased, the domain wall is pinned as long as $H_{eff} < W(m)$, when H_{eff} reaches a local maximum of $W(m)$ the domain wall jumps forward until the condition $H_{eff} < W(m)$ is met. The Barkhausen sizes S are just the changes in magnetization Δm occurring after these jumps or, in more mathematical terms, the first returns of the stochastic process described by $W(m)$. The random energy model in the form proposed by Néel, however, can not describe correctly the Barkhausen noise because the pinning field is essentially uncorrelated. Thus the first return distributions decays exponentially, while the experiments indicate a power law distribution.

In order to obtain a power law distribution of returns the pinning field has to be long-range correlated. This point was first realized by Bertotti [88, 89], who included a Brownian pinning field in a random energy model. The model, widely known as ABBM [16, 17], yields a quite accurate description of the Barkhausen noise statistics. In the ABBM model the magnetization evolves according to an overdamped equation of motion

$$\frac{dm}{dt} = ct - km + W(m), \quad (28)$$

where the external field increases at constant rate $H = ct$, k is the demagnetizing factor, and the damping coefficient has been set to unity rescaling the time units. The pinning field is a Brownian process where correlations grow as

$$\langle (W(m) - W(m'))^2 \rangle = D|m - m'|. \quad (29)$$

The main predictions of the ABBM model can be obtained deriving Eq. (28) with respect to time and defining $v \equiv dm/dt$

$$\frac{dv}{dt} = c - kv + vf(m), \quad (30)$$

where $f(m) \equiv dW/dm$ is an uncorrelated random field with variance D .

Expressing Eq. 30 as a function of v and m only

$$\frac{dv}{dm} = \frac{c}{v} - k + f(m), \quad (31)$$

we obtain a Langevin equation for a random walk in a confining potential, given by $U(v) = kv - c \log(v)$. Asymptotically, the statistics of v is ruled by the Boltzmann distribution

$$P(v, m \rightarrow \infty) \sim \exp(-U(v)/D) = v^{c/D} \exp(-kv/D). \quad (32)$$

The distribution in the time domain is obtained by a simple transformation and it is given by [16]

$$P(v) \equiv P(v, t \rightarrow \infty) = \frac{k^{c/D} v^{c/D-1} \exp(-kv/D)}{D^{c/D} \Gamma(c/D)}. \quad (33)$$

A consequence of Eq. (33) is that the domain wall average velocity is given by $\langle v \rangle = c/k$. For $c/D < 1$ the velocity distribution in Eq. 33 is a power law with an *upper* cutoff that diverges as $k \rightarrow 0$. In this regime, the domain wall moves in avalanches whose size and durations are also distributed as power laws. For $c/D > 1$ the motion is smoother with fluctuations that decrease as c/D increases.

The avalanche size distribution equals the distribution of first return times of a random walk in the confining potential $U(v)$. In the limit $k \rightarrow 0$, we can directly apply the exact result reported in Ref. [90] for the first return times of a random walk in a logarithmic potential, which implies that the avalanche exponents depends on c and are given by

$$\tau = 3/2 - c/2D \quad \alpha = 2 - c/D. \quad (34)$$

See also Ref. [43, 63] for alternative but not rigorous derivations of these results.

The scaling of the cutoff of the avalanche distributions in the ABBM model can be obtained similarly in the limit $c \rightarrow 0$ solving for the first return probability of a biased random walk and is given by

$$S_0 \sim k^{-2}. \quad (35)$$

Using similar arguments one can also show that the cutoff of avalanche durations scales as $T_0 \sim k^{-1}$ [50].

C. Spin models

In this section we discuss the attempts to understand the statistical properties of the Barkhausen effect by models of interacting spins, that can either be simulated on a computer or in some cases analyzed theoretically. This approach is conceptually simple and theoretically appealing, since it tries to derive directly macroscopic properties from a microscopic model, replacing the vectorial micromagnetic equations by simplified rules for the evolution of integer valued spins. The basis of this kind of approach is the notion of universality which is expected for critical phenomena: the values of the critical exponent and the shape of the scaling functions are independent on the microscopic details of the system, provided that the relevant symmetries of the problem are correctly taken into account. For this reason, we can expect to obtain the correct large scale behavior, such as the scaling properties of the Barkhausen effect, from relatively simple models.

1. The random field Ising model

Sethna et. al [91] have proposed the driven random-field Ising model as a prototype for hysteresis and avalanches at first-order phase transitions. The model was studied extensively analytically and numerically and the resulting scaling behavior was compared with the experimental results on the Barkhausen effect [69, 75, 76, 92, 93].

In this models, a spin $s_i = \pm 1$ is assigned to each site i of a d -dimensional lattice. The spins are coupled to their nearest-neighbors spins by a ferromagnetic interaction of strength J and to the external field H . In addition, to each site of the lattice it is associated a random field h_i taken from a Gaussian probability distribution with variance R , $P(h) = \exp(-h^2/2R^2)/\sqrt{2\pi}R$. The Hamiltonian thus reads

$$E = - \sum_{\langle i,j \rangle} J s_i s_j - \sum_i (H + h_i) s_i, \quad (36)$$

where the first sum is restricted to nearest-neighbors pairs. In the zero temperature dynamics used by Sethna et al. [91], the external field is ramped from $-\infty$ to ∞ and the spins align with the local field [94]

$$s_i = \text{sign}(J \sum_j s_j + h_i + H). \quad (37)$$

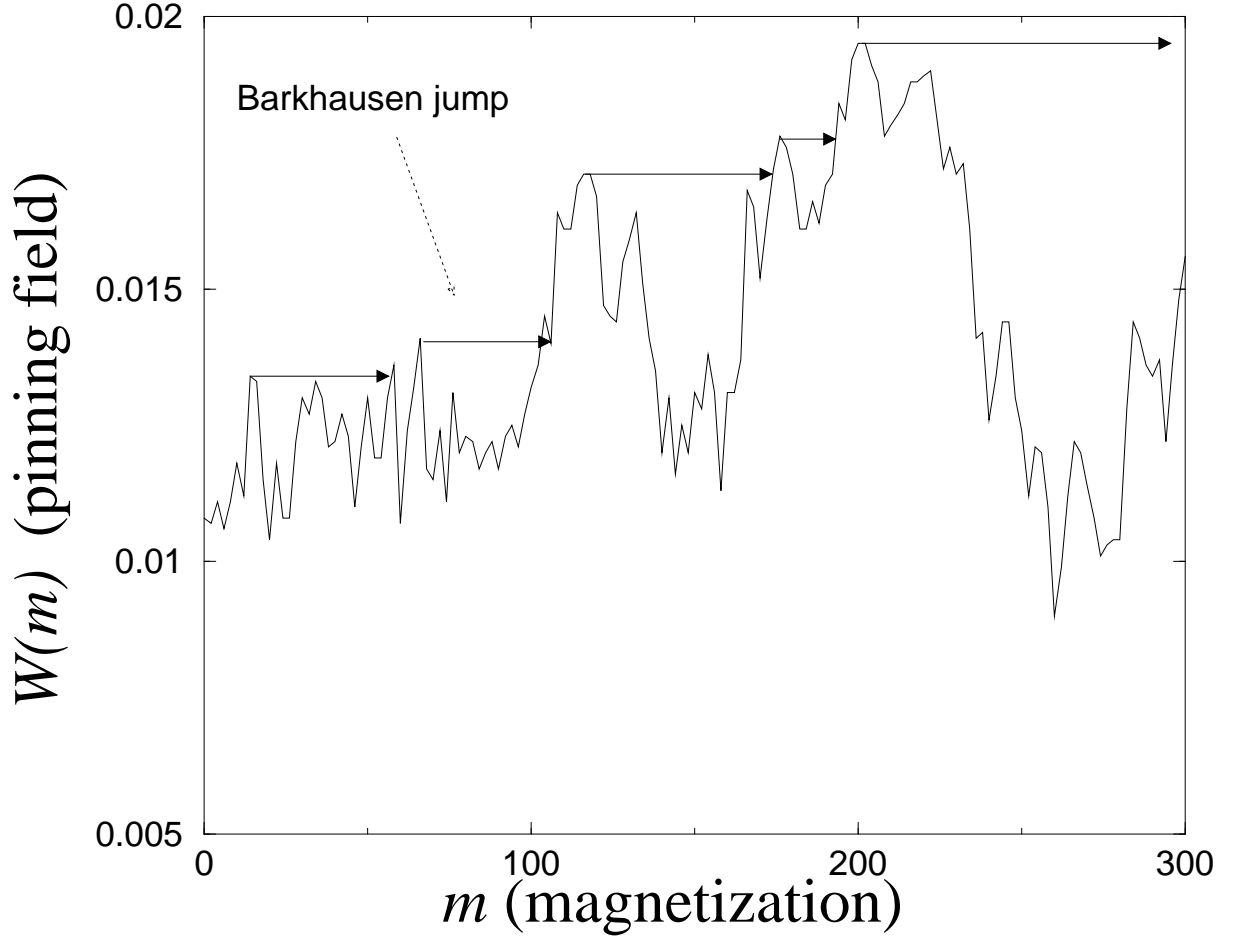


FIG. 21: The Barkhausen jumps (denoted by arrows) from the perspective of the random energy model.

In this way a single spin flip can lead the neighboring spins to flip, eventually trigger an avalanche.

For small values of the disorder R the first spin flips are likely to generate a big avalanche whose size is comparable to the system size, leading to a discontinuous magnetization reversal. On the other hand, a large disorder prevents the formation of large avalanches and the magnetization reversal is smooth. In fact, these two regimes are separated by a critical disorder R_c , where the avalanches are distributed as a power law. The behavior of the model close to R_c is very similar to that of equilibrium systems at the critical points and can thus be studied by standard methods, like mean-field theory and the renormalization group.

A first qualitative picture of the behavior of the RFIM can be obtained by mean-field theory [75, 91]. To this end, we consider Eq. 36 extending the sums to all the pairs of sites and obtain

$$E = - \sum_i (JM + H + h_i) s_i, \quad (38)$$

where $M = \sum_i s_i$. The magnetization can then be obtained self-consistently as

$$M = 1 - 2P(JM + H + h_i < 0) = 1 - 2 \int_{-\infty}^{-JM-H} \rho(h) dh. \quad (39)$$

This equation has a single valued solution for $R > R_c = \sqrt{(2/\pi)}J$, while the solution becomes multivalued for $R < R_c$. In the second case, we have an hysteresis loop with a jump at H_c and a diverging slope dM/dH . For high disorder there is no hysteresis, but this is an artifact of mean-field theory that is not observed in low dimensions. At the critical point $R = R_c$ the magnetization has a diverging slope, but no finite jump. In analogy with critical phenomena it is possible to obtain scaling laws describing the singularities occurring at the transition. In particular the magnetization

obeys the scaling law

$$M = |r|^\beta g_\pm(h/|r|^{\beta\delta}), \quad (40)$$

where $r \equiv (R - R_c)/R_c$ and $h \equiv (H - H_c)/H_c$ are the reduced control parameters, and $\beta = 1/2$, $\delta = 3$. The scaling function g_\pm is obtained as the root of a cubic equation.

The distribution of avalanche sizes near the critical point can be computed analytically in the framework of mean-field theory. The result can be summarized in the scaling form

$$P(S, r, h) = S^{-\tau} \mathcal{P}_\pm(S/|r|^{-1/\sigma}, h/|r|^{\beta\delta}), \quad (41)$$

where the exponents take the mean-field values $\tau = 3/2$, $\sigma = 1/2$. The scaling function \mathcal{P}_\pm can be evaluated exactly in terms of g_\pm and is given by

$$\mathcal{P}_\pm(x, y) = (1/\sqrt{2\pi}) \exp(-x(1 \mp \pi g_\pm(y)^2/4)^2/2). \quad (42)$$

In addition to the size distribution one can also define the distribution of durations T , which obeys an analogous scaling form

$$D(T, r, h) = T^{-\alpha} \mathcal{D}_\pm(T/|r|^{-1/(\sigma\nu z)}, h/|r|^{\beta\delta}), \quad (43)$$

where $\alpha = 2$, ν is the correlation length exponent ($\xi \sim r^{-\nu}$) and z is the dynamic exponent relating the correlation length to the characteristic time ($\xi \sim T_0^z$).

Mean-field theory has the advantage of being easily tractable and provides a qualitative picture of the behavior of the model, but the numerical values of the exponents are typically inaccurate in dimensions lower than the upper critical dimension, that for the RFIM it is equal to $d_c = 6$. To overcome this problem, one can perform a renormalization group analysis with an expansion in $\epsilon = 6 - d$ as in equilibrium critical phenomena. The renormalization group is quite involved and we do not discuss it here in detail, but just quote the main results (for a complete discussion the reader is referred to Ref. [75]). The exponent determining the scaling of the order parameter have been computed to first order in ϵ and are estimated to be $\beta = 1/2 - \epsilon/6$ and $\delta = 3 + \epsilon$. The avalanche exponent τ displays only corrections to order ϵ^2 and the cutoff exponent is estimated as $\sigma = 1/2 - \epsilon/12$.

Large scale numerical simulations have been performed, to obtain reliable estimate for the critical exponents in three dimensions. The avalanche size distribution is most naturally computed integrating the avalanches over the entire hysteresis loop. The exponent τ_{int} measured in this way can be related to the other exponents by a scaling relation $\tau_{int} = \tau + \sigma\beta\delta$. Typically the distribution displays an initial power law behavior and a cutoff that depends on the disorder R (see Fig. 22). The distribution for different values of R can then be collapsed using a scaling form of the type of Eq. 41 [69, 93]. The best numerical estimate for the exponents (or exponent combinations) in three dimensions is $\tau = 1.60 \pm 0.06$, $\tau_{int} = 2.03 \pm 0.03$, $1/\sigma = 4.2 \pm 0.3$, $\sigma\nu z = 0.57 \pm 0.03$, $\alpha = 2.02$, $\beta = 0.035 \pm 0.03$, $1/\nu = 0.71$ [93].

Looking at the results above one may be tempted to perform a direct comparison with experiments. However, this should be done with a grain of salt. The RFIM model in fact predicts scaling only close to a critical disorder R_c while in general there is no reason to believe that this condition is fulfilled in experiments. To relate the Barkhausen scaling behavior observed in experiments to a disorder induced phase transition, such as the one discussed here, it would be necessary to show that the cutoff to the scaling behavior scales with the disorder strength. Unfortunately such a measure has not been performed yet.

2. Random bonds, random anisotropies and other effects

The RFIM represents probably the simplest model to study the effect of disorder in ferromagnetic hysteresis and Barkhausen noise. The model displays a disorder induced transition with associated critical exponents, which has been recently observed in experiments. While random fields can be a useful theoretical idealization, they are not present in ferromagnetic materials. Thus an important question to address is whether the basic phenomenology of the RFIM carries over to more realistic types of disorder. While the answer to this question appears to be positive, it is still controversial whether the disorder induced phase transition is universal with respect to the type of disorder. A second related question is whether the inclusion of more realistic ingredients in the RFIM results or not in a change of the scaling exponents.

The first question was addressed by numerical simulations, considering random bonds, site dilution, and random (infinite) anisotropies. In the random bond Ising model (RBIM), the disorder enters into the exchange coupling J_{ij}

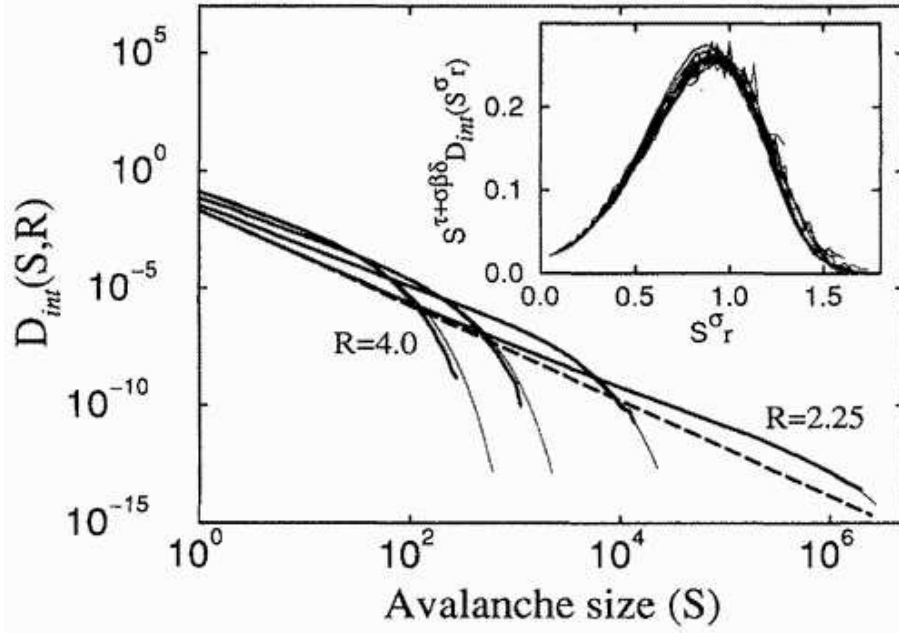


FIG. 22: The integrated avalanche distribution in the RFIM in $d = 3$ simulated in a lattice of 320^3 spins. The inset shows the data collapse. [From [69], Fig. 1, pg. 4528]

which is randomly distributed with mean J_0 and standard deviation R . Hysteresis in the RBIM was first studied in the spin glass limit ($J_0 = 0$) [94]. In analogy with the RFIM, the RBIM displays a disorder induced phase transition in the hysteresis loop. Some of the scaling exponents, including those ruling the avalanche distributions, have been evaluated and their values differ slightly from those measured in the RFIM. For instance, some reported values are $\tau_{int} \simeq 2$, $z \simeq 1.6$ and $\nu \simeq 1$ [95]. One should beware, however, that the lattice sizes used in this study are rather limited (up to 40^3) [95] compared to those used to estimate exponents in the RFIM (up to 320^3) [93].

In the site diluted Ising model (SDIM), the presence of non-magnetic impurities is treated by removing a fraction of spins in the lattice. The Hamiltonian is thus simply given by

$$E = -j \sum_{ij} J_{ij} c_i c_j s_i s_j - \sum_i H c_i \sigma_i \quad (44)$$

where $c_i = 0, 1$ indicates whether the spin is magnetic or not. Typically, the sum in the exchange interaction is not restricted to the nearest neighbors but extends to a larger range. Simulations of the SDIM in $d = 3$ yield exponents compatible with those of the RFIM, namely $\tau_{int} = 2.0 \pm 0.2$ [96].

The random (infinite) anisotropy model is obtained from a vectorial model (a lattice version of Eq. (61))

$$E = - \sum_{\langle ij \rangle} J \vec{s}_i \cdot \vec{s}_j - \sum_i K (\vec{s}_i \cdot \hat{n}_i)^2 + \vec{H} \cdot \vec{s}_i, \quad (45)$$

in the limit of $K \rightarrow \infty$. Thus to minimize the anisotropy energy, in each site the spin should be parallel to the quenched random direction \hat{n}_i . The original vectorial model becomes then effectively of Ising type as can be seen by introducing a fictitious spin $\sigma_i = \pm 1$ defining the sign of \vec{s}_i along its random axis (i.e. $\vec{s}_i = \hat{n}_i \sigma_i$). In terms of the new spin variables the Hamiltonian can be rewritten as

$$E = - \sum_{\langle ij \rangle} J_{ij} \sigma_i \sigma_j - \sum_i H_i \sigma_i, \quad (46)$$

with effective random bonds $J_{ij} \equiv J \hat{n}_i \cdot \hat{n}_j$ and random fields $H_i = n_z$. The model above was simulated numerically with a zero temperature dynamics analogous to the one employed in the RFIM and with two different distributions for the anisotropy axis. The measured exponents are in good agreement with those measured in the RFIM. In particular for the avalanche distribution, the reported values are $\tau_{int} = 2.06 \pm 0.05$ and $\tau_{int} = 2.10 \pm 0.05$ depending on the distribution [97]. A recently proposed analysis, based on the renormalization group, of the vectorial random

anisotropy model shows that the model should be described generically by the RFIM fixed point [98], thus supporting the conclusions of the simulations.

From the discussion above, we conclude that the disorder induced critical point in the RFIM represents a broad universality class describing different sorts of spin models. This fact, if confirmed by larger scale simulations and renormalization group calculation, is particularly interesting because it allows to concentrate on a relatively simple model (the RFIM) to understand quantitatively a more generic scaling behavior. There is, however, an important point still to be considered: the effect of long-range dipolar interactions. As we discussed in section IV A 2 the effect is twofold, interactions between spins in the bulk and surface charges at the boundary of the sample. The bulk interaction has not been studied deeply in the framework of spin models, apart from some numerical simulations in two dimensions [99, 100]. From simple power counting considerations, we would expect that dipolar forces are relevant in the renormalization group sense, thus modifying the numerical values of the critical exponents. Therefore, unless one can neglect dipolar forces (this could be the case in hard rare earth alloys with strong anisotropies), the numerical results obtained in the RFIM would not apply to real materials.

Surface effects have an even more drastic effect on the critical behavior discussed above. The presence of a demagnetizing field generates an effective correlation length, destroying scale invariance even at the critical point $R = R_c$. Nevertheless, this effect is small, since the demagnetizing factor tends to vanish for very large system sizes. Simulations of the RFIM in presence a demagnetizing field show remarkable features in the low disorder phase, where otherwise one expects the magnetization to change abruptly with a large jump. The demagnetizing field hinders the reversal process which splits in a series of avalanches of different sizes [101, 102]. The distribution of size is again a power law distribution and the cutoff is controlled by the demagnetizing factor (see Fig. 24) [101]. It is important to observe that this power law scaling is not related with the disorder induced critical point, since this behavior is observed generically for $R < R_c$, but can be explained considering the dynamics of a domain wall. Indeed for $R < R_c$, at the coercive field a domain is nucleated and starts to grow. When the domain is large enough the demagnetizing field reduces the effective field and eventually the growth stops. At this moment the spins that will flip when the external field is increased are likely to be those at the domain boundary. To understand this process in detailed one should thus analyze domain wall dynamics, as will be discussed in the next section.

D. Domain wall models

In order to minimize the exchange energy, a ferromagnetic material at sufficiently low temperature and zero field would display a uniform magnetization, oriented along an easy axis to lower the magnetocrystalline anisotropy energy. In most cases, however, this arrangement is hindered by a very high cost in magnetostatic energy, due to the discontinuities of the magnetization at the sample edges. Thus it is energetically favorable to create domains, which in the simplest situation span the sample from end to end. In this condition, the magnetization process occurs prevalently by domain wall motion, which can then be studied to recover the statistical properties of the Barkhausen noise [49, 50, 54, 103, 104, 105].

1. Energetics of a domain wall

We consider a flexible 180° domain wall separating two regions with opposite magnetization directed along the z axis. In absence of disorder the domain wall would be flat, but in general the wall will bend to accommodate pinning forces. If the surface has no overhangs, we can describe the position of the domain wall by a function $h(\vec{r}, t)$ of space and time (see Fig. 25). The energy associated with such a deformation field can be computed expanding the micromagnetic free energy discussed in Sec. IV A, and we can thus split the energy into the sum of different contributions due to exchange and magnetocrystalline interactions, magnetostatic and dipolar fields, and disorder [50].

The contribution from the magnetostatic energy, if the external field \vec{H} is applied along the z axis is given by

$$E_m = -2\mu_0(H + H_{dm})M_s \int d^2r h(\vec{r}, t), \quad (47)$$

where we have included the demagnetizing field H_{dm} which is in general a complicated function of $h(\vec{r}, t)$, depending also from the sample shape. In the simplest approximation, however, the intensity of the demagnetizing field will be proportional to the total magnetization. Considering the field constant through the sample, it can thus be written as

$$H_{dm} = -\frac{kM_s}{V} \int d^2r h(\vec{r}, t) \quad (48)$$

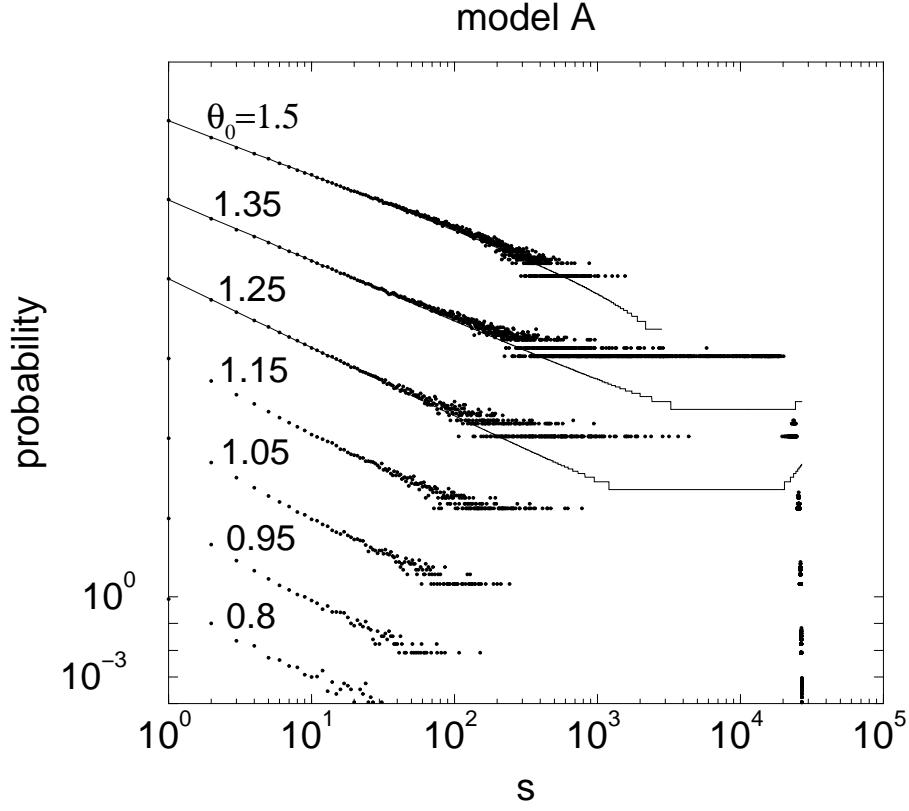


FIG. 23: The integrated avalanche distribution in the random infinite anisotropy model in $d = 3$ simulated in a lattice of 30^3 spins. The different curves correspond to different values of θ_0 , corresponding to the average angle between the field axis and the anisotropy axis [From Ref. [97], Fig. 8, pg. 134431-6].

where the demagnetizing factor k takes into account the geometry of the domain structure and the shape of the sample and V is a volume factor.

The interplay between magnetocrystalline anisotropy and exchange interactions is responsible for the microscopic structure of the domain wall. While a very sharp change of the spin orientation has a high cost in exchange energy, a very smooth rotation of the spins between two domains is prevented by the magnetocrystalline anisotropy. The balance between these two contributions determines the width of the domain wall and its surface energy. The total energy due to these contributions is proportional to the area of the domain wall

$$E_{dw} = \gamma_w \int d^2r \sqrt{1 + |\nabla h(\vec{r}, t)|^2}, \quad (49)$$

where $\gamma_w \simeq 2\sqrt{AK_0}$ is the domain wall surface energy. Expanding this term for small gradients we obtain

$$E_{dw} = \gamma_w S_{dw} + \frac{\gamma_w}{2} \int d^2r |\nabla h(\vec{r}, t)|^2, \quad (50)$$

where S_{dw} is the area of the undeformed wall. Thus the domain wall energy represents an elastic interaction that tends to keep the domain wall flat.

An additional elastic interaction is due to dipolar forces, since the local distortions of the domain wall are associated to discontinuities in the normal component of the magnetization. As discussed in Sec. IV A 2, this effect can be treated introducing magnetic charges on the domain wall surface (see Eq. 13). The surface charge density is zero when the magnetization is parallel to the wall and for small distortion it can be expressed as

$$\sigma(\vec{r}) = 2M_s \cos \theta \simeq 2M_s \frac{\partial h(\vec{r}, t)}{\partial x} \quad (51)$$

where θ is the local angle between the vector normal to the surface and the magnetization. The energy associated

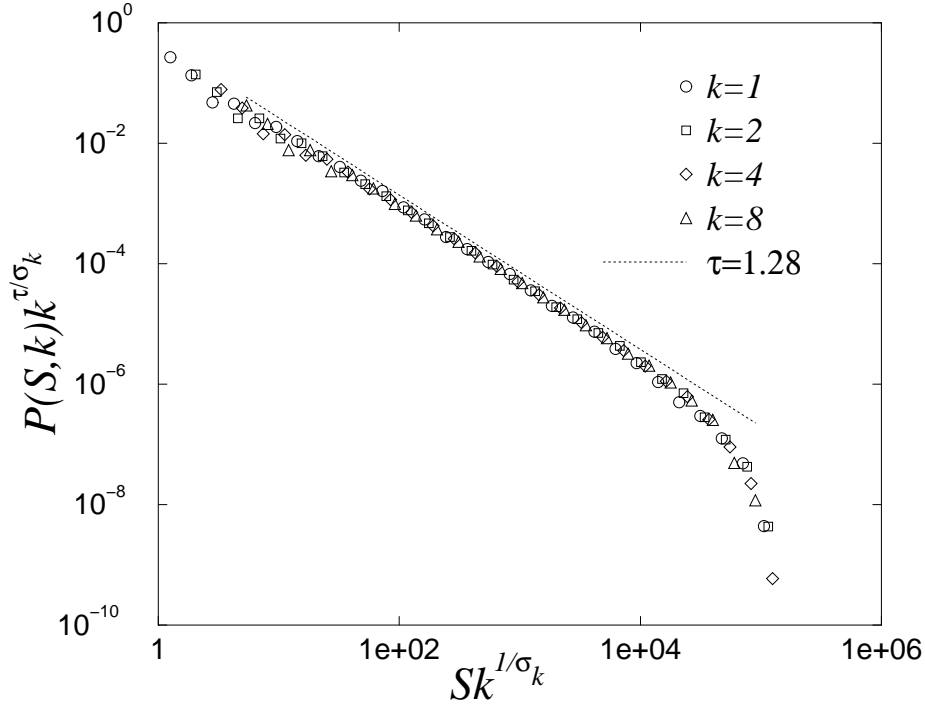


FIG. 24: Data collapse of avalanche size distribution $P(S) \sim S^{-\tau} f(S/S_0)$ simulated in the RFIM for $R < R_c$ in presence of a demagnetizing field, using different values of the demagnetizing factor k . The critical exponent τ is given by 1.28, while $S_0 \sim k^{-1/\sigma_k}$ with $1/\sigma_k \sim 0.7$ [From [101], Fig. 1, pg. 233].

with this distribution of charges is given by

$$E_d = \int d^2r d^2r' \frac{\mu_0 M_s^2}{2\pi |\vec{r} - \vec{r}'|} \frac{\partial h(\vec{r}, t)}{\partial z} \frac{\partial h(\vec{r}', t)}{\partial z'} \quad (52)$$

which integrating by part can also be written as

$$E_d = \int d^2r d^2r' K(\vec{r} - \vec{r}') (h(\vec{r}, t) - h(\vec{r}', t))^2 \quad (53)$$

where the non local-kernel is given by

$$K(\vec{r} - \vec{r}') = \frac{\mu_0 M_s^2}{2\pi |\vec{r} - \vec{r}'|^3} \left(1 - \frac{3(z - z')^2}{|\vec{r} - \vec{r}'|^2} \right). \quad (54)$$

The interaction is long range and anisotropic, as can be seen by considering the Fourier transform

$$K(p, q) = \frac{\mu_0 M_s^2}{4\pi^2} \frac{p^2}{\sqrt{p^2 + q^2}}, \quad (55)$$

where p and q are the two components of the Fourier vector along z and y . In the preceding derivation we have implicitly assumed an infinitely strong anisotropy, so that the magnetization never deviates from the easy axis. In practice, however, the magnetization will rotate slightly from the easy axis, producing additional volume charges as discussed in section IV A 2. This effect leads to a slight modification of the interaction kernel in Eq. (53)

$$\tilde{K}(p, q) \sim \frac{1}{\sqrt{Q}} \frac{p^2}{\sqrt{p^2 + Qq^2}}, \quad (56)$$

where $Q \equiv 1 + 2\mu_0 M_s^2/K$ is a material dependent constant [79].

The disorder present in the material in the form of non-magnetic impurities, lattice dislocations or residual stresses is responsible for the deformation and the pinning of the domain wall. In general, disorder can be modelled introducing a

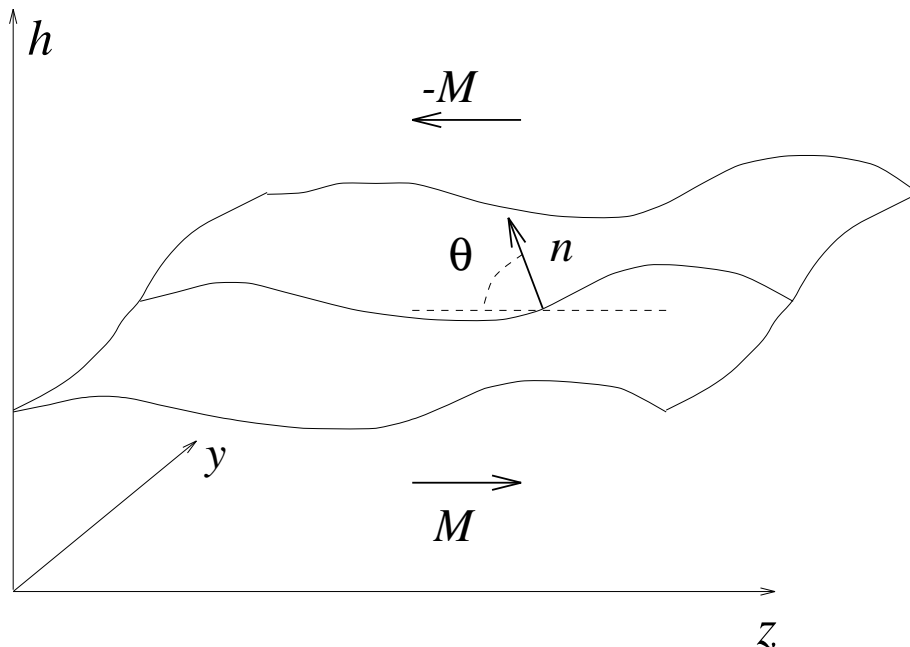


FIG. 25: A domain wall separating two regions of opposite magnetization. The discontinuities of the normal component of the magnetization across the domain wall produce magnetic charges.

random potential $V(\vec{r}, h)$, whose derivative gives the local pinning field $\eta(\vec{r}, h)$ acting on the surface. In the particular case of point-like defects, such as non-magnetic impurities, the random force is given by

$$\eta(\vec{r}, h) = - \sum_i f_p(\vec{r} - \vec{r}_i, h - h_i) \quad (57)$$

where (r_i, h_i) are the coordinates of the pinning centers and $f_p(x)$ is the individual pinning force, which typically has a range comparable with the domain wall width $\delta_w \simeq \sqrt{K/A}$. After coarse-graining at a scale larger than the typical distance between the pinning centers, this disorder can be replaced by a Gaussian random noise with correlations

$$\langle \eta(\vec{r}, h) \eta(\vec{r}', h') \rangle = \delta^2(\vec{r} - \vec{r}') R(h - h') \quad (58)$$

where $R(x)$ decays very rapidly for large values of the argument. It has been shown that the particular form of $R(x)$ (i.e. due to random-bond or random-field types of disorder) has not a relevant effect on the scaling laws associated the domain wall dynamics [106].

Another possible source of pinning is due to local variations of the domain wall energy γ_w [79], due for instance to random anisotropies. Thus the domain wall energy becomes a function of position $\gamma(\vec{r}, h)$ which we can expand about its average $\gamma_w + \eta(\vec{r}, h)$. Introducing this expression in Eq. 50, we obtain to lowest order an additional random term $\eta(\vec{r}, h)$, whose distribution and correlations can be directly related to the random anisotropies.

2. Domain wall dynamics and depinning transition

In most cases, the motion of the domain wall is strongly overdamped, since eddy currents cancel inertial effects. The equation of motion for the wall is thus given by

$$\Gamma \frac{\partial h(\vec{r}, t)}{\partial t} = - \frac{\delta E(\{h(\vec{r}, t)\})}{\delta h(\vec{r}, t)}, \quad (59)$$

where $E(\{h(\vec{r}, t)\})$ is the total energy functional, derived in the previous section, and Γ is an effective viscosity. We have neglected here thermal effects, since experiments suggest that these are not relevant for the Barkhausen effect in bulk three dimensional samples [53]. This could be different in thin films [107] where thermal activated motion can be described by adding an extra noise term to the equation of motion.

Collecting all the energetic contributions, we obtain the equation of motion for the domain wall [50]. In order to avoid a cumbersome notation all the unnecessary factors can be absorbed in the definitions of the parameters. The equation then becomes

$$\frac{\partial h(\vec{r}, t)}{\partial t} = H - \bar{k}\tilde{h} + \gamma_w \nabla^2 h(\vec{r}, t) + \quad (60)$$

$$\int d^2 r' K(\vec{r} - \vec{r}') (h(\vec{r}') - h(\vec{r})) + \eta(\vec{r}, h), \quad (61)$$

where the dipolar kernel K is reported Eq. (54), the effective demagnetizing factor is given by $\bar{k} \equiv 4\mu_0 k M_s^2 / V$ and $\tilde{h} \equiv \int d^2 r' h(\vec{r}', t)$. Owing to the fact that the demagnetizing field term is just an approximation, the dependence of k on the sample shape and size can be quite complex. Variants of Eq. (54) have been extensively studied in the past [49, 50, 54, 79, 103, 104, 105, 108, 109, 110, 111, 112, 113].

When the demagnetizing factor k is negligible, as for instance in a frame geometry, Eq. 61 displays a depinning transition as a function of the applied field H and the domain wall moves only if the applied field overcomes a critical field H_c . For fields $H > H_c$ the domain wall moves with an average velocity v that scales as

$$v \sim (H - H_c)^\beta \theta(H_c - H), \quad (62)$$

where $\theta(x)$ is the step function. The critical behavior associated to the depinning transition has been studied using renormalization group methods [106, 114, 115, 116], which show that at large length scales the critical exponents take mean-field values [49, 50]. This result is due to the linear dependence on the momentum of the interaction kernel (Eq. 54) in Fourier space [116, 117]. In general, if we consider an interface whose interaction kernel in momentum space scales as $K(q) = A_K |q|^\mu$, the upper critical dimension is given by $d_c = 2\mu$ and the values of the exponents depend on μ . Notice that here we define d as the internal dimension of the domain wall. Hence in the present analysis, we have a two dimensional interface ($d = 2$) moving in a three dimensional medium. While in general we would expect mean-field behavior, there are situations in which the dipolar coupling could be neglected with respect to the domain wall tension γ_w where one effectively could observe the critical behavior associated with $\mu = 2$.

In general, for interfaces close to the depinning transition, the response to small variations of the applied field occurs by avalanches whose sizes S are distributed as

$$P(S) \sim S^{-\tau} f(S/S_0), \quad (63)$$

where the cutoff scales as $S_0 \sim (H - H_c)^{-1/\sigma}$ and is related to the correlation length ξ by

$$S_0 \sim \xi^{d+\zeta}, \quad (64)$$

where ζ is the roughness exponent (Fig. 26). The correlation length diverges at the depinning transition as

$$\xi \sim (H - H_c)^{-\nu}, \quad (65)$$

which implies

$$\frac{1}{\sigma} = \nu(d + \zeta). \quad (66)$$

The average avalanche size also diverges at the transition

$$\langle S \rangle \sim (H - H_c)^{-\gamma}, \quad (67)$$

where γ is related to τ and σ by

$$\gamma = \frac{(2 - \tau)}{\sigma}, \quad (68)$$

and to ν and z by [106]

$$\gamma = (1 + \nu\zeta), \quad (69)$$

thus implying

$$\tau = 2 - \frac{1 + \nu\zeta}{\nu(d + \zeta)}. \quad (70)$$

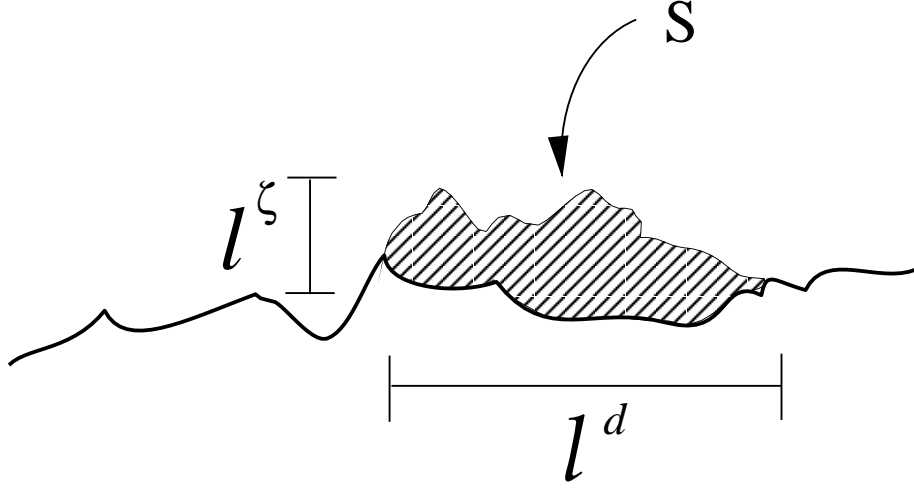


FIG. 26: The domain wall moves between two pinned configuration in an avalanche of size $S \sim l^{d+\zeta}$

The other exponent relevant for the Barkhausen effect describes the distribution of avalanche durations

$$P(T) \sim T^{-\alpha} g(T/T_0), \quad (71)$$

where the cutoff diverges at the transition as $T_0 \sim (H - H_c)^{-1/\Delta}$. From Eq. (65) and the relation $T_0 \sim \xi^z$ we obtain $\Delta = 1/z\nu$ and

$$\alpha = 1 + \frac{\nu d - 1}{z\nu}. \quad (72)$$

Finally, an additional symmetry of the equation of motion can be used to reduce the number of independent exponents through the relation

$$\nu(\mu - \zeta) = 1 \quad (73)$$

The renormalization group analysis allows for a determination of the critical exponents in the framework of $\epsilon = d_c - d$ expansion. As discussed above, for $\mu = 1$ we expect mean-field results $\tau = 3/2$ and $\alpha = 2$, while for $\mu = 2$ to first order in ϵ one obtains $\tau = 5/4$ and $\alpha = 11/7$. Recently a two loop expansion has been carried out, allowing for an estimate to order $O(\epsilon^2)$ of the exponents ($\tau = 1.24$ and $\alpha = 1.51$) [116]. Finally, numerical simulations yield $\tau = 1.27$ and $\alpha = 1.5$ for $\mu = 2$.

The discussion above applies strictly to the case $k = 0$ and scaling requires that H is close to H_c . If one would instead ramp the field slowly, sampling the avalanche distribution over all the values of the field, the result will be different. We need to integrate Eq. 63 over H [50]

$$p_{int}(S) = \int^{H_c} dH S^{-\tau} f(S(H - H_c)^{1/\sigma}) \sim S^{-\tau_{int}}, \quad (74)$$

with $\tau_{int} = \tau + \sigma$. Using the values of τ and σ reported above, we obtain $\tau_{int} = 1.72$ for $\mu = 2$ and $\tau_{int} = 2$ for $\mu = 1$. A similar discussion can be repeated for avalanche duration, yielding $\alpha_{int} = \alpha + \Delta$. The numerical result is $\alpha_{int} = 2.3$ and for $\mu = 2$ and $\alpha_{int} = 3$ for $\mu = 1$.

In a typical Barkhausen experiment, however, the situation changes since $k > 0$ and H is normally increased at constant rate. The effective field acting on the domain wall is given by $H_{eff} = ct - k\bar{h}$. Thus, according to Eq. 62, when $H_{eff} < H_c$ the domain wall is pinned and the effective field increases. As soon as $H_{eff} > H_c$ the domain wall acquires a finite velocity and \bar{h} increases. As a consequence, the effective field will be reduced until the domain wall stops. This process keeps the domain wall close to depinning transition, but criticality is only reached in the limit $c \rightarrow 0$ and $k \rightarrow 0$. A similar mechanism occurs in models of self-organized criticality [118].

The demagnetizing factor k represents a restoring force hindering the propagation of Barkhausen avalanches. Thus when $k > 0$, we expect to find a finite avalanche size cutoff S_0 . The domain wall can not propagate over distances larger than ξ , defined as the length at which the interaction term $A_K|q|^\mu$ is equal to the restoring force

$$A_K h \xi^{-\mu} \sim k \xi^d h \quad (75)$$

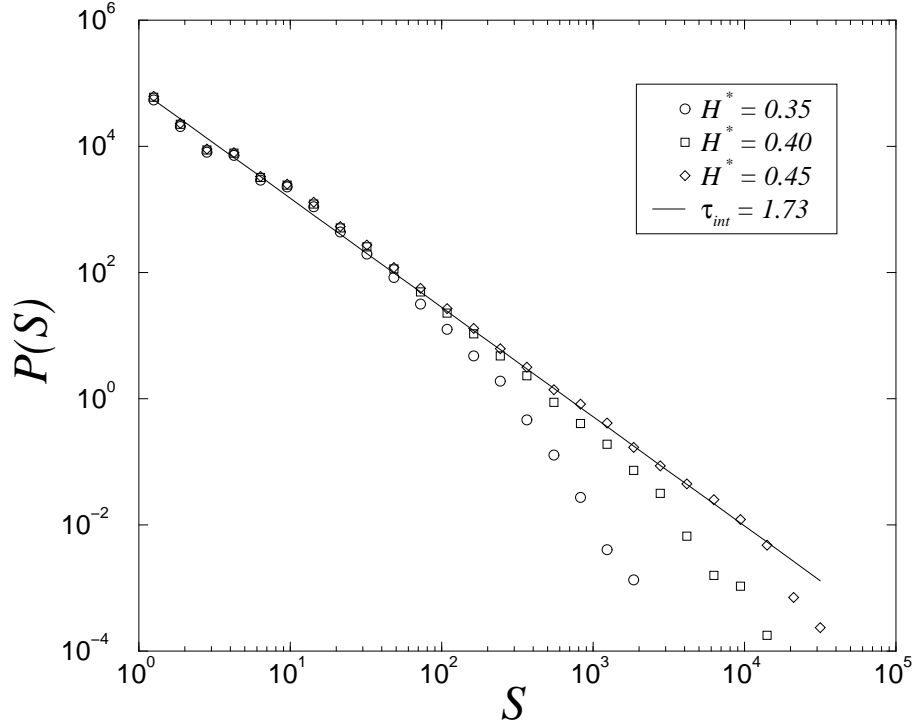


FIG. 27: The distribution of avalanche sizes in the short-range domain wall model at $k = 0$ when the field is swept from $H = 0$ to $H = H^* < H_c$. For $H^* \rightarrow H_c$, we obtain $\tau_{int} = \tau + \sigma$.

which implies

$$\xi \sim (k/A_K)^{-\nu_k} \quad \nu_k = 1/(\mu + d). \quad (76)$$

The avalanche size and duration distributions cutoff S_0 and T_0 can be obtained using the scaling relations reported above

$$S_0 \sim D(k/A_k)^{-1/\sigma_k}, \quad 1/\sigma_k = (d + \zeta)/(\mu + d) \quad (77)$$

and similarly

$$T_0 \sim (k/A_k)^{-\Delta_k}, \quad \Delta_k = z/(\mu + d), \quad (78)$$

where $D \equiv \sqrt{\langle \eta^2 \rangle}$ denotes the typical fluctuation of the disorder. Inserting in Eqs. (77-78) the renormalization group results to first order in ϵ [106, 114, 115] $\zeta = (2\mu - d)/3$ and $z = \mu - (4\mu - 2d)/9$, we obtain $1/\sigma_k = 2/3$ and $\Delta_k = (\mu - (4\mu - 2d)/9)/(\mu + d)$. Using the results obtained to order ϵ^2 [116], one obtains instead for $\mu = 2$, $1/\sigma_k = 0.71$ and $\Delta_k = 0.345$. The numerical values obtained from simulations are in good agreement with this prediction (see Fig. 28).

The mean-field theory, which provides a good qualitative description of the depinning transition and describes quantitatively the data for $d = d_c$ (apart from logarithmic corrections), is obtained discretizing the equation of motion, coupling all the sites with the average domain wall position \bar{h} [119]. The dynamics of such an infinite range model is described by

$$\frac{dh_i}{dt} = ct - k\bar{h} + J(\bar{h} - h_i) + \eta_i(h), \quad (79)$$

where J is an effective coupling and $i = 1, \dots, N$. Summing over i both sides of Eq. (79), one obtains an equation for the total magnetization m

$$\frac{dm}{dt} = \tilde{c}t - km + \sum_{i=1}^N \eta_i(h). \quad (80)$$

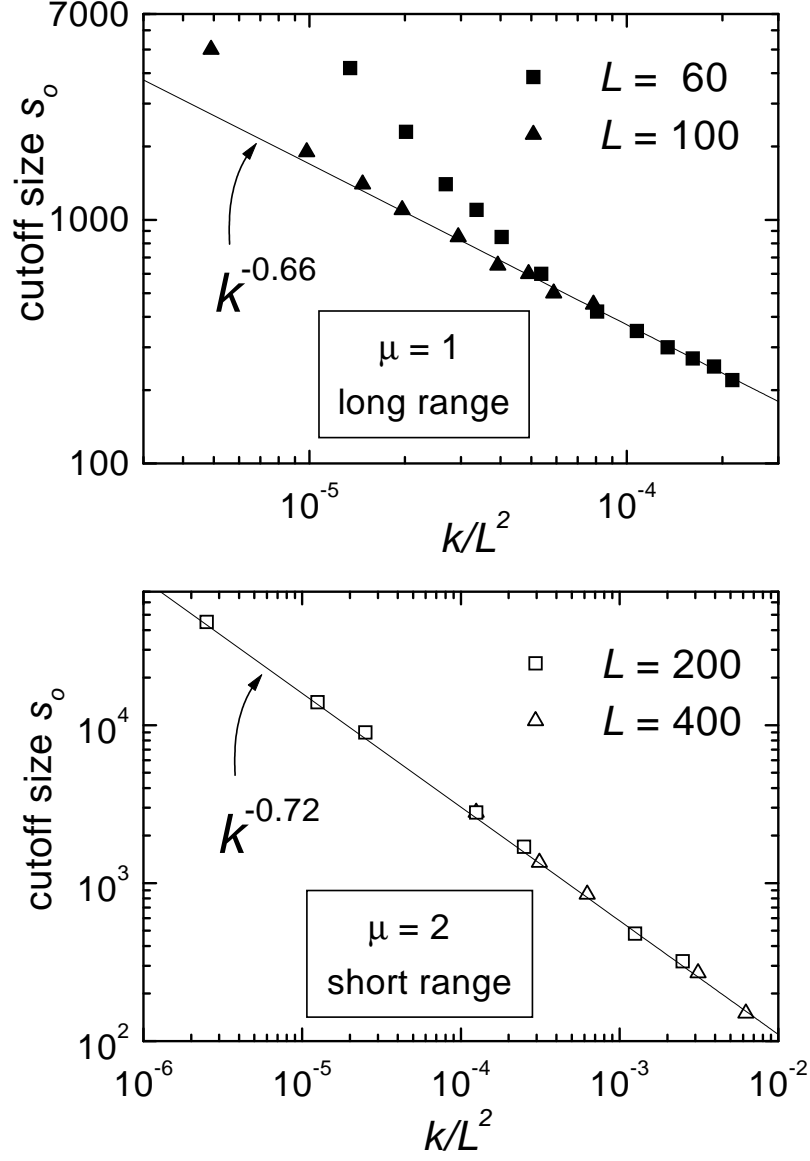


FIG. 28: The cutoff S_0 of the avalanche size obtained from numerical simulations for different demagnetizing factors. The two universality classes correspond to a kernel in the equation of the $|q|^\mu$ type in Fourier space, with $\mu = 1$ (long range dipolar interactions - up), and $\mu = 2$ (short range elastic interactions - down).

This equation has the same form of the ABBM model (see Eq. 28) [16].

To make the similarity more stringent, we should interpret $\sum_i \eta_i$ as an effective pinning $W(m)$, with Brownian correlations. When the domain wall moves between two pinned configuration W changes as

$$W(m') - W(m) = \sum_{i=1}^n \Delta\eta_i, \quad (81)$$

where the sum is restricted to the n sites that have effectively moved (i.e. their disorder is changed). The total number of such sites scales as $n \sim l^d$ and in mean-field theory is proportional to the avalanche size $S = |m' - m|$ (since $S \sim l^{d+\zeta}$ and $\zeta = 0$). Assuming that the $\Delta\eta_i$ are uncorrelated and have random signs, we obtain a Brownian

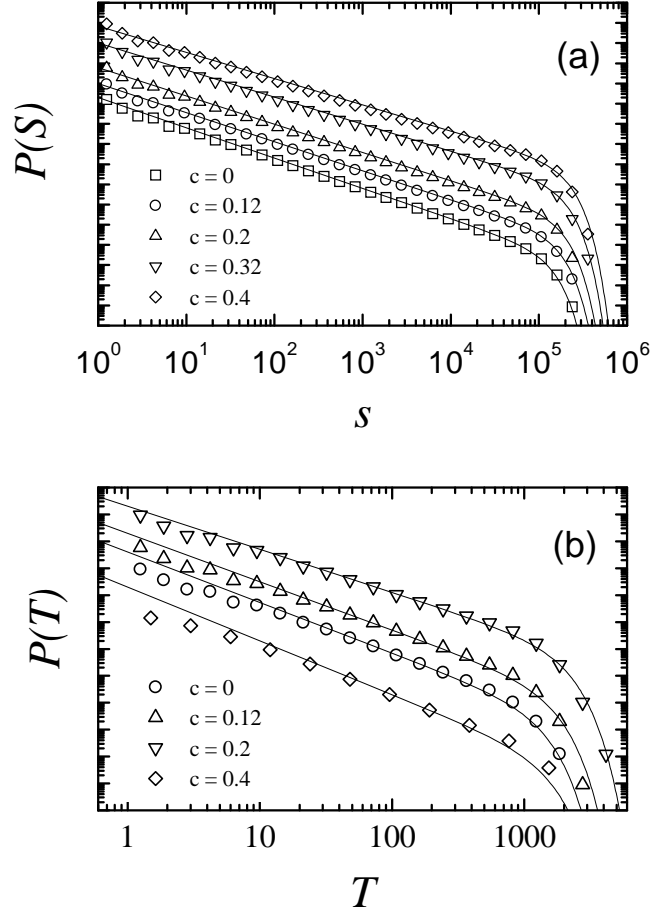


FIG. 29: (a) The distribution of avalanche sizes in the infinite-range model for different driving rates for $N = 32696$. The fit of the power-law part yields $\tau = 3/2 - c/2$, with $c = \tilde{c}/D$ and $1/D \simeq 1.2$. (b) The corresponding distribution of avalanche durations. The power-law part is fit with an exponent $\alpha = 2 - c$.

effective pinning field

$$\langle |W(m') - W(m)|^2 \rangle = D|m' - m|, \quad (82)$$

where D quantifies the fluctuation in W . Thus the Brownian pinning field, introduced phenomenologically in the ABBM model, is an effective description of the disorder resulting from the collective motion of a flexible domain wall. As a consequence of this mapping, we expect that the infinite range model displays the same frequency dependence of the exponents as in the ABBM model (Eq. 34). Simulations confirm this claim as shown in Fig. 29.

V. DISCUSSION OF THEORETICAL RESULTS

A. Avalanches distributions

The models discussed in Sec. IV provide different result and theoretical interpretation for the pulse distributions. While we have reported already the results obtained for the various models, for the sake of clarity we summarize here again the main conclusions. We have distinguished between two general classes of models: spin models and domain walls model. Rigorously speaking the second class is contained in the first, since a domain structure is typically present

model	τ	α	$\sigma\nu z$	$1/\sigma$	$1/\sigma_k$	Δ_k	τ_{int}	α_{int}
RFIM $d = 3$	1.60 ± 0.06	2.05 ± 0.12	0.57 ± 0.03	4.2 ± 0.3	-	-	2.03	2.81
MF (ABBM)	3/2	2	1/2	2	2	1	2	3
LRDW	1.5	2	0.5	2	0.65 ± 0.05	0.3 ± 0.1	2	3
SRDW	1.27 ± 0.02	1.50 ± 0.05	0.57 ± 0.02	2.2 ± 0.1	0.72 ± 0.03	0.39 ± 0.05	1.72	2.3

TABLE II: The values of critical exponents estimated from simulations of the RFIM [93] and domain wall models with short-range (SRDW) and long-range (LRDW) interactions [21, 120]. Mean-field (MF) results are the same for both classes of models and coincide with ABBM exponents. The exponent σ describes the scaling of the avalanche size cutoff with the reduced control parameter, $R - R_c$ in the RFIM and $H - H_c$ in domain wall models. For $k > 0$ and $R < R_c$ the RFIM reduces to the SRDW model and those exponents apply.

in spin systems, but the analysis of domain wall dynamics would be needlessly complicated. It is useful instead to treat separately the case in which domain wall propagation does not interfere with nucleation.

The two classes of models yield different interpretation of the origin of scaling in the Barkhausen pulse distributions. In spin models, scaling is ruled by the proximity to a disorder induced critical point. The cutoff to the power law scaling is determined by the distance from this critical point. The broadness of the critical region would justify the wide occurrence of scaling in experiments, without any apparent parameter tuning [69]. In domain wall models scaling is dictated by a different critical point: the depinning transition. The interplay between slow driving ($c \rightarrow 0$) and small demagnetization $k \rightarrow 0$ keeps the domain wall close to the depinning critical point. The cutoff of the distributions is then controlled by the value of k , which in strip geometries is typically small. A collection of the numerical estimates of the Barkhausen noise distribution exponents for the RFIM and domain wall models is reported in Table II.

Depending on the problem at hand the appropriate model for the Barkhausen noise may vary. In soft magnetic ribbons the domain structure is typically controlled by dipolar interactions and the sample shape, imposing a parallel set of domain walls spanning the sample from end to end. In this condition, the depinning scenario should apply as it is testified by the experimental findings. The avalanche exponents are in good agreement with the prediction of the depinning model and the cutoff is controlled by the demagnetizing factor.

In particular, experiments on polycrystalline SiFe are well described by the ABBM model or, equivalently, by a long-range depinning model. The exponents measured in amorphous alloys are instead well fitted by the short range interface model. This is due to the fact that in amorphous alloys the average anisotropy vanishes and thus dipolar interactions have no effect on the domain wall dynamics (i.e. Q in Eq. 56 is very large). On the contrary, in polycrystalline materials, every crystal is the source of a relevant anisotropy and long range effects occur. This is confirmed by the fact that long-range exponents are found when small crystallites are induced in an amorphous matrix by proper thermal annealing [21].

The scaling exponents measured in experiments on NiFe [51] wires and Vitrovac [25] could be also explained in this framework if one assumes that the Barkhausen signal was not stationary. This could occur if the field is not swept up to saturation so that the effective field varies and it is not kept around H_c as in most cases. Then one would obtain integrated exponents τ_{int} , α_{int} instead of τ and α . The striking similarity between the experimentally measured exponents and the theoretical ones (i.e. $\tau_{int} = 1.72$ and $\alpha_{int} = 2.3$) supports this conclusion.

Spin models could instead apply to cases in which the domain structure is more intricate and the effect of dipolar forces negligible. A typical example would be an hard magnetic materials, with strong local anisotropies. Systematic investigation of the Barkhausen effect in hard magnetic materials has just been started and a quantitative comparison between experiments and theory is still not possible.

An important problem to address, regardless of the theoretical framework, is the effect of the field rate on the Barkhausen noise statistics. As we discussed in section IV B the ABBM predicts a linear dependence from the exponents τ and α from the field rate, encoded in the parameter c . This result applies as well for the mean-field domain wall model (see Fig. 29) and agrees well with experiments on FeSi alloys. Simulations of the short-range domain wall model show that the scaling exponents do not change continuously as in mean-field, but a peak appears for large values of the jump size and grows with the rate [105] (see Fig. 30). While one could fit the result for higher driving rate with a different exponents, such a fit does not appear very reliable and a constant exponent coexisting with a growing peak seems a more appropriate approximation. A similar result is found in amorphous soft magnetic alloys, as shown in Fig. 5.

The effect of the driving rate on the avalanche distributions was analyzed in more general terms in Ref. [26]. A set of results can be derived under some basic assumptions:

- (i) The system is close to a critical point, so that in the adiabatic limit ($c \rightarrow 0$) the size and duration distributions are a power law.
- (ii) The avalanche signal is stationary under the time window considered.
- (iii) In the adiabatic limit, the average number of avalanche nucleation events per unit field increase is a smooth function of the driving field.

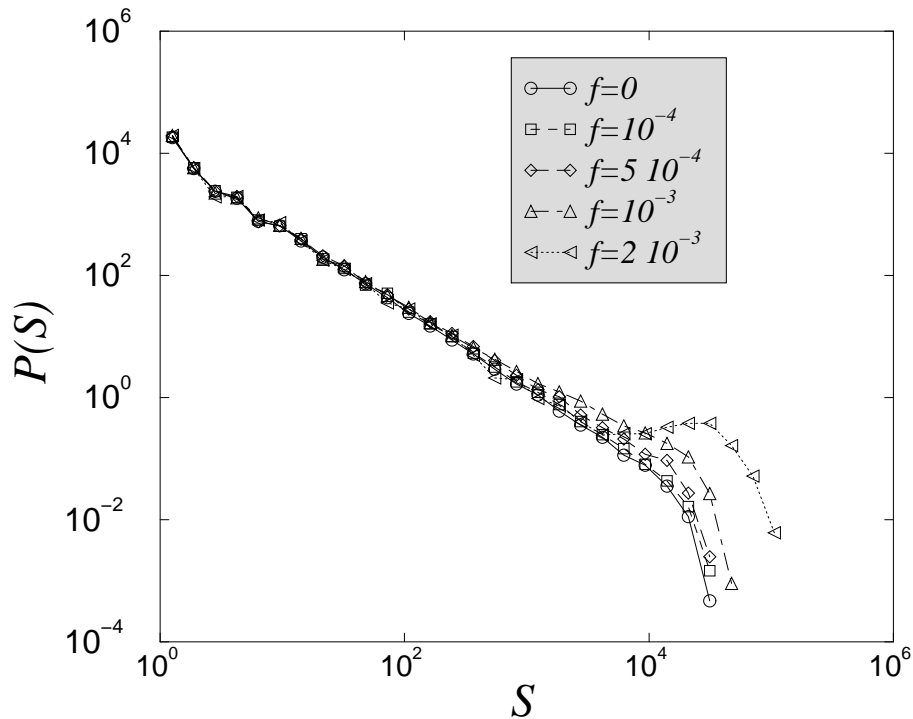


FIG. 30: The distribution of Barkhausen jump sizes from a short-range domain wall model for different driving field frequencies. While the scaling regime remains essentially unchanged a peak occurs around the cutoff. (See also Ref. [105])

(iv) For low c the avalanche dynamics is independent of c . (v) The field increases between avalanche nucleations is independent of the avalanche sizes. (vi) The avalanche sizes are uncorrelated in time. (vii) Avalanches are nucleated randomly in space.

All these assumption are reasonable both for the domain wall models and for spin models. Notice, however, that assumption (ii) restricts the derivation to a stationary signal and thus does not apply to distributions measured integrating along the entire hysteresis loop.

Under the assumptions above, one can show that the effect of the driving rate depends on the value taken by the exponent α in the duration distribution for $c \rightarrow 0$. For $\alpha > 2$ the distributions are unaffected by the driving rate, while for $\alpha < 2$ a peak appears at large sizes and durations. The interesting case is $\alpha = 2$, which corresponds to a linear dependence of the exponents from the driving rate c , recovering the ABBM result in Eq. 34. This general derivation provides an explanation of the results of experiments and numerical simulations, predicting the conditions under which drive dependent exponents should be observed.

B. The power spectrum

Explaining the power spectrum of the Barkhausen noise has been one of the main objectives of the past theoretical activity. In earlier approaches the power spectrum was considered as the result of a superposition of elementary independent events (see for instance [121, 122]) without a clear relation to the microscopic magnetization processes. A step forward in this direction was made in the framework of the ABBM model [16, 17].

From Eq. 28 one can derive a Fokker-Plank equation describing the evolution of the probability distribution $P(v, t|v_0)$ to have a velocity v at time t when the velocity at $t = 0$ is v_0 [16]

$$\frac{\partial P}{\partial t} = \frac{\partial}{\partial v} \left((kv - c)P + D \frac{\partial v P}{\partial v} \right). \quad (83)$$

Notice that, as in section IV B, we have rescaled time setting a damping constant equal to one. The velocity correlation function is defined as

$$G(t) \equiv \langle (v(t) - c/k)(v(0) - c/k) \rangle = \int dv dv_0 (v - c/k)(v_0 - c/k) P(v, t|v_0) P(v_0), \quad (84)$$

where $P(v_0)$ is given by Eq. 33. Deriving Eq. 84 and using Eq. 83, we obtain an evolution equation for $G(t)$

$$\frac{dG}{dt} = -kG, \quad (85)$$

which can be easily solved yielding

$$G(t) = c/k \exp -kt. \quad (86)$$

The power spectrum has thus a Lorentzian shape

$$F(\omega) = \frac{2c}{\omega^2 + k^2}. \quad (87)$$

This simple result contains several interesting predictions: (i) at large frequencies the spectrum decays as ω^{-2} . (ii) The scaling is cut off below a frequency $\omega_0 = 1/k$. (iii) The amplitude of the spectrum increases with the field driving rate c . These features describe qualitatively the shape of the experimentally measured power spectrum, but not quantitatively. For instance, the tail of the spectrum often decays with an exponent different than 2 and the cutoff frequency depends on k but not simply as $1/k$.

To reproduce the low frequency increase of the power spectrum, the ABBM model can be modified introducing a correlation length ξ^* in the pinning field [16]. This gives rise to a power spectrum of the type

$$F(\omega) \propto \frac{\omega^2}{(\omega^2 + k^2)(\omega^2 + \tau_c^{-2})}, \quad (88)$$

where $\tau_c \propto \xi^*$. The ABBM predictions for the power spectrum can be compared with numerical simulations of the infinite-range domain wall model (Eq. 79) for different values of c . The result in Fig. 31 are, as expected in good agreement with the theory.

Several attempts have been made in the past to link through scaling relations the power spectrum exponent to the scaling exponents describing the avalanche distributions [25, 50, 51, 75, 103]. The comparison between these results and experiments is, in most cases, not satisfactory. In any case, a simple exponent would just describe the tail of the power spectrum, while a complete theory should explain the entire shape observed experimentally. The problem was recently revisited in Ref. [74] where all the assumptions underlying previous scaling approaches [25, 50, 51, 75, 103] were carefully scrutinized and tested. Through a combination of analytical methods and numerical simulations, Kuntz and Sethna [74] found a scaling relation describing the high frequency tail of the spectrum which seems to be in good agreement with experiments [65].

The derivation of Ref. [74] follows different steps involving some assumptions which can be tested numerically and experimentally. Close to criticality one expect that the average size for an avalanche of duration T scales as $S(T) \sim T^{1/\sigma\nu z}$ and consistently the average shape scales as

$$v(T, t) = T^{1/\sigma\nu z - 1} f_{shape}(t/T), \quad (89)$$

where v is the signal voltage, t is the time and $f_{shape}(t/T)$ is a (possibly universal) scaling function.

The second assumption involves the probability $P(v|S)$ that a voltage v occurs in an avalanche of size S . This probability scales as:

$$P(v|S) = v^{-1} f_{voltage}(vS^{\sigma\nu z - 1}) \quad (90)$$

where $f_{voltage}$ is another universal scaling function. Using this equation one can show that the energy $E = \langle v^2 \rangle$ of an avalanche of size s scales as $E(S) \sim S^{2-\sigma\nu z}$. The analysis proceeds with the calculation of the voltage correlation function

$$G(t) \equiv \int dt' \langle v(t+t')v(t) \rangle, \quad (91)$$

which can be decomposed into various contributions for each avalanche $G(t|S)$. This quantity obeys a scaling law

$$G(t|S) = S^{2-\sigma\nu z} f_G(tS^{-\sigma\nu z}). \quad (92)$$

The contribution to the power spectrum is then obtained by a cosine transformation

$$F(\omega|S) = \int_0^\infty dt \cos(\omega t) G(t|S) = S^2 f_{energy}(\omega^{-1/\sigma\nu z} S). \quad (93)$$

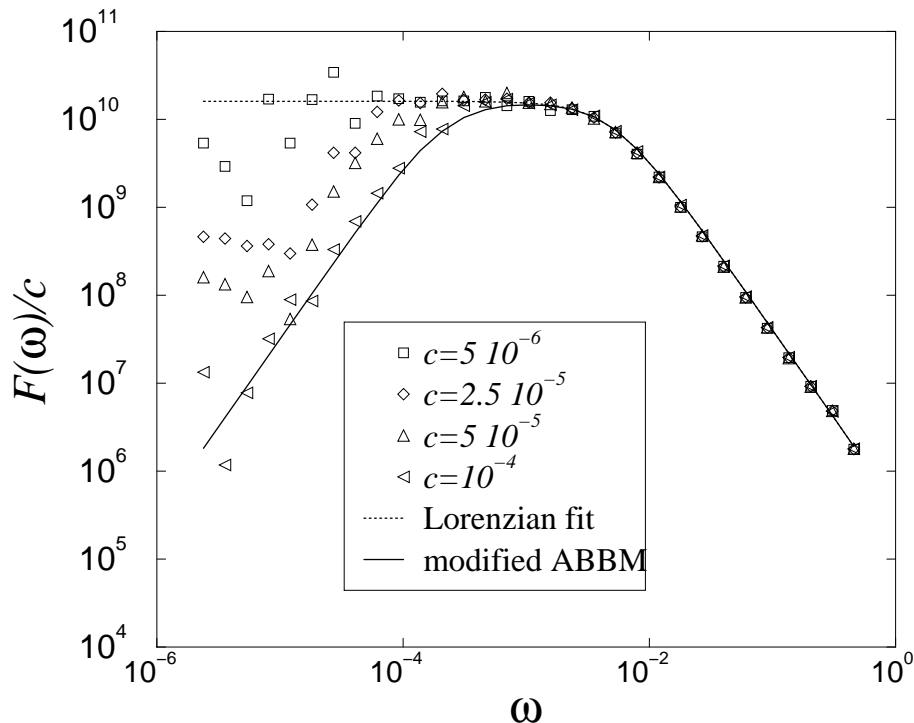


FIG. 31: The power spectrum measured in the infinite-range domain wall model for different field rates c . The tail is well fitted by a Lorentzian function with amplitude proportional to c . The entire spectrum is in perfect agreement with the ABBM result.

To obtain the power spectrum of the signal one should average Eq. 93 over different avalanche sizes. A naive estimate of the integral resulting from the average of Eq. 93 using $P(S) \sim S^{-\tau}$ leads to the incorrect prediction [25, 51, 75] $F(\omega) \sim \omega^{-(3-\tau)/\sigma\nu z}$. The reason behind this incorrect result comes from the fact that $f_{energy}(x) \sim 1/x$ for large x . Thus, if $\tau < 2$, the leading contribution to the averaged power spectrum comes from the upper cutoff in the size distribution, ultimately leading to the result [74]

$$F(\omega) \sim \omega^{-1/\sigma\nu z}. \quad (94)$$

Using mean field exponents $\sigma\nu z = 1/2$, we recover the ABBM result $F(\omega) \sim \omega^{-2}$. The result in Eq. 94 agrees reasonably well with experiments and is confirmed by numerical simulations of the domain wall model (see Figs. 31 and 32).

C. The avalanche shape

The problem of the Barkhausen avalanche shape was first introduced in Ref. [74] and proposed as a strong test to characterize the universality classes of the Barkhausen noise. Subsequently, Ref. [66] analyzed more systematically the results of numerical simulations for the RFIM with and without demagnetizing field. The conclusion reached is that the average avalanche shape is in both case symmetric and close to a parabolic shape. The pulse shape changes slightly with and without demagnetizing field although a reasonable collapse of the two set of curves can be obtained multiplying one set by a factor (see Fig. 33). Small differences emerge from a more detailed fitting procedure. A favorable comparison with experiments and a theoretical explanation of the numerical results is, however, still lacking.

The general problem of the shape of a stochastic excursion was recently addressed in more generality by Baldassarri et al. [123]. The authors show that for a broad class of stochastic processes the average shape of the excursion is a semicircle. This occurs irrespective of the value of the scaling exponent (the equivalent of $\sigma\nu z$). Thus in this sense the shape would appear to be more universal than the exponents. On the other hand, the shape and symmetry of the average shape can be changed at will introducing correlations in the stochastic process [123] and it is even possible to construct two stochastic processes with the same scaling exponents, but different shapes. This calls into question the idea that the shape is a universal function [124].

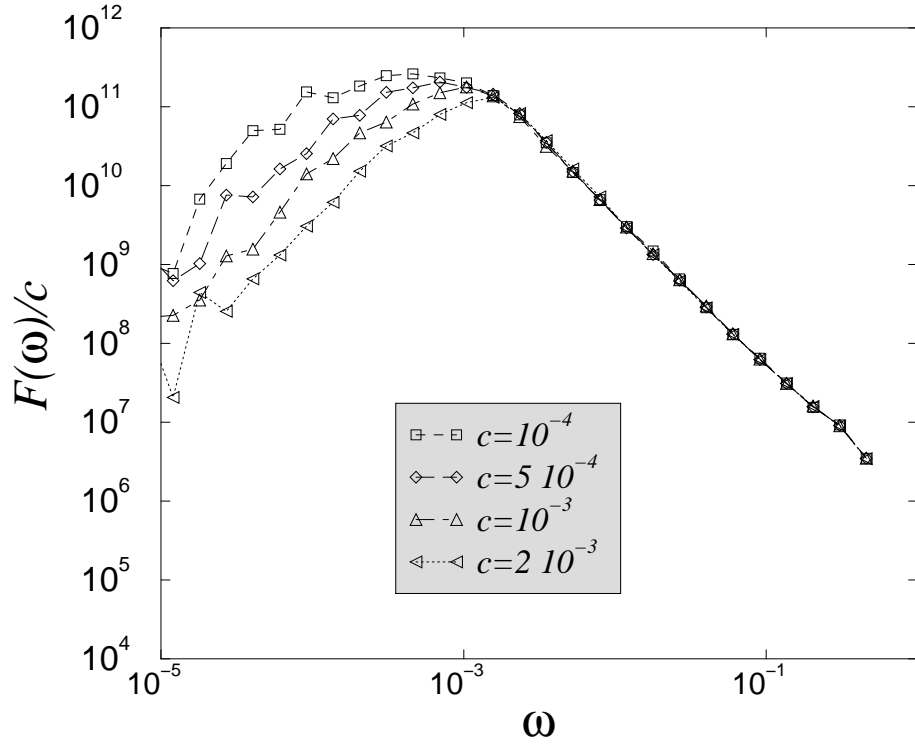


FIG. 32: The power spectrum measured in the short-range domain wall model for different field rates c . The tail is well fitted by a power law $\omega^{-1.8}$, in good agreement with Eq. 94, which predicts an exponent $1/\sigma\nu z = 1.77$.

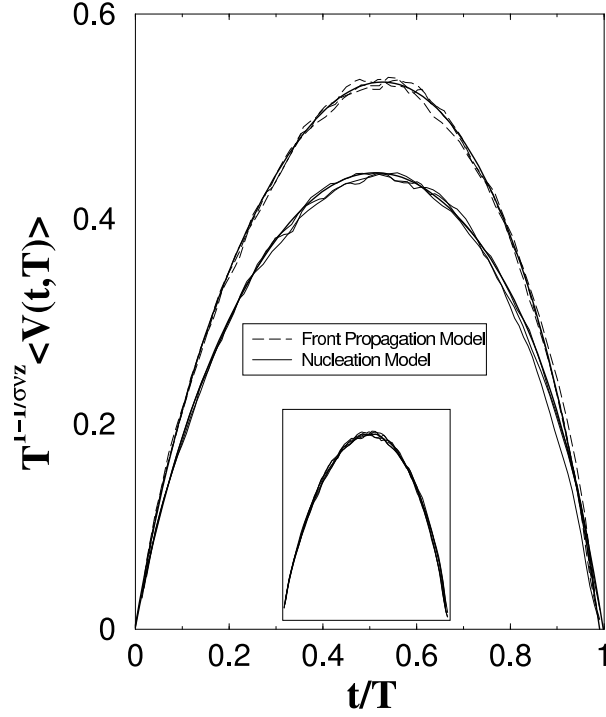


FIG. 33: The avalanche shapes for the RFIM with and without demagnetizing field (the second case is referred as front propagation). The shapes for different times have been collapsed using the value $1/z\sigma\nu = 1.72$ and $1/z\sigma\nu = 1.75$ in the two cases. An additional normalization factor allows to rescale the two set of curves together. [From [66], Fig. 1, pg. 046139-3]

The approach of Ref. [123] can be extended to compute the shape exactly of the Barkhausen pulses in the ABBM model [125]. Neglecting the contribution of the demagnetizing factor k , Eq. 31 describes the motion of a $1d$ random walk in a logarithmic potential $E(v) = -c \log(v)$, where the magnetization s plays the role of time. The corresponding Fokker–Planck equation is

$$\frac{\partial P(v, s)}{\partial s} = \frac{\partial}{\partial v} \left(-\frac{c}{v} + \frac{\partial}{\partial v} P(v, s) \right), \quad (95)$$

where $P(v, s)$ is the probability to find the walk in v at s . We are interested in a solution of this equation with the initial condition $P(v, 0) = \delta(v - v_0)$ and an absorbing boundary at the origin $v = 0$. Following Ref. [90] we can express this solution in terms of modified Bessel functions. For the case $0 < c < 1$, which is the condition of the ABBM model to have power laws in the avalanche distribution (see Eq. 1, and Ref. [16]), the probability $P(v, s|v_0, 0; c)$ for a walk starting at v_0 to be at v after a “time” s , in the limit $v_0 \rightarrow 0$ is simply proportional to a power of v times a Gaussian with variance s , and the average excursion of the walk is then obtained as

$$\langle v \rangle \propto \sqrt{s(S - s)} \quad (96)$$

This results means that the universal scaling function g_{shape} is proportional to a semicircle.

It is also possible to calculate the function f_{shape} in the time domain [125]. By definition, the avalanche size s at time t is given by the integral of $v(t, T)$ from time zero to time t :

$$s = \int_0^t dt' v(t', T) \propto T^{1/\sigma\nu z} \int_0^{t/T} f(x) dx, \quad (97)$$

which provides an expression of $s = s(t, T)$ as a function of t and T . If we now impose

$$v(t, T) = v(s = s(t, T), S(T)) \quad (98)$$

we get an integral equation for f_{shape} involving g_{shape}

$$f_{shape}(x) \propto g_{shape} \left(\int_0^x g(x') dx' \right). \quad (99)$$

Using the form of g_{shape} computed previously, we can solve this equation with the boundary conditions $f(0) = f(1) = 1$. The solution is

$$f_{shape}(x) \propto \sin(\pi x), \quad (100)$$

i.e. the universal function f_{shape} is proportional to an arch of sinusoid. Finally for the normalized avalanche one obtains

$$v(s, S) = S^{1-\sigma\nu z} \pi \sqrt{(s/S)(1 - s/S)}, \quad (101)$$

$$v(t, T) = T^{1/\sigma\nu z - 1} \pi/2 \sin(\pi t/T). \quad (102)$$

D. Two dimensions

The discussion presented so far focused on three dimensional systems, which is relevant for most Barkhausen noise experiments. The experimental results obtained in thin magnetic field require instead an analysis of two dimensional models. This task is not straightforward and several new features arise in two dimensions. The demagnetizing field, that plays a major role in determining the statistical properties of the Barkhausen noise, vanishes for very thin samples. For this reason, often we do not have have a simple parallel domain structure as in three dimensional ribbons and an analysis of single domain walls would not be appropriate. On the other hand, an approach in terms of spin models suffers for different difficulties, since there is no consensus on the presence of a disorder induced transition in two dimensions.

The RFIM has been extensively simulated in $d = 2$, using extremely large systems sizes (up to $(7000)^2$) [69, 93]. Despite this, it was not possible to obtain a reliable estimate of the threshold R_c for disorder induced transition. The simulations are consistent either with a vanishing threshold or with very large correlation critical exponents

(i.e. $\nu = 5.3 \pm 1.4$, $1/\sigma = 10 \pm 2$ with $R_c = 0.54$). An avalanche scaling exponent has also been estimated as $\tau_{int} = 2.04 \pm 0.04$. Additional results and analysis have appeared in the literature, but are not particularly reliable, being based on much smaller system sizes. Typically the presence of a disorder induced transition is assumed and exponents are evaluated [60, 126, 127]. A similar discussion would apply other models analyzed in the literature, like the RBIM [95, 128], the RFIM with site dilution [129] and dipolar interactions [99]. In summary, the large scale hysteretic behavior of disordered spin models in $d = 2$ is quite controversial and quantitative predictions seem at the moment not available. A possibility is that $d = 2$ is the lower critical dimensions, as it is expected for these models in equilibrium [130]. If this is the case, power law scaling may still be observed for low disorder, with the conjecture that $\tau = 3/2$ [69]. Nevertheless, we feel that at present the results of both experiments and models are still unreliable to make a comparison.

Even in thin films there are several cases in which a domain wall model may be appropriate. In particular, in the magnetooptical measurements of Ref. [32, 33] one observes directly Barkhausen jumps due to domain wall motion. The equation of motion for a single domain wall in two dimensions is similar to the one in three dimensions (e. g. Eq. 61) with some notable differences. For thin films with in plane magnetization the demagnetizing factor k is virtually zero and in Fourier space the dipolar kernel (Eq. 54) does not scale as q but as $q^2 \log(aq)$ where a is a small scale cutoff [131, 132]. Apart from the logarithmic correction, the dipolar term is similar to the domain wall energy and thus in principle should not significantly affect the universality class of the depinning transition. Numerical simulations, however, yield slightly different results in the two cases (for instance $\zeta = 1$ with long-range forces and $\zeta = 1.2$ without [133, 134]). While the short-range interface model has been studied extensively in two dimensions, less is known for the long-range problem. A result that could be relevant for the Barkhausen effect would be the avalanche distribution exponent which has been numerically estimated for short-range models: $\tau = 1.13 \pm 0.02$ [135], $\tau = 1.02 \pm 0.29$ [136]. The most reliable and precise estimate is probably $\tau = 1.115$ [137].

Before comparing simulation data with the experiments one has to be certain of the quantity effectively measured. When the demagnetizing factor is zero, a ramp up of the field does not lead to a Barkhausen stationary signal with $H_{eff} = H_c$, but the avalanches grow up to H_c . One would then measure an effective exponent $\tau_{int} = \tau + \sigma$. Given the relation $\sigma = \nu/(d + \zeta)$ and $\zeta = 1.25$ and $\nu = 1.33$ [115] we obtain $\tau_{int} \simeq 1.6$. If instead of ramping up the field, one would instead keep it fixed just below H_c as in Ref. [32, 33], then we would expect that the avalanche distribution scales with τ . Notice, however, that the avalanche “size” S defined in Ref. [32, 33] is not what we have defined, but is instead proportional to the change in the displacement Δh . Avalanches are only counted when the transverse length l (see Fig. 26) is larger than the system size L . Hence $S = L\Delta h$ with a constant L . Using scaling relation one can show that the exponent measured $\tau_h = ((\zeta + 1)\tau - 1)/\zeta \simeq 1.2$, which is still lower than the estimated value but could be consistent with the data.

Finally, we mention that spin models have been also used to study the dynamics of a single domain wall including overhangs. Simulations have shown a crossover from flat to fractal depending on the disorder strength [138]. The relation between these phenomenon and the Barkhausen noise still remains to be explored.

VI. CONCLUSIONS AND PERSPECTIVES

The Barkhausen effect has been studied for almost a century. While the essence of the phenomenon, i.e. an irregular magnetization reversal process occurring at the microscopic scale, was already indicated in the original paper by Barkhausen, a quantitative and detailed understanding was gained only recently. The key to this achievement is twofold: the injection in the field of methods and theories drawn from statistical mechanics of non-equilibrium critical phenomena and the identification of a standard experimental setup to collect reproducible and statistically significant data. These two aspects are tightly linked, since the necessity of rationalizing the experimental setup and to perform a detailed statistical analysis of the data was dictated by the theory, which was stimulated on its turn by the indication of scaling behavior coming from experiments.

The successful understanding outlined above is restricted mostly to the Barkhausen noise measured in bulk soft magnetic alloys, ribbons in particular. These are particularly instructive from the theoretical point of view because of the relatively simple parallel domain structure, induced by the interplay between dipolar forces and the sample geometry. The magnetization process is mainly due to domain wall motion in a disordered landscape which is responsible for the avalanche dynamics leading to the observed noise. The scaling behavior describing the statistical properties of the noise (avalanche distributions, power spectrum) can be related to an underlying domain-wall depinning transition. Critical phenomena are typically associated to a certain degree of universality: the scaling exponents do not depend on the microscopic details of the system but only on general symmetries, dimensionality, and long-range properties of the interactions. One would thus expect to be able to classify materials in broad universality classes, sharing the same critical exponents, irrespective to the microscopic details, such as sample composition, grain size or disorder strength.

To some extent experimental results confirm this expectation: polycrystalline SiFe alloys with different grain sizes and Si content, together with partially crystallized Co based alloys were all found to share the same critical exponents. Amorphous alloys of different composition are instead grouped in a different class characterized by a different set of exponents. These two groups of exponents coincide with those associated to the depinning transition of a domain wall, with or without long-range dipolar interactions. The latter are enhanced by local anisotropies, induced by the polycrystalline grains and absent in the amorphous structure. The domain wall depinning scenario successfully predicts additional features of the Barkhausen effect, such as the dependence on the field rate and the demagnetizing factor, and can thus be used as a basis to understand the role of the microstructure on the macroscopic magnetization properties.

The new frontier of the Barkhausen effect is represented mainly by thin films, as testified the recent literature. Inductive methods, that have played a leading role in noise measurements in bulk materials, become less effective as the thickness of the film is reduced to smaller and smaller sizes. Magneto optical techniques do not suffer of this problem and the improved resolution gained in time and space is allowing for precise noise measurements, joined to a direct visual inspection of domain wall dynamics. The effort in this direction, however, is still in process and a systematic analysis of the noise statistics in different materials has not yet been completed. Other techniques, such as magnetic force microscopy [139] or Hall sensors [140], are emerging as powerful tools to study the Barkhausen noise at the nanoscale. For instance, a recent experiment revealed Barkhausen jumps due to a domain wall depinning from the atomic Peierls potential [141]. As a note of warning, we note that these techniques reveal the magnetic properties of the surface and are thus not effective to study the crossover from bulk three-dimensional to thin two dimensional behavior. To this end, it would be desirable to improve inductive techniques, as recently proposed.

Apart from the experimental problems outlined above, thin films pose new theoretical challenges. It is unlikely that a simple translation of three-dimensional models to two dimensions will provide a significant understanding of the Barkhausen effect in thin films. The domain structure is in most cases more complicated than in the bulk and a single domain wall model will be inappropriate. The general framework of non-equilibrium critical phenomena and the understanding gained in domain wall and spin models could nevertheless lead to a successful theoretical understanding.

Finally, we would like to mention here hard ferromagnetic materials for which few Barkhausen noise measurements have been reported in the literature [142, 143, 144]. In these nucleation-type materials, the noise is not due to the motion of domain walls, but exclusively to grain reversal. Correlation between neighboring grains play a significant role [142], as well as the temperature. These systems, having large local anisotropies and nucleation fields, could be well represented by disordered spin models such as the RFIM. Recent studies of these models have contributed to renew the interest in the Barkhausen effect, but a clear experimental realization is still lacking.

VII. ACKNOWLEDGMENTS

We wish to thank all our collaborators who have greatly contributed to our current understanding of the Barkhausen effect: M. J. Alava, V. Basso, G. Bertotti, P. Cizeau, F. Colaiori, C. Castellano, R. da Silveira, A. Magni, L. Santi, R. L. Sommer, H. E. Stanley, M. B. Wiessmann. SZ thanks Ingeborg Walter and Michael Zaiser for their help in the translation.

APPENDIX A: TRANSLATION OF THE ORIGINAL PAPER BY BARKHAUSEN

Two phenomena discovered with the help of the new amplifier
by H. Barkhausen

1. Noise during magnetization of Iron

With the improvement of the new vacuum tube amplifier it is possible to generate easily a 10000 times larger current, which means a 100 million gain in power. With this apparatus, one can reveal electric or magnetic alternate fields that otherwise, due to their weakness, would be inaccessible to our knowledge. In some sense it is as if we discovered a microscope, and one with almost 10000 times magnification! Shortly after W. Shottky has indicated that, through a large amplification, one can, in some sense, hear the electrons flying in the amplifier tube, since the current they generate reveal the spontaneous fluctuations predicted by the kinetic gas theory.

I discovered a similar phenomenon two years ago in occasion of an experiment that I did in collaboration with Dr. T. Tuzek. Iron produces a noise when magnetized. As the magnetomotive force is smoothly varied, the molecular magnets flip in jumps to their new position. Because of this, they generate irregular induction pulses in a coil wound around the sample, that can then be heard as a noise in a telephone.

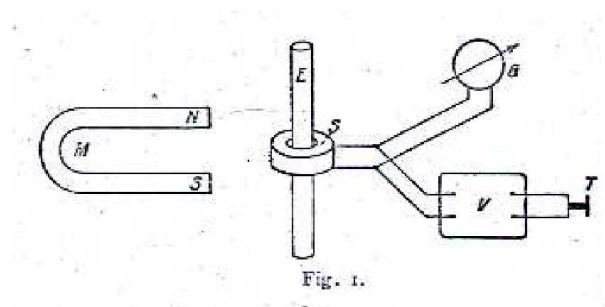


FIG. 34: Figure 1 of the original paper

I have now examined this phenomenon more closely. Fig. 34 shows the experimental apparatus. The iron sample *E* to be studied was put inside a small coil *S* with a diameter of 25mm and 300 turns. One end of the coil was connected to a telephone *T* through a 10000 times amplifier *V* and the other end to a mirror galvanometer *G*. The latter was so strongly damped that a deflection was staying almost unaltered for several seconds. Then each modification of the amplitude in practice is proportional to the corresponding modification of the induction flux of the coil. Displacing the U-shaped 10cm long magnet *M*, one could observe at the same time the modification of the induction and the noise strength. I determined the contribution of the iron sample to the former, measuring and subtracting the smallest observable deflection of the galvanometer for a given displacement of the magnet, but in absence of the iron sample. The displacement was made by hand. For this reason, the precision was not so large.

Next, it was shown that the noise became weaker for larger samples. 20mm large samples yielded effectively no more noise. As will be shown later, the reason for this is related to the too small variation of the induction (per unit area). The small magnet was not sufficient to magnetize strongly enough the large samples. So a pile of slabs gave rise to a weaker noise than a single slab coming from the same pile. The most suitable samples were found to be 1 to 1/2 mm large wires or 5 to 10mm thin ribbons. Employing stronger magnets one could also use stronger iron samples.

Later it was established on a large number of different samples that the noise was stronger as the iron was softer. Hardened steel gave almost no noise, while soft annealed iron yielded a particularly strong noise. The cause of this, however, was not the well known difficulty in magnetizing steel, that showed itself through a somewhat smaller deflection of the galvanometer given the same position of the magnet. The distinction in the noise existed also when soft iron was magnetized two to three times more weakly. Very soft iron still produced a noise when the magnet was moved at a 1/2m distance. When it was placed in the close vicinity, the noise was so strong that it could be heard clearly in the telephone even without the amplifier. The distinction between different kinds of iron is so large that one could really build on this a method to investigate iron.

The magnetic field variation was mostly done in such a way that the magnet was either displaced away by the side, turning it at 180° and then moving it back, or slowly turned away for 180° from a given position, in particularly close vicinity. The noise due to this motion was very strong in particular positions. The variations of the deflection of the galvanometer did not always correspond to the noise strength. When a variation in the direction *R* stopped at a point *A* (Fig. 35), all was suddenly quite and stayed perfectly quite as one made a variation back from *A* to *B*, even when the magnet was moved at will back and forth between *A* and *B*. As soon as the magnet overcome even slightly the position *A*, suddenly the full noise started again. In addition, by a further displacement in the direction *R*, the boundaries *A* and *B* were in some sense shifted away to the right. Then the boundary *A* remained again surprisingly sharp in correspondence to any motion between *A* and *B*. The boundary *B* was not sharp. The noise grew up slowly when one went back through *B* until *C*. At the same time, the boundary *A* became as well less sharp, in the sense sketched in Fig. 36. The galvanometer also showed quite strong variations in the region between *A* and *B*. No jump could be detected during its motion, when *A* was crossed and the noise suddenly started. Clearly the observation method was not very precise.

For thick samples it would be perhaps the same for a stronger field, but the region *A-B* was not reachable with the changes produced by the present magnet. Thus, as remarked above, with this no noise could be generated.

One could maybe explain this peculiar behavior of iron in the following way: the individual molecular magnets group themselves into assemblies of various sizes with different degrees of stability. Noise results only from the disruption or formation of greater assemblies. For a motion corresponding to Fig. 35, only small assemblies are modified in the region *A-B* and noise is does not start. For a motion across *B* in the direction *-R*, little by little also medium and large assemblies get involved. In the direction *+R*, all small and middle size assemblies have been already dissolved in the first change coming from far away up to *A*. Only the largest and more stable assemblies in this direction are

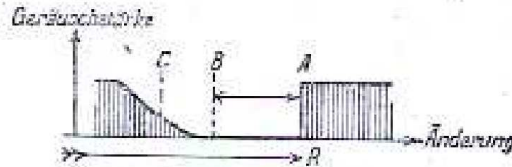


Fig. 2.

FIG. 35: Figure 2 of the original paper

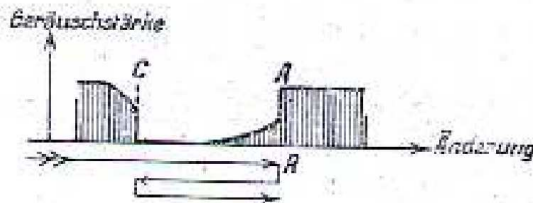


Fig. 3.

FIG. 36: Figure 3 of the original paper

still remaining. Those will be first dissolved by a further change beyond A.

In good agreement with this idea, moving across B one hears a uniform, low sough, while a loud crackling noise starts across A. For very slow variations, for instance when the magnet is moved far away from the sample, one can clearly distinguish isolated snapping hits. It appears that in steel the molecular magnets do not have the ability to join in large assemblies. In this material one only hears the low sough. Also the behavior described in Fig. 36 is in agreement with this idea. The weak assemblies, magnetized in the backward motion (from B to C in Fig. 35), are overcome again in the direction R, before A is reached.

A phenomenon occurring in a stripe, thin as paper, of soft iron sheet is still non clearly understood. A turn of the magnet by 180° gave rise to the stronger noise when the magnet was placed at a distance of 10cm. By turning it at shorter distance, the noise was surprisingly very weak, even when the magnet was turned very slowly.

A similar analysis would be desirable with the magnetodetector of Marconi and with the telegraph, also in view of practical applications.

Dresden, Institut für Schwachstromtechnik, Mai 1919.

-
- [1] Barkhausen, H. (1919). Zwei mit Hilfe der neuen Verstärker entdeckte Erscheinungen. *Physik Z.* **20**, 401–403.
 - [2] Weiss, P. (1907). L'hypothèse du champ moléculaire et la propriété ferromagnétique. *J. de Phys.* **6**, 661–690.
 - [3] Elmore, W. (1938). The magnetic structure of Cobalt. *Phys. Rev.* **53**, 757–764.
 - [4] Williams, H. J., and Shockley, W. (1949). A simple domain structure in an iron crystal showing a direct correlation with the magnetization. *Phys. Rev.* **75**, 178–183.
 - [5] Kittel, C. (1949). Physical theory of ferromagnetic domains. *Rev. Mod. Phys.* **21**, 541–583.
 - [6] McClure, J. C., and Schöeder, K. (1976). The magnetic Barkhausen effect. *CRC Crit. Rev. Solid State Mater. Sci.* **6**, 45–83.
 - [7] Tebble, R. S., and Newhouse, V. L. (1953). The Barkhausen effect in single crystals. *P. Phys. Soc. Lond. B* **66**, 633–641.
 - [8] Rudyak, V. M. (1971). The Barkhausen effect. *Sov. Phys. USP* **13**, 461–478.
 - [9] Mazzetti, P., and Montalenti, G. (1965). The theory of the power spectrum of the Barkhausen noise. In "Proceedings of the International Conference on Magnetism, Nottingham, 1964", pp. 701–706, The Institute of Physics and The Physical Society, London.
 - [10] Grosse-Nobis, W. (1977). Frequency spectrum of the Barkhausen noise of a moving 180° domain wall. *J. Magn. Magn. Mat.* **4**, 247–253.

- [11] Grosse-Nobis, W., and Lieneweg, U. (1978). Spatial extent of the flux due to local irreversible changes of the magnetic polarization in ferromagnetic strips and rods. *J. Magn. Magn. Mat.* **9**, 343–348.
- [12] Baldwin, J. A., and Pickles, G. M. (1972). Autocorrelation function of Barkhausen noise in simple materials. *J. Appl. Phys.* **43**, 1263–1268.
- [13] Baldwin, J. A., and Pickles, G. M. (1972). Power spectrum of Barkhausen noise in simple materials. *J. Appl. Phys.* **43**, 4746–4749.
- [14] Wiegman, N. J., and Stege, R. (1978). Barkhausen effect in magnetic thin films: general behaviour and stationarity along the hysteresis loop. *Appl. Phys.* **16**, 167–174.
- [15] Bertotti, G., and Fiorillo, F. (1981). Barkhausen noise and domain structure dynamics in SiFe at different points of the magnetization curve. *J. Magn. Magn. Mat.* **23**, 136–148.
- [16] Alessandro, B., Beatrice, C., Bertotti, G., and Montorsi, A. (1990). Domain wall dynamics and Barkhausen effect in metallic ferromagnetic materials. I. Theory. *J. Appl. Phys.* **68**, 2901–2908.
- [17] Alessandro, B., Beatrice, C., Bertotti, G., and Montorsi, A. (1990). Domain wall dynamics and Barkhausen effect in metallic ferromagnetic materials. II. Experiments. *J. Appl. Phys.* **68**, 2908–2915.
- [18] Cote, P. J., and Meisel, L. V. (1991). Self-organized criticality and the Barkhausen effect. *Phys. Rev. Lett.* **67**, 1334–1337.
- [19] Meisel, L. V., and Cote, P. J. (1992). Power laws, flicker noise, and the Barkhausen effect. *Phys. Rev. B* **46**, 10822–10828.
- [20] Bak, P., Tang, C., and Wiesenfeld, K. (1987). Self-organized criticality: An explanation of the $1/f$ noise. *Phys. Rev. Lett.* **59**, 381–384.
- [21] Durin, G., and Zapperi, S. (2000). Scaling exponents for Barkhausen avalanches in polycrystalline and amorphous ferromagnets. *Phys. Rev. Lett.* **84**, 4075–4078.
- [22] Alessandro, B., Bertotti, G., and Montorsi, A. (1988). Phenomenology of Barkhausen effect in soft ferromagnetic materials. *J. de Phys.* **49**, C8–1907.
- [23] Wiegman, N. J. (1979). Barkhausen noise in magnetic thin films. Master’s thesis, Technische Universiteit, Eindhoven. Available on line: <http://alexandria.tue.nl/extra3/proefschrift/PRF3A/7909139.pdf>.
- [24] Santi, L., Sommer, R., Magni, A., Durin, G., Colaiori, F., and Zapperi, S. (2003). Dynamic hysteresis in Finemet thin films. *IEEE Trans. Magn.* **39**, 2666–2668.
- [25] Spasojevic, D., Bukvic, S., Milosevic, S., and Stanley, H. E. (1996). Barkhausen noise: elementary signals, power laws, and scaling relations. *Phys. Rev. E* **77**, 2531.
- [26] White, R., and Dahmen, K. A. (2003). Driving rate effects on crackling noise. *Phys. Rev. Lett.* **91**, 085702.
- [27] Wiegman, N. J. (1977). Barkhausen effect in magnetic thin films: experimental noise spectra. *Appl. Phys.* **12**, 157–161.
- [28] Hubert, A., and Schäfer, R. (1998). Magnetic domains. Springer, New York.
- [29] Puppini, E., Vavassori, P., and Callegaro, L. (2000). A focused magneto-optical Kerr magnetometer for Barkhausen jump observations. *Rev. Sci. Instr.* **71**, 1752–1755.
- [30] Puppini, E. (2000). Statistical properties of Barkhausen noise in thin Fe films. *Phys. Rev. Lett.* **84**, 5415–5418.
- [31] Puppini, E., and Ricci, S. (2000). Statistical fluctuations during magnetization reversal in Fe films. *IEEE Trans. Magn.* **36**, 3090–3092.
- [32] Kim, D.-H., Choe, S.-B., and Shin, S.-C. (2003). Direct observation of Barkhausen avalanche in Co thin films. *Phys. Rev. Lett.* **90**, 087203.
- [33] Kim, D.-H., Choe, S.-B., and Shin, S.-C. (2003). Time-resolved observation of Barkhausen avalanche in Co thin films using magneto-optical microscope magnetometer. *J. Appl. Phys.* **93**, 6564–6566.
- [34] Coyne, P. J., and Kramer, J. J. (1974). The shape of individual Barkhausen pulses. *AIP Proc.* **24**, 726–728.
- [35] Porteseil, J. L., and Vergne, R. (1979). Irreversible processes in Bloch wall motion. *J. Appl. Phys.* **50**, 2131–2133.
- [36] Vergne, R., Cotillard, J. C., and Porteseil, J. L. (1981). Quelques aspects statistiques des processus d’aimantation dans les corps ferromagnétiques. Cas du déplacement d’une seule paroi de Bloch à 180° dans un milieu monocristallin aléatoirement perturbé. *Rev. Phys. Appl.* **16**, 449–476.
- [37] Porteseil, J. L., Cotillard, J., Vergne, R., and Ferrari, G. (1981). Etude expérimentale des mécanismes d’activation thermique dans le déplacement d’une paroi de Bloch à 180° . *J. Phys. (Paris)* **42**, 1253–1261.
- [38] Williams, H. J., Shockley, W., and Kittel, C. (1950). Studies of propagation velocity of a ferromagnetic domain boundary. *Phys. Rev.* **80**, 1090–1096.
- [39] Lieneweg, U. (1974). Barkhausen noise of 3% Si-Fe strips after plastic deformation. *IEEE Trans. Magn.* **10**, 118–120.
- [40] Alessandro, B., Bertotti, G., and Fiorillo, F. (1989). Statistical properties of Barkhausen noise in soft magnetic materials. *Phys. Scripta* **39**, 256–258.
- [41] Geoffroy, O., and Porteseil, J. L. (1994). Scaling properties of irreversible magnetization and their consequences on the macroscopic behaviour of soft materials. *J. Magn. Magn. Mat.* **133**, 1–5.
- [42] Bertotti, G., Fiorillo, F., and Sassi, M. (1982). Investigation on the magnetization reversal propagation in a (110)[001] 3% SiFe single crystal. *J. Magn. Magn. Mat.* **26**, 234–236.
- [43] Durin, G., Magni, A., and Bertotti, G. (1995). Fractal properties of the Barkhausen effect. *J. Magn. Magn. Mat.* **140-144**, 1835–1836.
- [44] Storm, L., Heiden, C., and Grosse-Nobis, W. (1966). The power spectrum of the Barkhausen noise of grain oriented three-percent silicon iron. *IEEE Trans. Magn.* **2**, 434–438.
- [45] Komatsubara, M., and Porteseil, J. L. (1985). Influence of the magnetising frequency on the Barkhausen noise power of non-oriented Si-steel sheets. *J. de Phys.* **46**, C6–173–178.
- [46] Komatsubara, M., and Porteseil, J. L. (1986). Barkhausen noise behaviour in grain oriented 3% Si Fe and the effect of local strain. *IEEE Trans. Magn.* **MAG-22**, 496–498.

- [47] Rautioaho, R., Karjalainen, P., and Moilanen, M. (1986). Coercivity and power spectrum of Barkhausen noise in structural steels. *J. Magn. Magn. Mat.* **61**, 183–192.
- [48] Jansen, K., Grosse-Nobis, W., and Klebrink, H. (1982). Propagation properties of irreversible magnetizing processes in amorphous and crystalline material. *J. Magn. Magn. Mat.* **26**, 267–269.
- [49] Cizeau, P., Zapperi, S., Durin, G., and Stanley, H. E. (1997). Dynamics of a ferromagnetic domain wall and the Barkhausen effect. *Phys. Rev. Lett.* **79**, 4669–4672.
- [50] Zapperi, S., Cizeau, P., Durin, G., and Stanley, H. E. (1998). Dynamics of a ferromagnetic domain wall: avalanches, depinning transition and the Barkhausen effect. *Phys. Rev. B* **58**, 6353–6366.
- [51] Lieneweg, U., and Grosse-Nobis, W. (1972). Distribution of size and duration of Barkhausen pulses and energy spectrum of Barkhausen noise investigated on 81% Nickel-iron after heat treatment. *Inter. J. Magnetism* **3**, 11–16.
- [52] Lieneweg, U. (1977). Increased Barkhausen noise of hard-drawn 50% Nickel-Iron at low temperatures. *J. Magn. Magn. Mat.* **4**, 242–246.
- [53] Urbach, J. S., Madison, R. C., and Markert, J. T. (1995). Reproducible noise in a macroscopic system: magnetic avalanches in Permivar. *Phys. Rev. Lett.* **75**, 4694–4697.
- [54] Urbach, J. S., Madison, R. C., and Markert, J. T. (1995). Interface depinning, self-organized criticality, and the Barkhausen effect. *Phys. Rev. Lett.* **75**, 276–279.
- [55] O’Brien, K., and Weissman, M. B. (1994). Statistical characterization of Barkhausen noise. *Phys. Rev. E* **50**, 3446–3452.
- [56] Petta, J. R., Weissman, M. B., and O’Brien, K. (1996). Multiple magnetization paths in Barkhausen noise. *Phys. Rev. E* **54**, R1029–1031.
- [57] Grosse-Nobis, W., and Wagner, W. (1977). Fluctuations of the driving field in a tape wound core of Metglas 2826. *J. Magn. Magn. Mat.* **6**, 77–79.
- [58] Yamada, K., and Saitoh, T. (1992). Observation of the Barkhausen effect in ferromagnetic amorphous ribbons by sensitive pulsed magnetometer. *J. Magn. Magn. Mat.* **104–107**, 341–342.
- [59] Durin, G., Magni, A., and Bertotti, G. (1996). Measurements of the Barkhausen effect in FeCoB alloys. *J. Magn. Magn. Mat.* **160**, 299–301.
- [60] Zheng, G.-P., Li, M., and Zhang, J. (2002). Dynamics of Barkhausen jumps in disordered ferromagnets. *J. Appl. Phys.* **92**, 883–888.
- [61] Zani, M., and Puppini, E. (2003). Negative Barkhausen jumps in amorphous ribbons of Fe₆₃B₁₄Si₈Ni₁₅. *J. Appl. Phys.* **94**, 5901–5904.
- [62] Bertotti, G., Durin, G., and Magni, A. (1994). Scaling aspects of domain wall dynamics and Barkhausen effect in ferromagnetic materials. *J. Appl. Phys.* **75**, 5490–5492.
- [63] Durin, G., Magni, A., and Bertotti, G. (1995). Fractals, scaling and the question of self-organized criticality in magnetization processes. *Fractals* **3**, 351.
- [64] McMichael, R. D., Swartzendruber, L. J., and Bennet, L. H. (1993). Langevin approach to hysteresis and Barkhausen noise jump modelling in steel. *J. Appl. Phys.* **73**, 5848–5850.
- [65] Durin, G., and Zapperi, S. (2002). On the power spectrum of magnetization noise. *J. Magn. Magn. Mat.* **242–245**, 1085–1088.
- [66] Mehta, A., Mills, A., Dahmen, K., and Sethna, J. (2002). Universal pulse shape scaling function and exponents: a critical test for avalanche models applied to Barkhausen noise. *Phys. Rev. E* **65**, 046139.
- [67] Basso, V., Bertotti, G., Duhaj, P., Ferrara, E., Haslar, V., Kraus, L., Pokorny, J., and Zaveta, K. (1996). Microstructural and magnetic investigation of partially crystallized amorphous ribbons. *J. Magn. Magn. Mat.* **157–158**, 217–219.
- [68] Durin, G., and Zapperi, S. (1999). Barkhausen noise in soft magnetic materials under applied stress. *J. Appl. Phys.* **85**, 5196–5198.
- [69] Perkovic, O., Dahmen, K., and Sethna, J. P. (1995). Avalanches, Barkhausen noise, and Plain Old Criticality. *Phys. Rev. Lett.* **75**, 4528–4531.
- [70] Porteseil, J. L., and Vergne, R. (1979). Homothétie interne dans le déplacements d’une paroi de Bloch. *C.R. Acad. Sc. Paris.* **B-288**, 343–345.
- [71] Bertotti, G., and Montorsi, A. (1990). Dependence of Barkhausen noise on grain size in ferromagnetic materials. *J. Magn. Magn. Mat.* **86**, 214–216.
- [72] Durin, G. (1997). The Barkhausen effect: new perspectives for an old problems. In “Noise in Physical Systems and 1/f Fluctuations” (C. Claeys, and E. Simoen, eds.), pp. 577–582, World Scientific, Singapore.
- [73] Petta, J. R., Weissman, M. B., and Durin, G. (1998). Barkhausen pulse structure in an amorphous ferromagnet: characterization by high order spectra. *Phys. Rev. E* **57**, 6363–6369.
- [74] Kuntz, M. C., and Sethna, J. P. (2000). Noise in disordered systems: The power spectrum and dynamic exponents in avalanche models. *Phys. Rev. B* **62**, 11699–11708.
- [75] Dahmen, K., and Sethna, J. P. (1996). Hysteresis, avalanches, and disorder-induced critical scaling: A renormalization-group approach. *Phys. Rev. B* **53**, 14872–14905.
- [76] Sethna, J., Dahmen, K. A., and Myers, C. R. (2001). Crackling noise. *Nature* **410**, 242–244.
- [77] Petta, J. R., Weissman, M. B., and Durin, G. (1998). Determination of Barkhausen signal scaling from high order spectral analysis. *IEEE Trans. Magn.* **34**, 1171–1173.
- [78] Néel, L. (1955). Energie des parois de Bloch dans le couches minces. *C. R. Acad. Sci. Paris* **241**, 533–536.
- [79] Néel, L. (1946). Bases d’une nouvelle theorie generale du champ coercitif. *Ann. Univ. Grenoble* **22**, 299–343.
- [80] Hirth, J., and Lothe, J. (1992). Theory of Dislocations. Krieger Publishing Company, Melbourne.
- [81] Groma, I., and Bakó, B. (1998). Probability distribution of internal stresses in parallel straight dislocation systems. *Phys.*

- Rev. B* **58**, 2969–2974.
- [82] Székely, F., Groma, I., and Lendvai, J. (2000). Characterization of self-similar dislocation patterns by X-ray diffraction. *Phys. Rev. B* **62**, 3093–3098.
- [83] Gonzalez, J., Chubykalo, O., and Gonzalez, J. (1997). Quantitative analysis of the collective behavior in a micromagnetic model. *Phys. Rev. B* **55**, 921–930.
- [84] Chubykalo, O. A., Gonzalez, J., and Gonzalez, J. M. (1998). Avalanches as propagating domain walls in a micromagnetic model. *Physica D* **113**, 382–386.
- [85] Chubykalo, O. A., Gonzalez, J. M., and Gonzalez, J. (1998). Barkhausen jump distributions in a micromagnetic model. *J. Magn. Magn. Mat.* **184**, L257–261.
- [86] Néel, L. (1942). Théorie des lois d’aimantation de Lord Rayleigh. I: Le déplacements d’un paroi isolée. *Cah. Phys.* **12**, 1–20.
- [87] Néel, L. (1943). Théorie des lois d’aimantation de Lord Rayleigh. II: Multiples domaines et champ coercitif. *Cah. Phys.* **13**, 18–30.
- [88] Bertotti, G. (1986). Statistical interpretation of magnetization processes and eddy current losses in ferromagnetic materials. In "Proc. of the 3rd Int. Conf. Physics of Magnetic Materials" (W. Gorzkowski, H. Lachowicz, and H. Szymczak, eds.), pp. 489–508, World Scientific, Singapore.
- [89] Bertotti, G. (1987). Dynamics of magnetic domain walls and Barkhausen noise in metallic ferromagnetic systems. In "Magnetic Excitations and Fluctuations II" (U. Balucani, S. W. Lovesey, M. G. Rasetti, and V. Tognetti, eds.), pp. 135–139, Springer, Berlin.
- [90] Bray, A. J. (2000). Random walks in logarithmic and power-law potentials, nonuniversal persistence, and vortex dynamics in the two-dimensional XY model. *Phys. Rev. E* **62**, 103–112.
- [91] Sethna, J. P., Dahmen, K., Kartha, S., Krumhansl, J. A., J., Roberts, B. W., and Shore, D. (1993). Hysteresis and hierarchies: Dynamics of disorder-driven first-order phase transformations. *Phys. Rev. Lett.* **70**, 3347–3350.
- [92] Dahmen, K., and Sethna, J. P. (1993). Hysteresis loop critical exponents in $6-\epsilon$ dimensions. *Phys. Rev. Lett.* **71**, 3222–3225.
- [93] Perkovic, O., Dahmen, K. A., and Sethna, J. P. (1999). Disorder-induced critical phenomena in hysteresis: Numerical scaling in three and higher dimensions. *Phys. Rev. B* **59**, 6106–6119.
- [94] Bertotti, G., and Pasquale, M. (1990). Hysteresis phenomena and Barkhausen-like instabilities in the Sherrington-Kirkpatrick spin glass model. *J. Appl. Phys.* **67**, 5255–5257.
- [95] Vives, E., and Planes, A. (1994). Avalanches in a fluctuationless phase transition in a random-bond Ising model. *Phys. Rev. B* **50**, 3839–3848.
- [96] Vives, E., and Planes, A. (2000). Hysteresis and avalanches in disordered systems. *J. Mag. Magn. Mat.* **221**, 164–171.
- [97] Vives, E., and Planes, A. (2001). Hysteresis and avalanches in the random anisotropy Ising model. *Phys. Rev. B* **63**, 134431.
- [98] da Silveira, R. A., and Zapperi, S. (2003). Critical hysteresis from random anisotropy. *Phys. Rev. B* **69**, in press.
- [99] Magni, A., Beatrice, C., Durin, G., and Bertotti, G. (1999). Stochastic model for magnetic hysteresis. *J. Appl. Phys.* **86**, 3253–3261.
- [100] Magni, A., and Vertesy, G. (2000). Dipolar-random-field Ising model: An application to garnet films. *Phys. Rev. B* **61**, 3203–3206.
- [101] Durin, G., and Zapperi, S. (2002). Complex dynamics of magnetic domain walls. *Phys. A* **314**, 230–234.
- [102] Carpenter, J. H., and Dahmen, K. A. (2003). Barkhausen noise and critical scaling in the demagnetization curve. *Phys. Rev. B* **67**, 020412(R).
- [103] Narayan, O. (1996). Self-similar Barkhausen noise in magnetic domain wall motion. *Phys. Rev. Lett.* **77**, 3855–3858.
- [104] Bahiana, M., Koiller, B., de Queiroz, S. L. A., Denardin, J. C., and Sommer, R. L. (1999). Domain size effect in Barkhausen noise. *Phys. Rev. E* **59**, 3884–3887.
- [105] de Queiroz, S. L. A., and Bahiana, M. (2001). Finite driving rates in interface models of Barkhausen noise. *Phys. Rev. E* **64**, 066127.
- [106] Narayan, O., and Fisher, D. S. (1993). Threshold critical dynamics of driven interfaces in random media. *Phys. Rev. B* **48**, 7030–7042.
- [107] Lemerle, S., Ferré, J., Chappert, C., Mathet, V., Giamarchi, T., and Doussal, P. L. (1998). Domain wall creep in ultrathin films. *Phys. Rev. Lett.* **80**, 849–852.
- [108] Hilzinger, H.-R. (1976). Computer simulation of magnetic domain wall pinning. *Phys. Status Solidi A* **38**, 487–496.
- [109] Hilzinger, H. R. (1977). Scaling relations in magnetic, mechanical and superconducting pinning theory. *Philos. Mag.* **36**, 225–234.
- [110] Enomoto, Y. (1994). Bloch wall motion in random impurities. *J. Magn. Magn. Mat.* **129**, L146–150.
- [111] Enomoto, Y. (1994). Magnetic domain wall depinning in a disordered medium. *J. Magn. Magn. Mat.* **138**, L1–5.
- [112] Elmer, F. J. (1995). A model for Barkhausen noise. *J. Magn. Magn. Mat.* **140-144**, 1839.
- [113] Enomoto, Y. (1997). Crossover behavior of magnetization noise properties in disordered ferromagnets. *J. Magn. Magn. Mat.* **174**, 155–159.
- [114] Nattermann, T., Stepanow, S., Tang, L. H., and Leschhorn, H. (1992). Dynamics of interface depinning in a disordered medium. *J. Phys. II (France)* **2**, 1483–1488.
- [115] Leschhorn, H., Nattermann, T., Stepanow, S., and Tang, L. H. (1997). Driven interface depinning in a disordered medium. *Ann. Physik* **6**, 1–34.
- [116] Chauve, P., and adn K. J. Wiese, P. L. D. (2001). Renormalization of pinned elastic systems: how does it work beyond one loop. *Phys. Rev. Lett.* **86**, 1785–1788.

- [117] Ertas, D., and Kardar, M. (1994). Critical dynamics of contact line depinning. *Phys. Rev. E* **49**, R2532–2535.
- [118] Dickman, R., Munoz, M. A., Vespignani, A., and Zapperi, S. (2000). Paths to Self-organized criticality. *Braz. J. Phys.* **30**, 27–39.
- [119] Fisher, D. S. (1985). Sliding charge-density waves as a dynamic critical phenomenon. *Phys. Rev. B* **31**, 1396–1427.
- [120] Durin, G., and Zapperi, S. (2000). Universality and size effect in the Barkhausen noise. *J. Appl. Phys.* **87**, 7031–7033.
- [121] Mazzetti, P. (1962). Study of non-independent random pulse trains with application to the Barkhausen noise. *Il Nuovo Cimento* **25**, 1322–1342.
- [122] Arquès, P. (1968). Sur certains problèmes statistiques liés à l’effet de Barkhausen. *J. de Phys.* **29**, 369–384.
- [123] Baldassarri, A., Colaïori, F., and Castellano, C. (2003). Average shape of a fluctuation: Universality in excursions of stochastic processes. *Phys. Rev. Lett.* **90**, 060601.
- [124] Colaïori, F., Baldassarri, A., and Castellano, C. (2003). Average trajectory of returning walks. *Phys. Rev. E*, in press.
- [125] Colaïori, F., Durin, G., and Zapperi, S. (2004). Shape of a Barkhausen pulse. *J. Magn. Magn. Mat.*, in press.
- [126] Tadić, B., and Nowak, U. (2000). Barkhausen avalanches in anisotropic ferromagnets with 180° domain walls. *Phys. Rev. E* **61**, 4610–4613.
- [127] Zheng, G., and Li, M. (2002). Universality of dynamic scaling for avalanches in disordered Ising systems. *Phys. Rev. E* **66**, 036108.
- [128] Vives, E., Goicoechea, J., Ortín, J., and Planes, A. (1995). Universality in models for disordered induced phase transitions. *Phys. Rev. E* **52**, R5–8.
- [129] Tadic, B. (1996). Nonuniversal scaling behavior of Barkhausen noise. *Phys. Rev. Lett.* **77**, 3843–3846.
- [130] Imry, J., and Ma, S. K. (1975). Random-Field Instability of the Ordered State of Continuous Symmetry. *Phys. Rev. Lett.* **35**, 1399–1401.
- [131] Nattermann, T. (1983). Interface phenomenology, dipolar interaction, and the dimensionality dependence of the incommensurate-commensurate transition. *J. Phys. C* **16**, 4125–4135.
- [132] Chui, S. (1995). Fluctuations and elastic properties of domain walls in two-dimensional dipolar systems. *Phys. Rev. B* **51**, 250–257.
- [133] Tanguy, A., Gounelle, M., and Roux, S. (1998). From individual to collective pinning: Effect of long-range elastic interactions. *Phys. Rev. E* **58**, 1577–1590.
- [134] Zapperi, S., and Zaiser, M. (2001). Depinning of a dislocation: effect of long range interactions. *Mat. Sci. Eng. A* **309-310**, 348–351.
- [135] Paczuski, M., Maslov, S., and Bak, P. (1996). Avalanche dynamics in evolution, growth, and depinning models. *Phys. Rev. E* **53**, 414–443.
- [136] Chen, L. W., and Marchetti, M. C. (1995). Interface motion in random media at finite temperature. *Phys. Rev. B* **51**, 6296–6308.
- [137] Alava, M. J. (2002). Scaling in self-organized criticality from interface depinning? *J. Phys. Cond. Mat.* **14**, 2353–2360.
- [138] Ji, H., and Robbins, M. (1991). Transition from compact to self-similar growth in disordered systems: Fluid invasion and magnetic-domain growth. *Phys. Rev. A* **44**, 2538–2542.
- [139] Schwarz, A., Liebmann, M., Kaiser, U., Wiesendanger, R., Noh, T. W., and Kim, D. W. (2004). Visualization of the Barkhausen effect by Magnetic Force Microscopy. *Phys. Rev. Lett.* **92**, 077206.
- [140] Damento, M., and Demer, L. (1997). Investigation of local events of magnetization reversal in a Nd-Fe-B magnet by use of a Hall-effect microprobe. *IEEE Trans. Magn.* **23**, 1877–1880.
- [141] Novoselov, K. S., Geim, A. K., Dubonos, S. V., Hill, E. W., and Grigoreva, I. V. (2003). Subatomic movements of a domain wall in the Peierls potential. *Nature* **426**, 812–816.
- [142] Cuntze, G., Brendel, H., and Hubert, A. (1996). Barkhausen noise from sintered permanent magnets. *IEEE Trans. Magn.* **32**, 4359–4361.
- [143] Thompson, P. J., and Street, R. (1997). Magnetic viscosity and Barkhausen noise in NdFeB-type permanent magnets. *J. Magn. Magn. Mat.* **171**, 153–162.
- [144] Basso, V., Beatrice, C., Bertotti, G., Durin, G., Bue, M. L., and Sasso, C. (2004). Barkhausen noise in nucleation-type hard magnetic materials. *J. Magn. Magn. Mat.*, in press.